On Local Optima in Minimum Time Control of the Restricted Three-Body Problem

Jean-Baptiste Caillau and Ariadna Farrés

Abstract The structure of local minima for time minimization in the controlled three-body problem is studied. Several homotopies are systematically used to unfold the structure of these local minimizers, and the resulting singularity of the path associated with the value function is analyzed numerically.

Keywords Circular restricted three body problem · Optimal control · Shooting · Homotopy · Swallowtail singularity

1 Introduction

There is currently a renewed interest in space missions with electric propulsion. See for instance the BepiColombo [2] or Lisa [9] programs. Very important models for such missions are the two and three-body controlled problems; in particular, the circular restricted three-body problem provides a dynamically relevant and challenging model for missions in the Earth-Moon or Sun-Earth systems. We recall that we take an inertial reference frame such that the line joining the Earth and Moon remains fixed on the x-axis, the z-axis is parallel to the angular velocity of the couple and the y-direction completes a positive triad. We also normalize the units of distance and time such that the distance between the two primaries is one and the period of rotation is 2π, then the equations of motion for the mass-less satellite under the gravitational influence of the two primaries is given by (see, e.g., [5])

J.-B. Caillau (✉)
UBFC & CNRS/INRIA, Math. Institute, Université de Bourgogne,
9 Avenue Alain Savary, 21078 Dijon Cedex, France
e-mail: jean-baptiste.caillau@u-bourgogne.fr

A. Farrés
Dpt. Matematica Aplicada i Analisi, Universitat de Barcelona,
Gran Via de Les Corts Catalanes 585, 08007 Barcelona, Spain
e-mail: ariadna.farres@maia.ub.es

B. Bonnard and M. Chyba (eds.), *Recent Advances in Celestial and Space Mechanics*,
Mathematics for Industry 23, DOI 10.1007/978-3-319-27464-5_7

$$
\begin{aligned}
\dot{x} &= v_x,\\
\dot{y} &= v_y,\\
\dot{z} &= v_z,\\
\dot{v}_x &= 2v_y + x - (1-\mu)\frac{x+\mu}{r_1^3} - \mu\frac{x+\mu-1}{r_2^3} + \varepsilon u_1,\\
\dot{v}_y &= 2v_x + \left(1 - \frac{(1-\mu)}{r_1^3} - \frac{\mu}{r_2^3}\right) + \varepsilon u_2,\\
\dot{v}_z &= -\left(\frac{(1-\mu)}{r_1^3} - \frac{\mu}{r_2^3}\right) z + \varepsilon u_3,
\end{aligned}
\tag{1}
$$

where $\mu \in (0, 1/2]$ is the mass parameter of the system ($\mu = m_2/(m_1 + m_2)$—for the Earth-Moon case we have $\mu = 0.012153$), $r_1 = \sqrt{(x-\mu)^2 + y^2 + z^2}$, $r_2 = \sqrt{(x-\mu+1)^2 + y^2 + z^2}$ and $u = (u_1, u_2, u_3)$ is the thrust direction on the small satellite (where $|u| \leq 1$) and ε is the maximal thrust. Our aim is to find a steering law for Earth-Moon transfer orbits minimizing the transfer time. (For the minimum fuel case, see [3]; see [10] as well for a nice numerical study.)

This problem can be formulated as:

$$
\begin{aligned}
&\min t_f = \int_0^{t_f} dt,\\
&\dot{x} = F(x,u) = F_0(x) + \varepsilon \sum_{i=0}^{3} F_i(x) u_i,\\
&|u| \leq 1,\\
&x(0) \in \mathscr{X}_0,\\
&x(t_f) \in \mathscr{X}_1.
\end{aligned}
\tag{2}
$$

where $\mathscr{X}_0$ and $\mathscr{X}_1$ are the initial and final sets; in our case $\mathscr{X}_0$ is a point on a GEO orbit (or the whole GEO orbit) and $\mathscr{X}_1$ will be either L_2 or a point on a MO orbit. In this paper, we will focus on the coplanar case and thus we will only consider a two-input control in the orbital plane. More realistic models should, of course, take into account the fact that the initial and final orbits do not need to belong to the orbital plane of the circular motion of the two primaries (see [5] for an example of 3D minimum time computation).

As it is proved in [5], controllability holds for any $\varepsilon > 0$ for a fixed $\mu \in (0, 1)$ (see [8] for the two-body case, $\mu = 0$), provided the Jacobi constant, J_c, or *energy*, is not greater that $J_c(L_2)$. (Caveat: In [5], Poincaré terminology is used so what is nowadays termed the L_1 Lagrange point was called L_2, and conversely. Here, we use the modern standards and by L_1 we mean the Lagrange point with lowest energy.) Let us recall that

$$
J_c(q, \dot{q}) = \frac{1}{2}|\dot{q}|^2 - \frac{1-\mu}{|q+\mu|} - \frac{\mu}{|q-1+\mu|} - \frac{1}{2}|q|^2.
$$

In order to connect orbits around the primaries, it is transparent from the proof that the energy has to be raised beyond $J_c(L_1)$ through the action of the control; it turns out that, for relevant boundary conditions, a time minimizing transfer will actually pass quite close to the L_1 point in the phase space. In this respect, for an important class of endpoint values, one can approximately decompose a min time transfer into two two-body problems coupled by an intermediary L_1 target. A byproduct of this heuristic interpretation is the role of the rotation numbers (or homology, see [7] for a first numerical study) around each primary. As it is well known, many local minima exist for min time two-body transfers [8], so we propose here a detailed and systematic study of this phenomenon in the restricted three-body setting. The idea is to use a homotopy in the covering angle coordinate of the initial orbit to unfold the structure of these local time minimizers. For a fixed level of thrust ε, we parameterized the solution (computed by single shooting suitably initialized—we build on [5] results) by the angular position on it; performing a homotopy on this angle reveals the connection between the different local minima. Moreover, we investigate the interplay between these local minima and the fact that, when the thrust level is decreased one needs to "make more turns" to depart from the initial orbit (*resp.* reach the final orbit); this analysis is drawn using another homotopy, on ε, to follow the characteristics (aka extremals, that are state and costate solutions of the maximum principle) through some specific singularities.

The paper is organized in two sections and four appendices. Section 2 is devoted to transfers towards the L_1 Lagrange points. First, extremals with fixed initial point on the GEO orbit are computed, in combination with homotopies w.r.t either the position angle, θ_0, or the maximum thrust allowed, ε; then extremals with free θ_0 (that is with initial submanifold the whole GEO orbit) are computed, again with a homotopy on ε. The numerical computations reveal the existence of possible cut points, that is of several candidates as global optimizers having the same cost but different structures. The same analysis is performed in Sect. 3 on transfers from the GEO towards an orbit around the Moon, referred to as MO; in this case, a homotopy on the radius of this target circular orbit is also computed. The aim of this paper is to provide a rather extensive numerical study of the problem so that detailed results are archived into several appendices: The first two provide a comprehensive list of tables of shooting initializations allowing to reproduce the results in Sects. 2 and 3, while the last two ones give a precise account of the computations of (what might be) cut points for the GEO to L_1 and MO targets, respectively.

2 Transfer from a GEO to L_1

In this section we will explore the nature of the first phase of an Earth-Moon transfer. Hence, we focus on the minimum-time transfer trajectories from a GEO orbit to the L_1 point. Finding a global minima is a hard task as in many cases it will be hard to determine if we have a global minima or just a local one. We will use indirect methods based on the Pontryagin Maximum Principle to determine local minima, using the package `hampath` [4]. First, we use the initial conditions from [5] and refine them so that they meet the constraints of our problem. The solutions in [5] where found doing homotopies from the 2BP to the 3BP, using μ as the continuation parameter. Then we will perform different homotopies with respect to the position of the initial orbit and with respect to ε, the thrust value. The idea is to understand the global structure, and find all the possible local minimum-time transfer trajectories for a given thrust value, ε, and classify the different type of solutions. In order to analyse this minimum-time transfer we propose two different boundary value problems: (a) a fixed initial condition on the GEO orbit (point-to-point problem), or (b) a free initial condition on the GEO orbit (circle-to-point problem). Both problems will be solved using a shooting method. In order to find a minimum-time transfer trajectory, it is clearly better to leave the initial condition in the departure orbit free. But due to the small radius of convergence of the shooting method, a first exploration fixing the initial position is required. Moreover, it might be possible, that in a concrete mission scenario, the initial position on the GEO orbit is fixed.

2.1 Fixed Initial Point on a GEO

In this section we discuss the results for the minimum-time transfer problem for a fixed point on a GEO orbit to L_1. The boundary conditions are:

$$x(t_0) - x_0 = 0, \quad x(t_f) - x_f = 0, \quad h(t_f) = 0, \tag{3}$$

where $x(t)$ represents the position and velocity of the spacecraft at time t, x_0 is a fixed initial condition on a circular orbit around the Earth of radius r_0; x_f is the position in the phase space that we want to reach with minimum time (here $x_f \equiv L_1 = (0.8369, 0, 0, 0)$), and $h(t_f)$ is the Hamiltonian of the PMP that has to be maximised. We parameterise an initial condition on a circular orbit by its radius r_0 and angle $\theta_0 \in [-\pi, \pi)$. Accordingly,

$$x_0 = (r_0 \cos\theta_0 - \mu, r_0 \sin\theta_0, -v_0 \sin\theta_0, v_0 \cos\theta_0), \tag{4}$$

where $v_0 = \sqrt{(1-\mu)/r_0}$ (velocity required to have a circular orbit around the Earth using a 2BP approximation). In this section we will use $r_0 = 0.109689855932071$ and $v_0 = 3.000969693845573$. Notice that $r_0 = 0.10968 \approx 42,164$ km which corresponds to a GEO orbit ($\approx$ 35.786 km *above the Earth surface*). Later we might want to discuss the effect of taking a smaller r_0 but given the nature of the problem, the results should be very similar and we should experience just some more turns around the Earth before getting on an excursion towards L_1. In [5], the authors considered $r_0 = 0.109689855932071$, $\tilde{v}_0 = 2.878597058456258$. We have done a homotopy with respect to the initial velocity on the orbit for a fixed point placed at $\theta_0 = \pi$. Tables 1 and 2 summarize these results for different values of ε. (For $\varepsilon = 3$N we had a problem during the continuation process and the local minima found has $t_f < 0$, so we will not use this as reference value.) Caveat: The $T_{\max}$ variable name in graph legends refers to ε.

Table 1 ε, t_f and p_0 of the local minima for $r_0 = 0.109689855932071$, $\tilde{v}_0 = 2.878597058456258$ and $\theta_0 = \pi$ (see [5])

ε (N)	t_f (UT)	p_0
10.0	1.47056664	(2.57392200 1.58804145 0.06972900 0.07817485)
5.0	2.28408175	(2.54649996 2.42058400 0.10200404 0.11955574)
4.0	3.14537620	(9.72954854 1.31678527 0.05736254 0.42386881)
3.0	3.82670885	(11.03739342 −0.29053787 −0.00260636 0.49490659)
2.5	4.39877672	(11.19394050 −2.02820238 −0.06740069 0.48674283)
1.5	6.67073313	(4.56115506 −0.98210983 −0.02417903 −0.03690623)
1.0	8.44011820	(−22.71568672 9.43440236 0.36634939 −0.86734182)

Table 2 ε, t_f and p_0 of the local minima for $r_0 = 0.109689855932071$, $v_0 = 3.000969693845573$ and $\theta_0 = \pi$ (results after continuation from Table 1)

ε (N)	t_f (UT)	p_0
10.0	1.4833856	(3.83493364 1.72669505 0.07642569 0.13229597)
5.0	2.3063975	(5.63281024 2.42739999 0.10473957 0.24553557)
4.0	3.3788754	(14.73978122 0.81593498 0.03725883 0.63113008)
3.0	−3.6981165	(−12.78641230 0.12268080 0.01238500 −0.58331391)
2.5	4.2681801	(13.40062243 −1.57809214 −0.05401807 0.60223014)
1.5	6.4693309	(8.27460406 −2.03560608 −0.06799797 0.14339434)
1.0	10.4302927	(41.66289104 −1.40939476 −0.04832354 1.81224566)

2.1.1 Homotopy w.r.t θ_0

As the initial manifold is a whole orbit, the initial position on the GEO shall be left free. Nevertheless, due to the small radius of convergence of the shooting method and the large dimension of the phase space, taking as initial conditions the local minima in Table 2 the shooting method does not converge. This is why we decided to proceed more systematically and solve for a large range of θ_0. We have taken for $\varepsilon = 10$N, 5N and 1N the local minima in Table 2 and perform a homotopy with respect to θ_0 (Eq. 4), i.e. we change the initial position on the GEO orbit. For each ε we start at $\theta_0 = \pi$ (which corresponds to the values in Table 2) and perform two continuations: one from $\theta = \pi \mapsto 21\pi$ and the other from $\theta = \pi \mapsto -21\pi$. In order to have a good precision along the path, we have divided the homotopies into smaller blocks of length 2π, for example for the homotopy from $\theta = \pi \mapsto 21\pi$ we split it in small homotopies from $\theta = (2k+1)\pi \mapsto (2k+2)\pi$, for $k = -10, \ldots, 9$. When we go from one block to another we refine the initial condition taking the last point on the previous block. We proceed in this way not to deprecate precision along the continuation path. The homotopy will be stopped when `hampath` fails to continue for different reasons (e.g., the norm of the shooting function becomes to big, the continuation step-size is to small). Note that the homotopy is actually done on $\theta_0 \in \mathbb{R}$, using implicitly the variable in the covering of the initial orbit diffeomorphic to $\mathbf{S}^1$ (Tables 3, 4, 5, 6, 7, 8, 9, 10 and 11).

Figures 1, 2 and 3 show the homotopy path for $\varepsilon = 10$N, 5N and 1N respectively. On the left-hand side of each Figure we plot the continuation parameter, θ_0, versus the transfer time, t_f, and on the right-hand side we plot $\theta_0(\text{mod } 2\pi) \in [-\pi, \pi]$ versus t_f (Tables 12, 13 and 14). The plots on the right-hand side illustrate that for a given initial position on the departure orbit there are different local minima solutions. We recall that each point on the curve is a solution to the minimum-time transfer from GEO to L_1 for a fixed initial position on the GEO. The red points correspond to the local minima on the projection of the homotopic path on the θ_0–t_f plane, and they are candidates for being local minima when the initial position on a GEO orbit is left free (Sect. 2.2). The initial conditions for these local minima are summarized in Tables 12, 13 and 14. Notice that the three curves for $\varepsilon = 10$N, 5N and 1N (Figs. 1, 2 and 3 respectively) present a similar behaviour; as we increase θ_0 (i.e. we change the initial position on the GEO following the clockwise direction) the transfer time, t_f, decreases until we reach a global minima and then t_f grows drastically. Also notice that for $\varepsilon = 10$N and 5N (Figs. 1 and 2) after t_f has drastically increased the homotopic curve takes a turn and θ_0 starts to decrease and we find different local minima. For both curves we find different local minima and one clear global minima. In the case of $\varepsilon = 1$N (Fig. 3) after reaching the global minima t_f also increases drastically but the continuation scheme is stopped before we can see a similar behaviour to what we obtained previously. We expect that things will continue to grow as for $\varepsilon = 10$N but need a sharper continuation scheme.

As we have mentioned before, for a given initial condition on the GEO orbit and a fixed ε we have many different local minimum time−transfer orbits from GEO to L_1. In Tables 4, 5, 6 and 7 we summarize the different local minima for $\varepsilon = 10$ and $\theta_0(\text{mod } 2\pi) = 0, \pi/2, \pi$ and $-\pi/2$ respectively. In Fig. 4 we plot the transfer trajectory of the solutions in Table 4, corresponding to $\theta_0(\text{mod } 2\pi) = 0$ and $\varepsilon = 10$N and $k = 2$. In Fig. 5 we plot the variation of the Jacobi constant J_c along time for the trajectories that appear in Fig. 4.

As we can see in Fig. 4 there are two types of trajectories. The first type, that we call $\mathscr{T}_1$ and correspond to $k = 1, \ldots, 12$ from Table 4, where the trajectory gives several turns around the Earth and then heads towards L_1 directly. The number of turns around the Earth will depend on the initial condition and, as we can see in Fig. 5, the extra turns correspond to a decrease and later increase of J_c before reaching $J_c(L_1)$. For all these orbits the final transfer to L_1 is the same. The second type of orbits, that we call $\mathscr{T}_2$ and corresponds to $k = 14$ and 15. Here the trajectories do a large excursion to get to L_1. This large excursion corresponds to large increase on J_c, high above $J_c(L_1)$. The transition between one kind of trajectories and the other (solution $k = 13$) corresponds to intermediary excursions of the trajectory and are the solutions while t_f drastically increases in Fig. 1. In Figs. 6 and 7 we show the same results for $\varepsilon = 1$N. Here we only find trajectories of type $\mathscr{T}_1$. This is because the continuation method failed at some point, but this does not mean that trajectories of type $\mathscr{T}_2$ do not exist for $\varepsilon = 1$N.

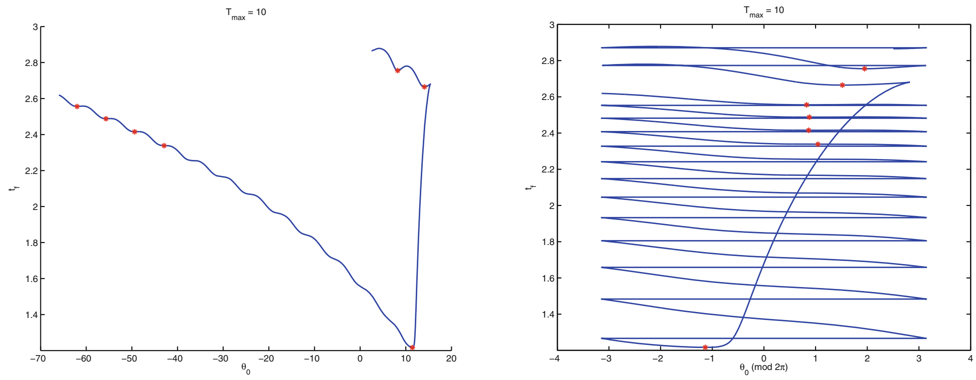

Fig. 1 For $\varepsilon = 10\text{N}$: Projection of the homotopic path θ_0 versus t_f (*left*), $\theta_0 (\text{mod } 2\pi)$ versus t_f (*right*). GEO to L_1 transfer, where the initial point on a GEO is fixed to $(r_0 \cos\theta_0 - \mu, r_0 \sin\theta_0, v_0 \cos\theta_0, v_0 \sin\theta_0)$

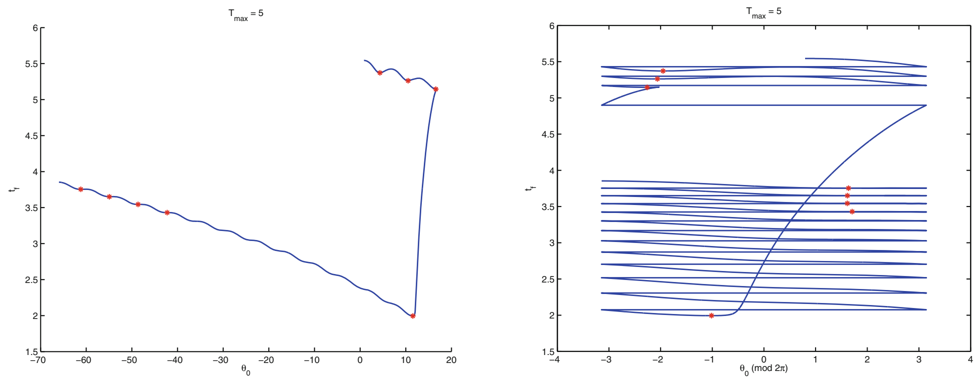

Fig. 2 For $\varepsilon = 5\text{N}$: Projection of the homotopic path θ_0 versus t_f (*left*), $\theta_0 (\text{mod } 2\pi)$ versus t_f (*right*). GEO to L_1 transfer, where the initial point on a GEO is fixed to $(r_0 \cos\theta_0 - \mu, r_0 \sin\theta_0, v_0 \cos\theta_0, v_0 \sin\theta_0)$

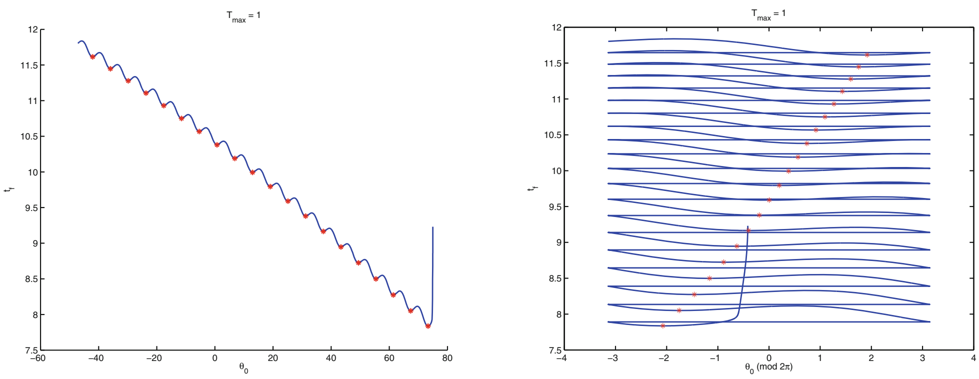

Fig. 3 For $\varepsilon = 1\text{N}$: Projection of the homotopic path θ_0 versus t_f (*left*), $\theta_0 (\text{mod } 2\pi)$ versus t_f (*right*). GEO to L_1 transfer, where the initial point on a GEO is fixed to $(r_0 \cos\theta_0 - \mu, r_0 \sin\theta_0, v_0 \cos\theta_0, v_0 \sin\theta_0)$

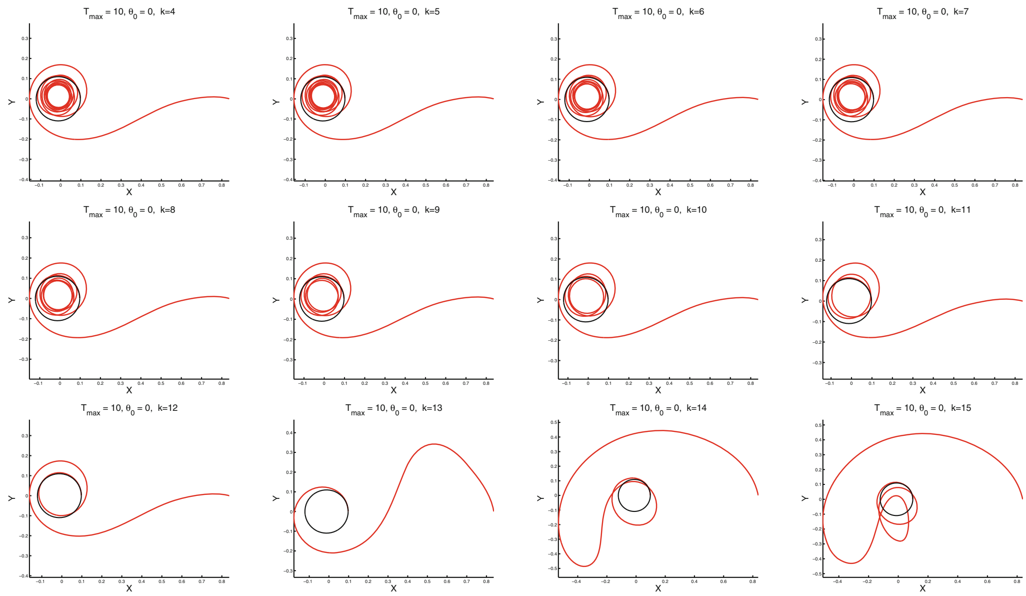

Fig. 4 Transfer trajectories of the local minima for $\varepsilon = 10$N and $\theta_0 = 0$ (Table 4). The initial condition on the GEO orbit is $x_0 = (-r_0 - \mu, 0, 0, v_0)$

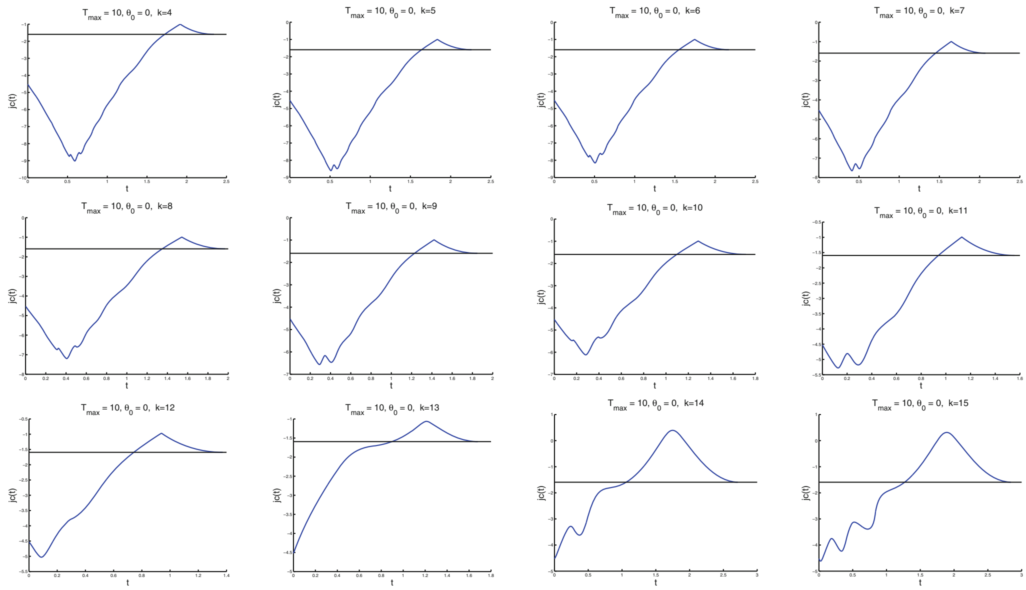

Fig. 5 Variation of J_c of the local minima for $\varepsilon = 10$N and $\theta_0 = 0$ (Table 4). The initial condition on the GEO orbit is $x_0 = (-r_0 - \mu, 0, 0, v_0)$

Finally, we have done a small exploration on the different characteristics of the minimum time−transfer trajectories that appear in Figs. 1, 2 and 3. For each minimum-time transfer orbit, parameterised by θ_0, we have computed the maximal value for J_c along the orbit, $\max_{t\in[t_0:t_f]}(J_c(t))$, the norm of the adjoint vector at t_0, $|p(t_0)|$, and the number of turns that the trajectory makes around the Earth, N_{ET}, before the trajectory reaches $J_c(L_1)$. These results are summarized in Figs. 8, 9

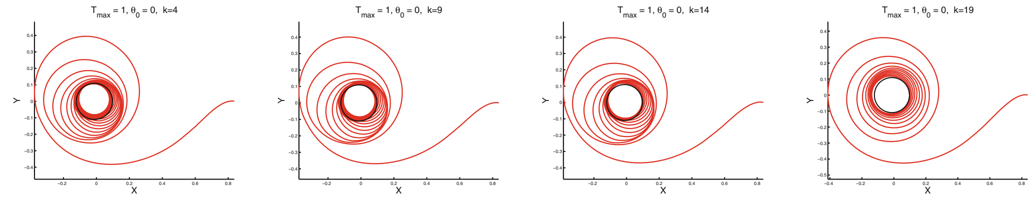

Fig. 6 Transfer trajectory of the local minima for $\varepsilon = 1$N and $\theta_0 = 0$ (Table 8). The initial condition on the GEO orbit is $x_0 = (-r_0 - \mu, 0, 0, v_0)$

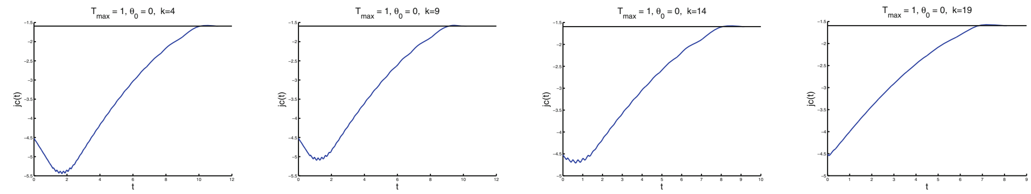

Fig. 7 Variation of Jacobi constant of the local minima for $\varepsilon = 1$N and $\theta_0 = 0$ (Table 8). The initial condition on the GEO orbit is $x_0 = (-r_0 - \mu, 0, 0, v_0)$

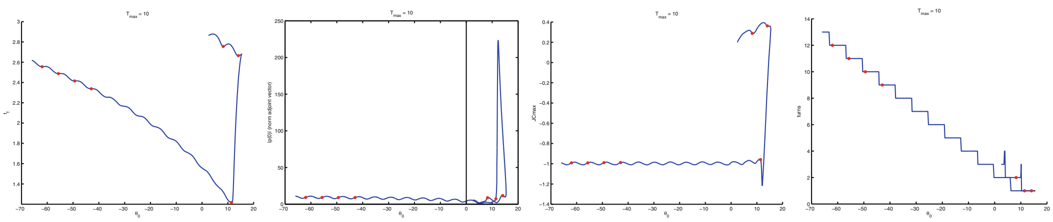

Fig. 8 For $\varepsilon = 10$N. From *left* to *right* θ_0 versus t_f, θ_0 versus $|p(t_0)|$, θ_0 versus $\max_{t\in[t_0:t_f]}(J_c(t))$, and θ_0 versus N_{ET}

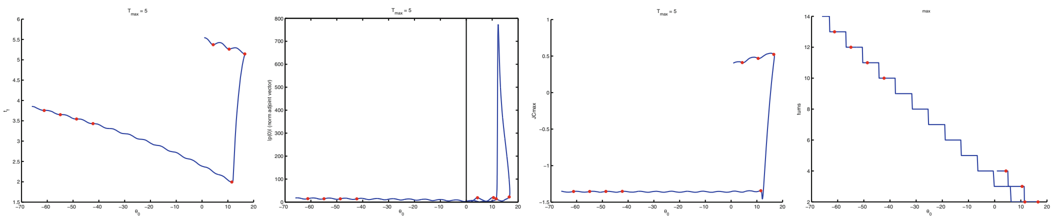

Fig. 9 For $\varepsilon = 5$N. From *left* to *right* θ_0 versus t_f, θ_0 versus $|p(t_0)|$, θ_0 versus $\max_{t\in[t_0:t_f]}(J_c(t))$, and θ_0 versus N_{ET}

and 10 for $\varepsilon = 10$N, 5N and 1N respectively. In each figure we see: t_f versus θ_0, $|p(t_0)|$ versus θ_0, $\max_{t\in[t_0,t_f]}(J_c(t))$ versus θ_0 and N_{ET} versus θ_0. Notice that the number of turns decreases as we reach the global minima, which will display 1 turn for $\varepsilon = 10$N, 2 turns for $\varepsilon = 5$N and 10 turns for $\varepsilon = 1$N. We observe that the maximum value reached by the Jacobi constant J_c can be used to filter out solutions far away for what seems to be the global minimum (for this one, the value of J_c is close to $J_c(L_1)$). Finally, looking at $|p(t_0)|$ we see a strong increase when the homotopic path moves from one type of trajectory to the other. We recall that the points in red in Figs. 8, 9 and 10 correspond to the local minima of the projection of the homotopic

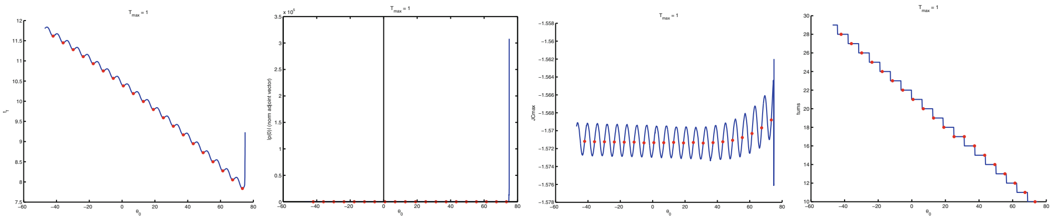

Fig. 10 For $\varepsilon = 1$N. From *left* to *right* θ_0 versus t_f, θ_0 versus $|p(t_0)|$, θ_0 versus $\max_{t\in[t_0:t_f]}(J_c(t))$, and θ_0 versus N_{ET}

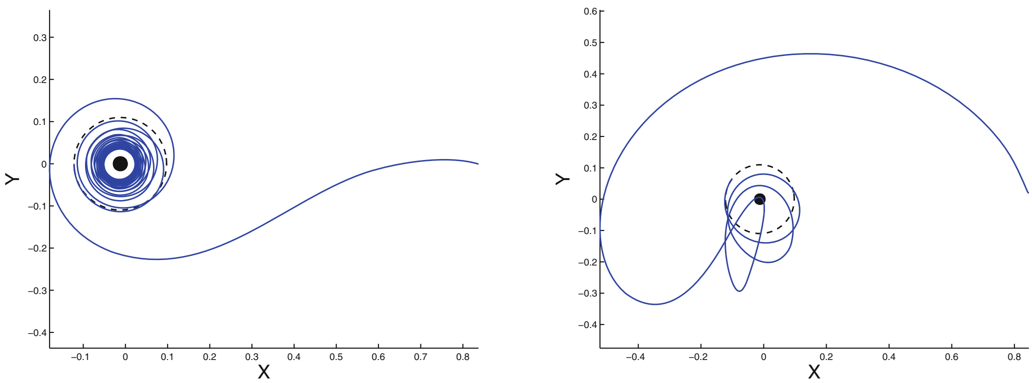

Fig. 11 Transfer trajectories of the two ends of the homotopic curve θ_0 versus t_f

path θ_0 versus t_f. All these local minima are summarized in Tables 12, 13 and 14 for $\varepsilon = 10$N, 5N and 1N respectively.

Moreover, for $\varepsilon = 10$N, we have continued the two extremes of the homotopic curve w.r.t θ_0 to see if there are other connections. We have seen that both extremes die when the associated transfer trajectory has a close encounter with the Earth. On one end of the curve we see type $\mathscr{T}_1$ trajectories where the transfer trajectory spirals towards the Earth and then outwards before a direct transfer to L_1. We think that if we continue decreasing θ_0 in this direction, the trajectory will collide with the Earth. On the other end of the curve we see type $\mathscr{T}_2$ trajectories, where the transfer trajectory experiences a fast close approach with the Earth. In Fig. 11 we can see the two solutions at the two extremes of the path.

2.1.2 Homotopy w.r.t. ε

In this section, we have taken the different solutions for $\varepsilon = 10$N and a fixed initial condition $\theta_0(\text{mod } 2\pi) = 0, \pi/2, \pi$ and $-\pi/2$, summarized in Table 4, 5, 6 and 7. For each initial condition we perform a homotopy with respect to ε from 10N to 1N. In Fig. 12 we summarize the results for the different values of $\theta_0(\text{mod } 2\pi)$. As we can see, for each fixed $\theta_0(\text{mod } 2\pi)$ the behaviour of the family of homotopic curves is very similar. For most local minima, t_f increases as ε decreases. In some of the cases, at some point the slope of $\varepsilon(t_f)$ experiences a drastic change and t_f

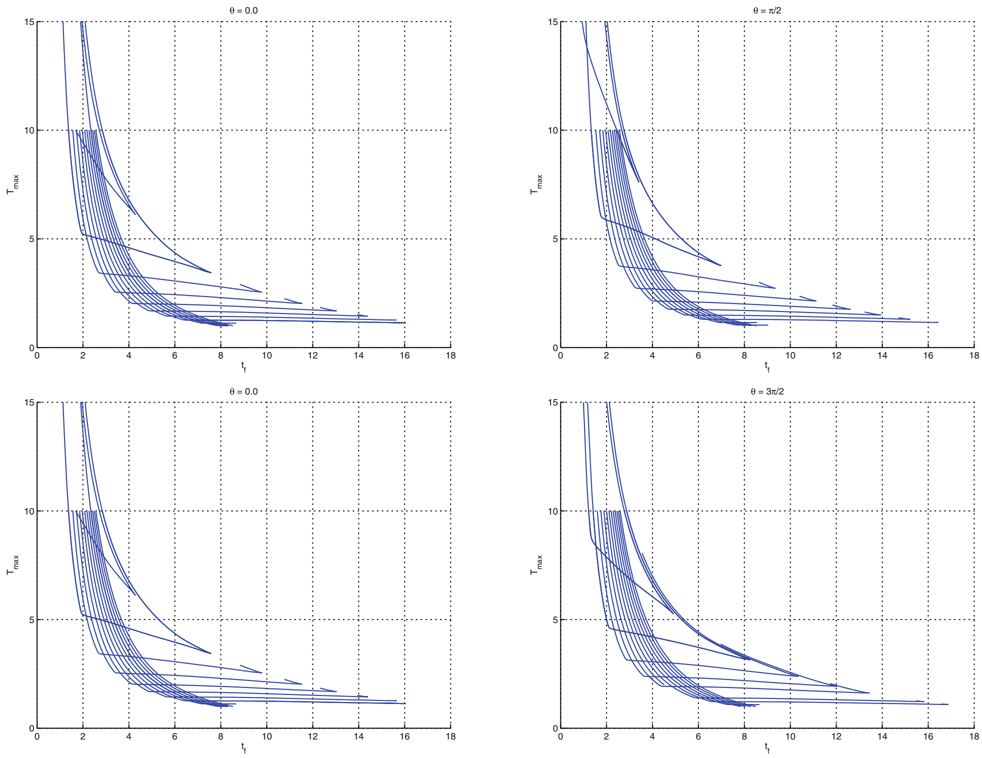

Fig. 12 Homotopy with respect to ε for θ_0 fixed: $\theta_0 = 0$ (*top-left*), $\theta_0 = \pi/2$ (*top-right*), $\theta_0 = \pi$ (*bottom-left*), $\theta_0 = -\pi/2$ (*bottom-right*)

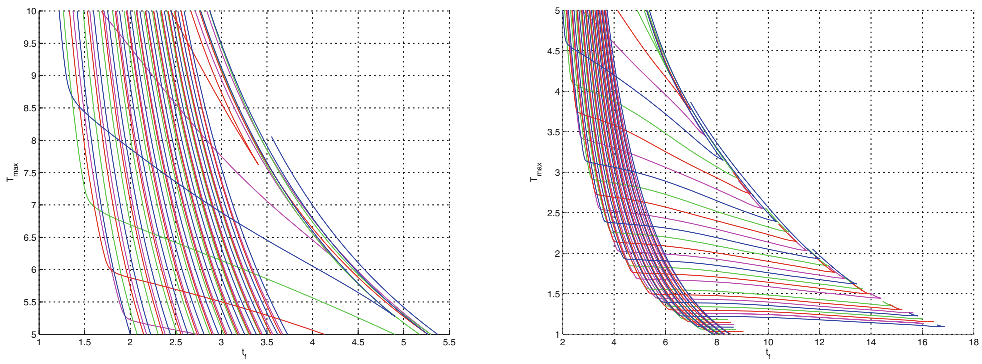

Fig. 13 Homotopy with respect to ε for θ_0 fixed: $\theta_0 = 0$ (*magenta*), $\pi/2$ (*red*), π (*green*), $-\pi/2$ (*blue*). *Left* zoom for $\varepsilon \in [5:10]$, *Right* zoom for $\varepsilon \in [1:5]$

increases very quickly for small variations of ε. Then at some point the homotopy curve has a turning point and ε starts to grow, and we are not able to reach lower values for ε. Nevertheless, there are other cases where ε just decreases and reaches $\varepsilon = 1$N with no drastic changes on the curve. We believe that for these last cases a similar behaviour will be observed for $\varepsilon < 1$N. In Fig. 13 we summarize all the local minima for $\theta_0 (\text{mod } 2\pi) = 0$ (magenta), $\pi/2$ (red), π (green) and $-\pi/2$ (blue). For $\varepsilon \in [5:10]$ (left) and $\varepsilon \in [1:5]$ (right). In Fig. 14 we show the variation of the type of solutions along time for one of these families ($\theta_0 = 0$, $k = 2$ in Table 4),

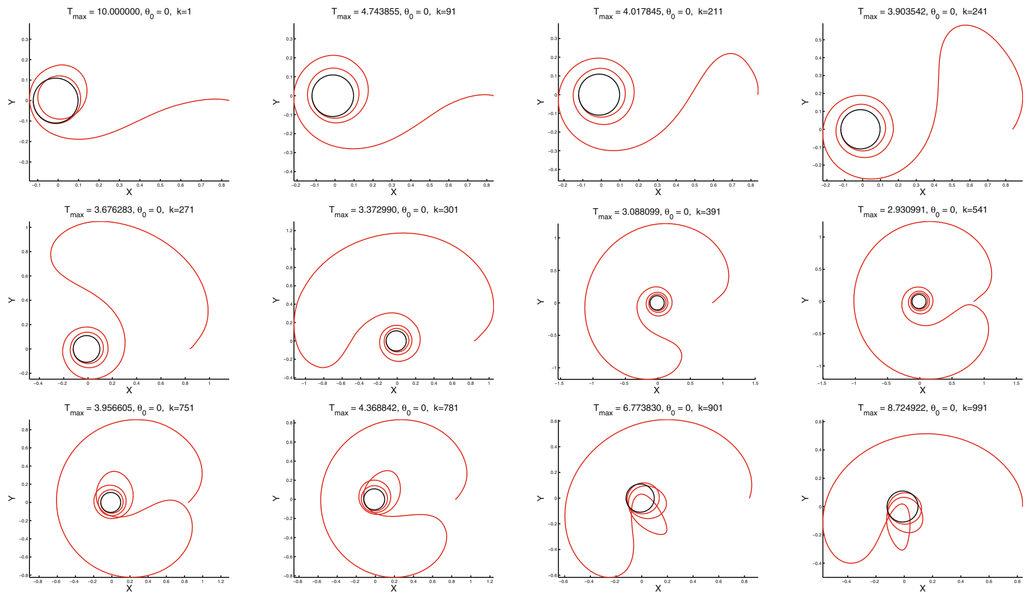

Fig. 14 Transfer trajectories from GEO to L_1 for θ_0 fixed and different ε. Here $\theta_0 = 0$ and all the orbits belong to the homotopic curve generated by $k = 2$ from Table 4 when we use ε as the homotopy parameter

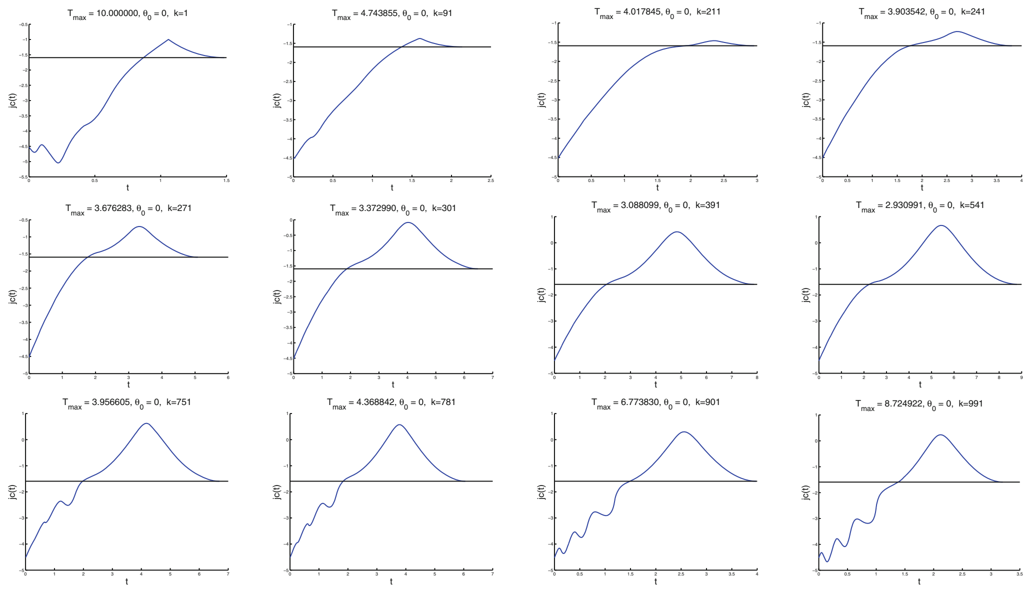

Fig. 15 Variation of the Jacobi constant along time for a transfer trajectories from GEO to L_1 for θ_0 fixed and different ε. Here $\theta_0 = 0$ and all the orbits belong to the homotopic curve generated by $k = 2$ from Table 4 when we use ε as the homotopy parameter

which corresponds to one of the homotopy paths where $\varepsilon(t_f)$ experiences two drastic changes. As we can appreciate, the orbits on the first part of the homotopic curve are type $\mathscr{T}_1$. When the slope of the path experiences its first drastic change, the transfer trajectories start to do big excursions on the phase space before heading towards L_1 and we begin to observe type $\mathscr{T}_2$ trajectories. Eventually, when ε starts to grow the

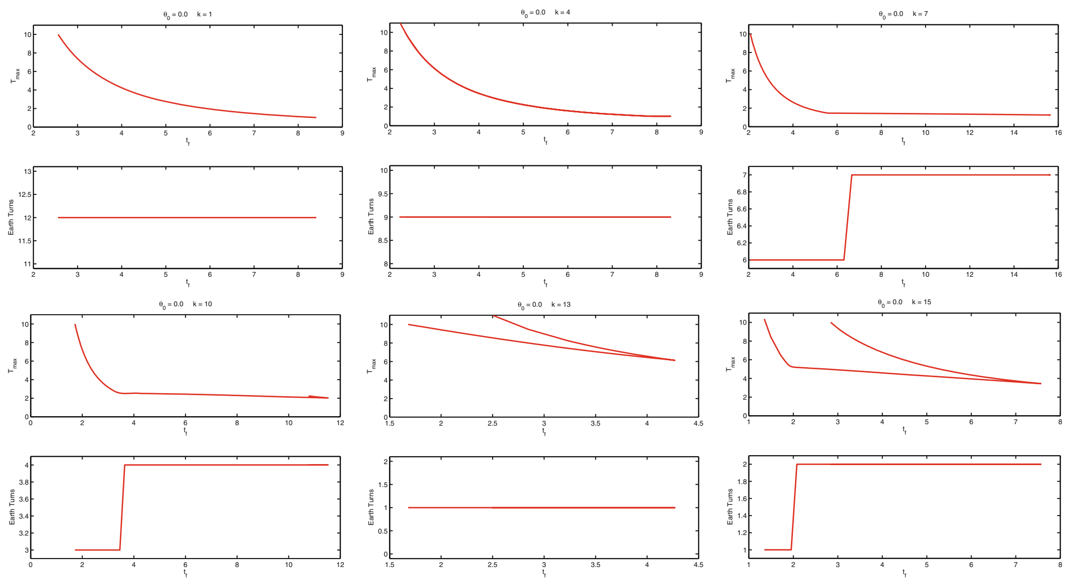

Fig. 16 For the local minima for $\theta_0 = 0$ and $\varepsilon = 10$ ($k = 1, 4, 7, 10, 13, 15$): homotopic curve ε versus t_f (subplots on the *top*) and N_{ET} versus t_f (subplots on the *bottom*)

trajectories remain of type $\mathscr{T}_2$ and some of them experience close approaches with the Earth. Hence, these paths connect type $\mathscr{T}_1$ transfer trajectories with type $\mathscr{T}_2$. Finally, in Fig. 15 the variation of the Jacobi constant is displayed with respect to time for the trajectories in Fig. 14.

Finally, we think it is worth saying that for a fixed θ_0, along each of the different homotopic paths that we have generated by varying ε summarized in Fig. 12, the number of turns the trajectory gives around the Earth, N_{ET}, is kept constant before the first drastic change on the homotopic paths slope. There the number of turns increases in 1 and remains constant along that path, even when ε starts to increase. This phenomena can be seen in Fig. 16, where we plot some of the homotopic curves, the variation of the number of turns around the Earth versus t_f. In order to understand better this phenomenon, for each curve we have plotted on top the corresponding homotopic curve (t_f vs. ε) and on the bottom (t_f vs. N_{ET}). So if we assume that for a given ε^* there is a minimum number of turns around the Earth that the trajectory must give before $J_c(x(t)) > J_c(L_1)$, which will allow the trajectory to reach L_1, this gives us a criteria to chose one of the solutions for $\varepsilon = 10$N and get to ε^* by following its homotopic path w.r.t. ε.

2.2 Free Initial Point on a GEO

In this section we discuss the results for a minimum-time transfer from a GEO orbit to L_1. The main difference with respect to the previous section is that here we just impose the initial condition to be on a GEO orbit but we do not fix the position on it. Hence, the boundary conditions are:

$$x(t_0) \in \mathscr{M}_0, \quad p(t_0) \perp T_{x(t_0)}\mathscr{M}_0, \quad x(t_f) - x_f = 0, \quad h(t_f) = 0, \tag{5}$$

where $\mathscr{M}_0$ represents the GEO orbit. The first two boundary conditions are written as

$$\begin{aligned} (x_0 + \mu)^2 + y_0^2 - r_0^2 &= 0, \\ \dot{x}_0^2 + \dot{y}_0^2 - v_0^2 &= 0, \\ (x_0 + \mu)\dot{x}_0 + y_0\dot{y}_0 &= 0, \\ (x_0 + \mu)p_{y0} - y_0 p_{x0} + v x_0 p_{\dot{y}0} - v y_0 p_{\dot{x}0} &= 0, \end{aligned} \tag{6}$$

where r_0 is the radius of the GEO orbit and v_0 is the corresponding velocity; $x(t_0) = (x_0, y_0, \dot{x}_0, \dot{y}_0)$ is the coordinate vector of the spacecraft and $p(t_0) = (p_{x0}, p_{y0}, p_{\dot{x}0}, p_{\dot{y}0})$ is the adjoint vector, both evaluated at t_0. The other boundary conditions are the same as in Sect. 2.1. We recall that all the solutions found in Sect. 2.1, where we fix the initial condition on the GEO orbit, are not necessarily solutions of this more general problem. Here the boundary conditions are more restrictive as we impose the transversality condition on $p(t_0)$. Only the local minima in the projection (θ_0, t_f) of the homotopic paths in Figs. 1, 2 and 3 will be good initial conditions to be local minima of this problem. The values for (x_0, p_0) are summarized in Tables 12, 13 and 14 for $\varepsilon = 10$N, $5N$ and 1N, respectively. In this section we have taken some of the local minima for $\varepsilon = 10$N and for each one we have performed homotopies with respect to the thrust magnitude $\varepsilon \in [1 : 10]$N. The initial conditions corresponding to the local minima from Figs. 1 and 3 in Sect. 2.1 are summarized in Tables 12 and 14.

On the left-hand side of Fig. 17 we show the continuation curve for the local minima number 4, 5, 6 and 7 for $\varepsilon = 10$N from Table 12. Minima 4 and 5 are $\mathscr{T}_1$ type solutions and the homotopic curves are plotted in magenta and blue respectively. Minima 6 and 7 are $\mathscr{T}_2$ solutions and the homotopic curves are plotted in red and green respectively. Notice that the homotopic paths with respect to ε do not connect the two type of solutions $\mathscr{T}_1$ and $\mathscr{T}_2$. On the right-hand side of Fig. 17 we compare

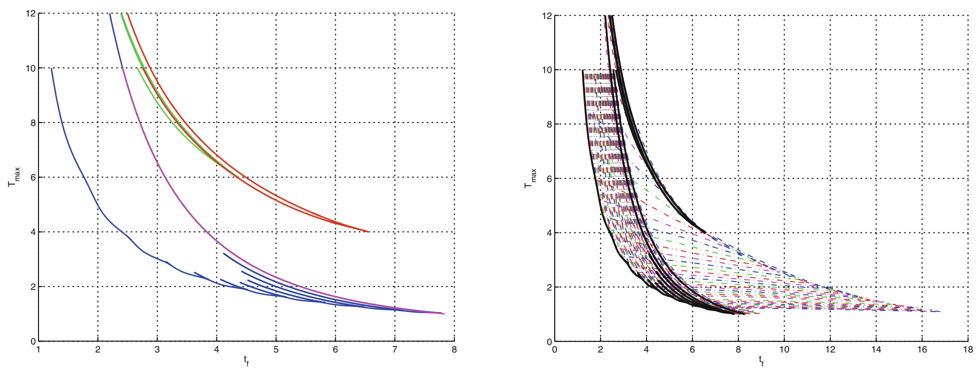

Fig. 17 Homotopy w.r.t ε for a transfer orbit from GEO to L_1. *Left* the initial condition on the orbit is considered free. *Right* comparison between letting the initial condition free (*black line*) and fixing it to $\theta_0 = 0, \pi/2, \pi, -\pi/2$

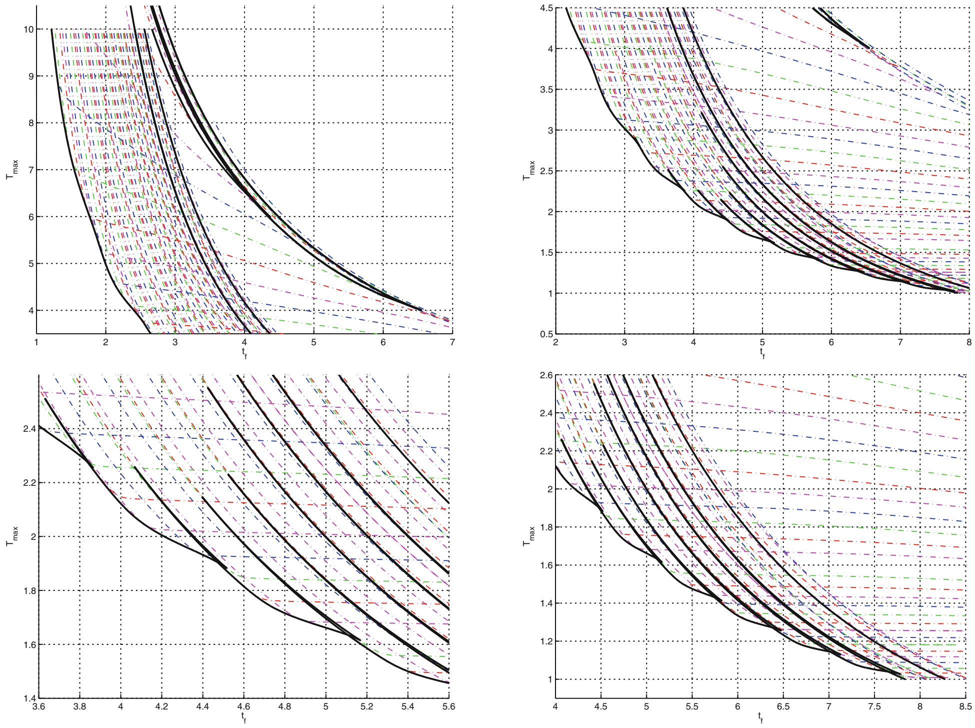

Fig. 18 Homotopy w.r.t ε: Comparison between letting the initial condition free (*black line*) and fixing it to $\theta_0 = 0, \pi/2, \pi, -\pi/2$

these homotopic curves (now plotted in black) with the homotopic curves for θ_0 fixed. The curves for $\theta_0 = 0, \pi/2, \pi$ and $-\pi/2$ are plotted in blue, magenta, green and red respectively. In Fig. 18 we have plotted different zooms of these last plot. Notice that for $\varepsilon < 3$N the projection of the homotopic path in the ε–t_f plane self-intersects several times. Hence, we have at least two different solutions with the same cost. These are candidates to be cut points. We will describe them in more detail in the next section (Tables 15, 16, 17 and 18).

Finally, in Fig. 19 we show information on the orbital parameters for one of the continuation curves, the one corresponding to the candidate to "global" minima. On the top left hand-side we show θ_0 the argument of the initial condition on the GEO orbit versus ε, and on the top right hand-side we show $\theta_0(\text{mod } 2\pi)$ verus ε. On the bottom left hand-side we show θ_0 versus the number of turns around the Earth, and on the bottom right hand-side we show θ_0 versus the norm of the adjoint vector for $t_0 = 0$, $|p(t_0)|$. As we can see, θ_0 can be used to parameterize the homotopic curve.

2.3 Cut Points

As we can appreciate in Fig. 18, the homotopic path for the GEO to L_1 transfer with θ_0 free has several turning points and the path self-intersects several times. These intersections are cut point candidates. We recall that, in optimal control, a *cut point*

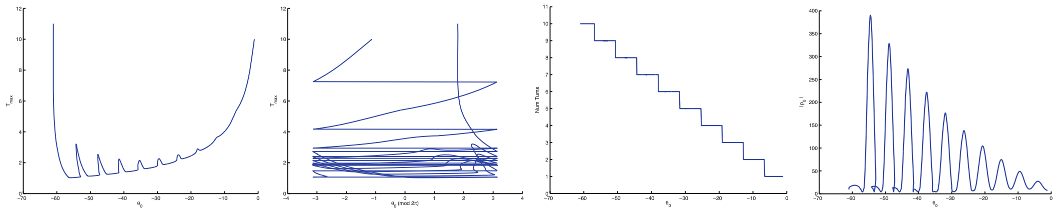

Fig. 19 Homotopy of the candidate for global minimum with respect to ε. From *left* to *right* ε versus θ_0 the argument on the GEO orbit, ε versus $\theta_0 (\text{mod } 2\pi)$, N_{ET} versus θ_0, $|p(t_0)|$ versus θ_0

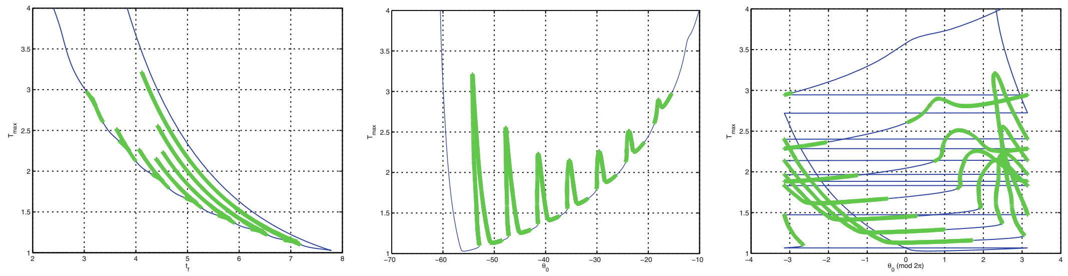

Fig. 20 Homotopy of the local minima. *Left* ε versus t_f, *Centre* ε versus θ_0, *Right*: ε versus θ_0 (mod 2π). The *green* points correspond in both cases the neighbourhood of the cut points ($t_f \in [t_f cut - 0.15, t_f cut + 0.15]$)

is the first point in the extremal where the solution ceases to be globally minimizing. Typically, two different extremals with the same cost are candidates for defining such a point. From now on we call the couple $\{(x_0, p_0), (x_1, p_1)\}$ a cut point if they are two different initial conditions such that for the same ε^* they generate two local optimal solutions for the GEO to L_1 transfer problem with the same transfer time t_f^*. We find these initial conditions on the self-intersections of the ε versus t_f projection of homotopic path in Fig. 17. To fix notation, (x_0, p_0) will be the "first" point on the homotopic path that reaches (ε^*, t_f^*) and (x_1, p_1) will be the "second" point to reach (ε^*, t_f^*). In Table 3 we summarize all the cut points that we have found for $\varepsilon \in [1, 10]$. We have computed these points by refining the intersections found in Fig. 18. In Fig. 20 we plot the different projections of the homotopy path that we have already seen, where we have highlighted in green the solutions close to the cut points. On the left hand side of Fig. 20 we have the t_f versus ε projection, on the centre we have the θ_0 versus ε projection and on the right hand side we have θ_0 mod 2π versus ε projection.

For all seven cut points we have done the same analysis. First of all we have taken both points and computed the transfer trajectory, the variation of $J_c(t)$, the control law $\mathbf{u}(t)$ and $(H_1(t), H_2(t))$. We have also integrated both trajectories backwards and forward in time covering the time range $[-t_f, 2t_f]$, where t_f is the transfer time. As we will see, the main difference between both solutions appears when we look at the integration of the trajectory backwards in time $t \in [-t_f, 0]$ and on the control $u(t)$ at the beginning of the transfer trajectory. Secondly, we have taken a neighbourhood of the cut point and checked the variation of different orbital parameters for the optimal

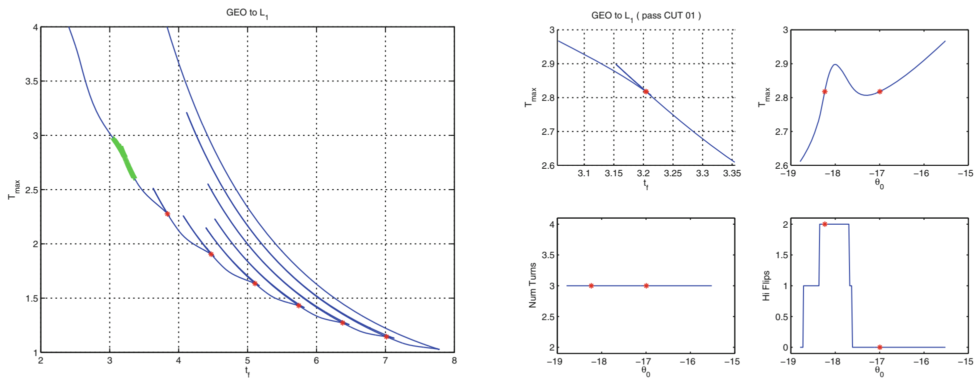

Fig. 21 For cut point n^o 1: *Left* t_f versus ε homotopic curve with highlight of the cut passage in *green*; *Right* analysis of the cut passage: (*top-left* subplot) t_f versus ε zoom, (*top-right* subplot) θ_0 versus ε, (*bottom-left* subplot) θ_0 versus N_{ET}, (*bottom-right* subplot) θ_0 versus N_{ZH}. *Red* points are values corresponding the each cut point

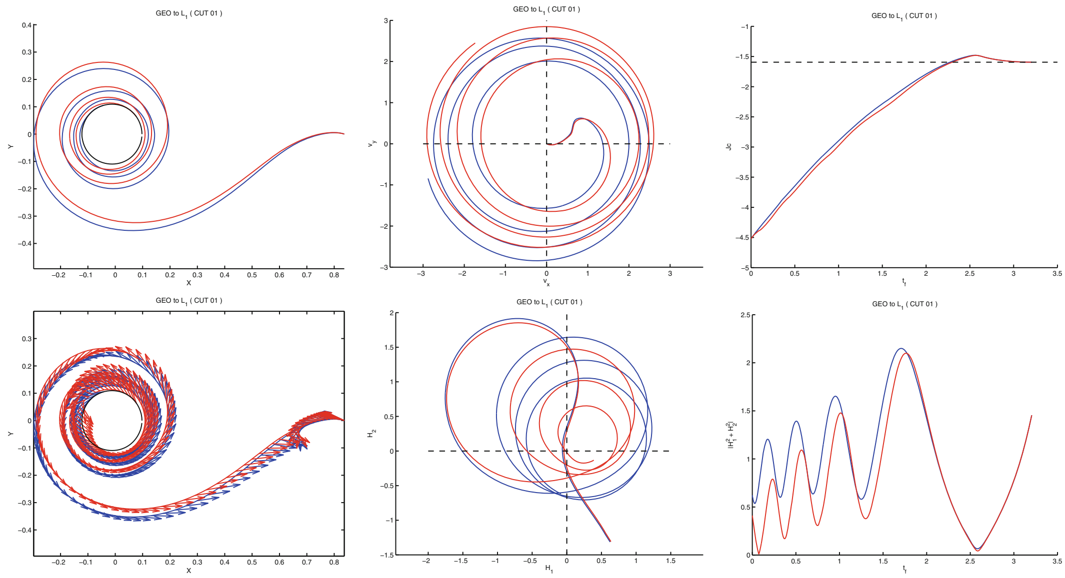

Fig. 22 For cut point n^o 1: *blue* orbits correspond to the first cut value and *red* orbits to the second cut value. *Top-Left* $\{XY\}$ projection of the transfer trajectory, *Top-Centre* $\{\dot{X}\dot{Y}\}$ projection of the transfer trajectory, *Top-Right* t versus J_c (energy variation along the transfer trajectory), *Bottom-Left* control along the trajectory, *Bottom-Centre* H_1 versus H_2, *Bottom-Right* t versus $|(H_1, H_2)|$

transfer orbits on the homotopic path. For all cut points, if ε^*, t_f^* is the value of the thrust magnitude and transfer time at the cut point, we analyse the solutions that are close to the cut point, i.e. $t_f \in [t_f^* - 0.15 : t_f^* + 0.15]$. The plots corresponding to these simulations are summarized in Appendix "Summary of the cut points on the GEO to L_1 transfer" here we will only describe the results for the cut points number 1 and 5 in Table 3, where Figs. 21, 22 and 23 correspond to the 1st cut point and Figs. 24, 25 and 26 correspond to the 5th cut point. The first cup point occurs at $\varepsilon^* \approx 2.8177314$N and $t_f^* \approx 3.2044271$. On the left-hand side of Fig. 21, we have plotted the whole homotopic curve and highlighted in green the first cut region, i.e.

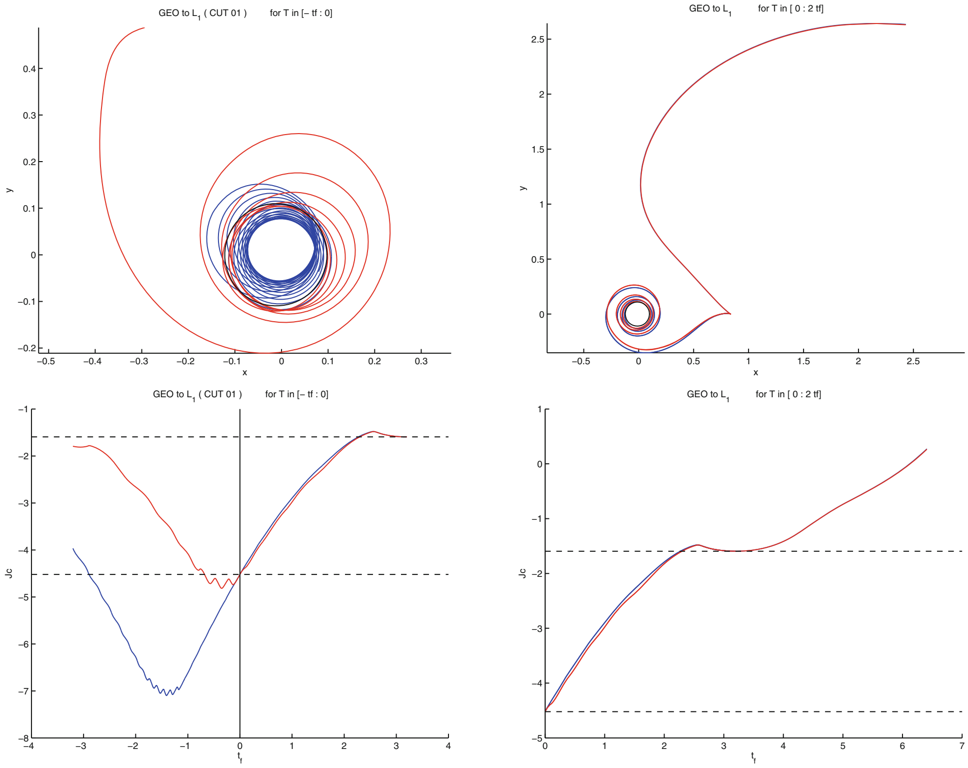

Fig. 23 For cut point n^o 1: *Left* optimal solutions for $t \in [-t_f, 0]$ (XY projection and J_c variation), *Right* optimal solutions for $t \in [0, 2t_f]$ (XY projection and J_c variation)

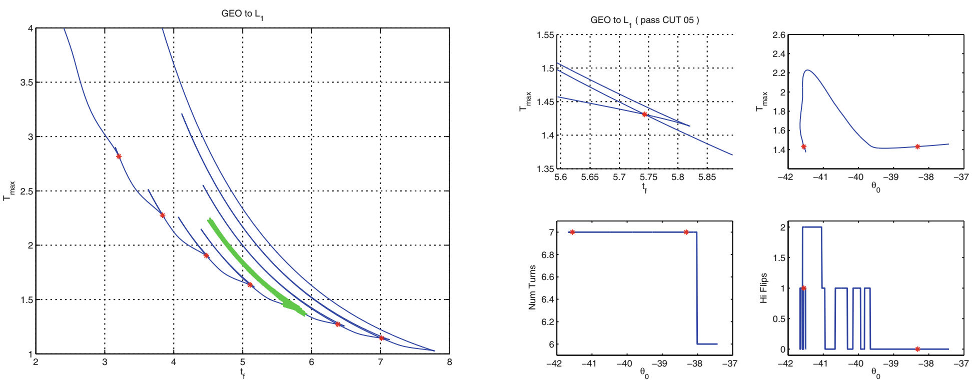

Fig. 24 For cut point n^o 5: *Left* t_f versus ε homotopic curve with highlight of the cut passage in *green*; Right analysis of the cut passage: (*top-left* subplot) t_f versus ε zoom, (*top-right* subplot) θ_0 versus ε, (*bottom-left* subplot) θ_0 versus N_{ET}, (*bottom-right* subplot) θ_0 versus N_{ZH}. *Red* points are values corresponding the each cut point

solutions with a transfer time between $[t_f - 0.15 : t_f + 0.15]$. On the right-hand side we have 4 subplots, the two subplots on the top are a zoom of the cut region t_f versus ε (left), and the θ_0 versus ε projection of the cut region (right). The two subplots on the bottom show θ_0 versus N_{ET}, the number of turns around the Earth before going towards L_1 (left), and θ_0 versus N_{ZH}, the number of times $|(H_1, H_2)|$ get close to

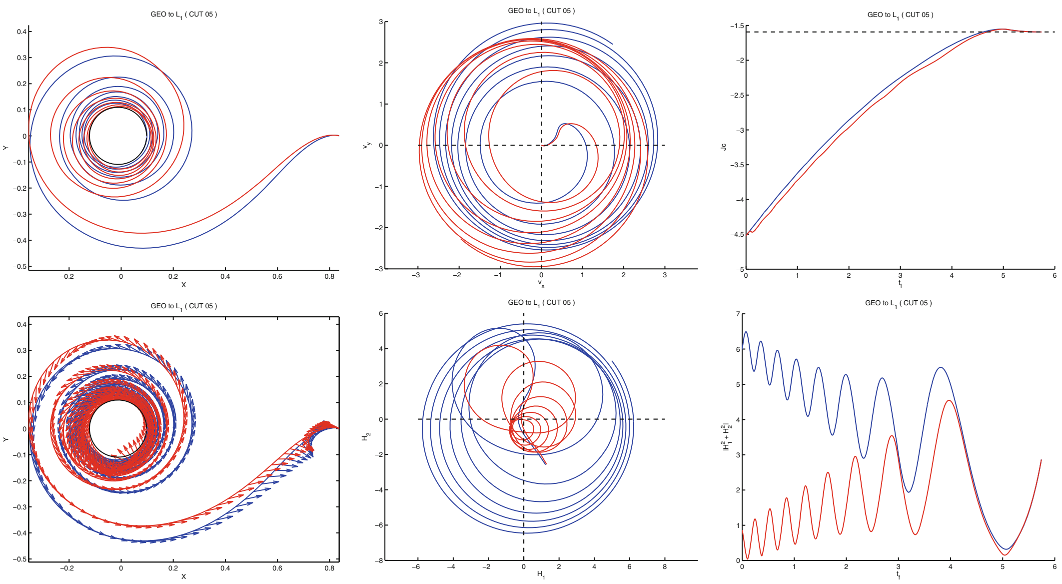

Fig. 25 For cut point n^o 5: *blue* orbits correspond to the first cut value and *red* orbits to the second cut value. *Top-Left* $\{XY\}$ projection of the transfer trajectory, *Top-Centre* $\{\dot{X}\dot{Y}\}$ projection of the transfer trajectory, *Top-Right* t versus J_c (energy variation along the transfer trajectory), *Bottom-Left* control along the trajectory, *Bottom-Centre* H_1 versus H_2, *Bottom-Right* t versus $|(H_1, H_2)|$

zero (right). As we can see, the number of turns around the Earth remains constant $N_{ET} = 3$, but $N_{ZH} = 0$ for the first cut point and 2 for the second cut point. In Fig. 22 we show different aspects of both transfer trajectories. The curves in blue correspond to the first cut point, (x_0, p_0), and the curves in red to the second cut point, (x_1, p_1). The three plots on the top, from left to right correspond to the $\{x, y\}$ projection on the transfer trajectory, to the $\{\dot{x}, \dot{y}\}$ projection of the transfer trajectory, and to the evolution of J_c along the transfer trajectory. The three plots on the bottom, from left to right correspond to the $\{x, y\}$ projection of the trajectory and the control law $\mathbf{u}(t)$, to the projection of (H_1, H_2), and to the variation of $|(H_1, H_2)|$ along time. In these plots we can see that the main difference between the two transfer trajectories lies on the control law. The control $\mathbf{u}(t)$ for the second cut point (red curve) has a drastic change of its orientation at the beginning of the transfer trajectory. This translates on (H_1, H_2) passing close to zero—possible discontinuity of the control. This effect is not observed for the first cut point (blue curve). In Fig. 23 we see for both cut points the integration backwards in time ($t \in [-t_f : 0]$) and forward in time ($t \in [0 : 2t_f]$), as well as the corresponding variation of $J_c(t)$. Again, the curves in blue are related to the first cut point and the curves in red to the second cut point. As we can see, there is practically no qualitative difference for the evolution of both transfer trajectories if we integrate forward in time. While we do see a difference between the evolution backwards in time. Notice that the first cut point (blue curve) spirals towards the Earth and $J_c(t)$ decreases drastically, while the second cut point (red curve) spirals outwards and $J_c(t)$ will quickly start to grow.

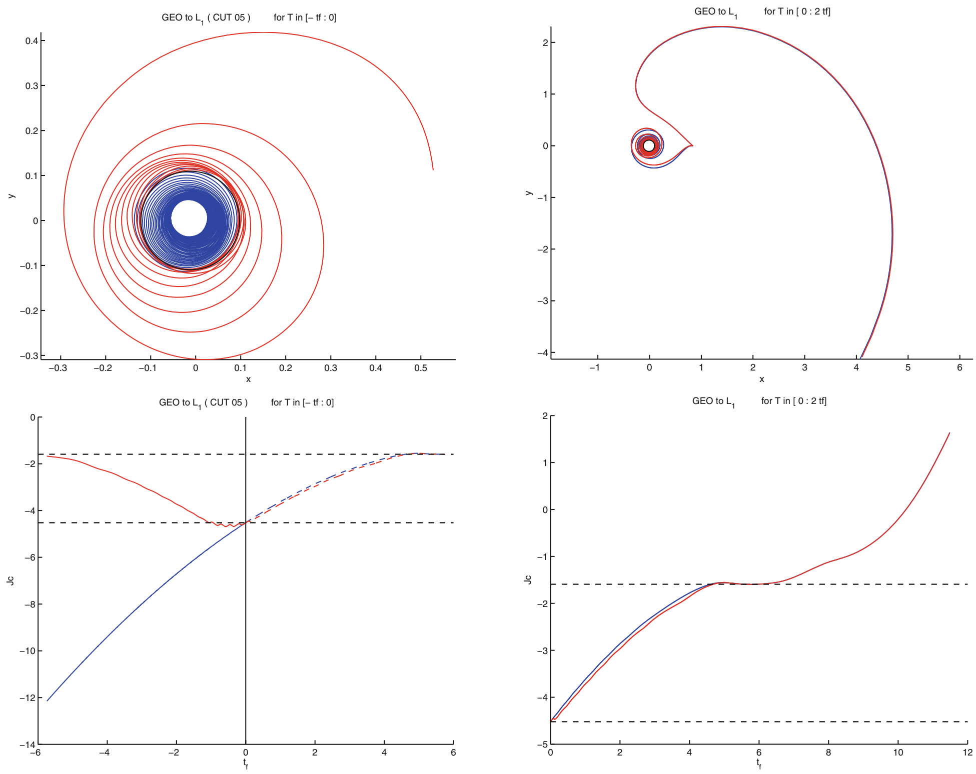

Fig. 26 For cut point n^o 5: *Left* optimal solutions for $t \in [-t_f, 0]$ (XY projection and J_c variation), *Right* optimal solutions for $t \in [0, 2t_f]$ (XY projection and J_c variation)

Cut point number 5 corresponds to $\varepsilon^* \approx 1.4309308$N and $t_f^* \approx 5.7431841$. On the left hand-side of Fig. 24, we have highlighted in green the cut region. On the right-hand side we also have 4 subplots with a zoom of this cut region and the variation of N_{ET} and N_{ZH} for the different points on the curve. As we can see the main difference between the cut points is the N_{ZH} that is 0 for the first cut point and 1 for the second cut point. In Fig. 25 we compare the transfer orbits of the two cut points (x_0, p_0) (blue curve) and (x_1, p_1) (red curve). Where we show the $\{x, y\}$ and $\{\dot{x}, \dot{y}\}$ projections of the trajectory and $J_c(t)$. We also show the evolution of the control along the trajectory and (H_1, H_2). As it happened for the first cut point, the main difference between both trajectories is on the control at the beginning of the transfer trajectory, where the red curve experiences a drastic change on the direction of $\mathbf{u}(t)$ opposed to a smooth behaviour of $\mathbf{u}(t)$ for the red curve. This can be seen as a close approach of (H_1, H_2) to zero. Finally in Fig. 23 we show the integration backwards and forward in time for the two cut points, and the corresponding variation of $J_c(t)$. As it happened for cut point number 1, there is no qualitative difference for the evolution forward in time. While for the integration backward in time we have the same behaviour as bellow, the first cut point (blue curve) spirals inwards towards the Earth, while the second cut point (red curve) spirals outwards.

As previously indicated, the results for the other cut points are summarized in Appendix “Summary of the cut points on the GEO to L_1 transfer”. As we can see there is a pattern that repeats for all the cut points that might be useful to detect this phenomena. The main difference between the two solutions appears on the control law at the beginning on the transfer trajectory: where the red curve (corresponding to the second cut point) always experiences a drastic change on its orientation, which is related to (H_1, H_2) passing close to zero, and the blue curve (corresponding to the first cut point) has a smooth behaviour along the first phase of the transfer trajectory. The other difference between both solutions appears when we integrate them backwards in time $t \in [-t_f : 0]$, where one solution spirals towards the Earth and the other outwards.

3 Transfer from a GEO to MO

In this section we will focus on the transfer from a GEO to a Moon orbit (MO). Throughout the section we will do a similar analysis to the one done in Sect. 2 for the GEO to L_1 transfer. We will also use indirect shooting methods based on Pontryagin maximum principle and the package `hampath` to find different local minima. First we will focus on the two point boundary value problem where the initial condition on the GEO orbit is fixed and perform homotopies with respect to (a) the position on the GEO orbit and (b) the thrust magnitude ε. Second, we will focus on the boundary value problem where the initial condition on the GEO orbit is free. For all these explorations the position on the arrival Moon orbit is free.

3.1 Fixed Initial Point on a GEO

Here we summarize the results for a minimum-time transfer from a GEO to a MO, where the position on the GEO orbit is fixed, hence the Boundary Conditions are:

$$x(t_0) - x_0 = 0, \quad x(t_f) \in \mathscr{M}_1, \quad p(t_f) \perp T_{x(t_f)}\mathscr{M}_1, \quad h(t_f) = 0, \tag{7}$$

where as before, $x(t)$ is the position and velocity of the spacecraft at time t; $p(t)$ is the adjoint vector at time t; x_0 is a fixed initial condition on a GEO orbit; $\mathscr{M}_1$ represents the desired Moon orbit; and $h(t_f)$ is the Hamiltonian of the PMP evaluated at the final point. The two point boundary conditions for the arrival point, $x(t_f)$ and $p(t_f)$, can be written as

$$\begin{aligned}
(x_f + \mu - 1)^2 + y_f^2 - r_1^2 &= 0,\\
\dot{x}_f^2 + \dot{y}_f^2 - v_1^2 &= 0,\\
(x_f + \mu - 1)\dot{x}_f + y_f\dot{y}_f &= 0,\\
(x_f + \mu - 1)p_{yf} - y_f p_{xf} + \dot{x}_f p_{\dot{y}f} - \dot{y}_f p_{\dot{x}f} &= 0,
\end{aligned} \tag{8}$$

where r_1 is the radius of the arrival Moon orbit and $v_1 = \sqrt{\mu/r_1}$ the corresponding velocity for the circular orbit, $x(t_f) = (x_f, y_f, \dot{x}_f, \dot{y}_f)$ are the coordinates of the spacecraft and $p(t_f) = (p_{xf}, p_{yf}, p_{\dot{x}f}, p_{\dot{y}f})$ is the adjoint vector, both evaluated at t_f, As in Sect. 2.1, we parameterize the position of the spacecraft on the initial GEO orbit using its radius r_0 and the angle $\theta_0 \in [-\pi, \pi]$. Hence, $x_0 = (r_0 \cos\theta_0 - \mu, r_0 \sin\theta_0, -v_0 \sin\theta_0, v_0 \cos\theta_0)$, with $v_0 = \sqrt{(1-\mu)/r_0}$. We will also use: $r_0 = 0.109689855932071$ and the corresponding $v_0 = 3.000969693845573$ for a GEO orbit. For the arrival Moon orbit, we consider $r_1 = 0.034$ and $v_1 = \sqrt{\mu/r_1} = 0.59786$. First of all we need a good initial condition to start exploring type of solutions. We have considered one of the local minima for the GEO to L_1 transfer found in Sect. 2.1: $\{t_f, (x_0, p_0)\}$, and use it as initial guess for the GEO to MO problem. For the initial condition to converge we use a slightly larger transfer time as initial guess, i.e. $\hat{t}_f = t_f + h$. We have considered for $\varepsilon = 10$N:

$$\begin{cases} t_f = 1.483385683993085, \\ x_0 = (r_0 - \mu,\ 0.0,\ 0.0,\ -v_0), \\ p_0 = (3.8349336494018,\ 1.7266950508752,\ 0.0764256922941,\ 0.1329597699146), \end{cases}$$

which corresponds to the transfer orbit shown on Fig. 27. Using this as initial guess and taking as transfer time $\hat{t}_f = t_f + h$ for $h = 5 \cdot 10^{-3}$, $5 \cdot 10^{-2}$ and 10^{-1} we have found three different classes of minimum time transfer solutions from GEO to MO.

1. For $h = 5 \cdot 10^{-3}$, transfer orbit on Fig. 28 left (blue curve):

$$\begin{aligned} \hat{t}_f &= 1.562091470465241, \\ \hat{x}_0 &= (-0.1218428559320,\ 0.0000000000000,\ 0.0000000000000,\ -3.0009696938455), \\ \hat{p}_0 &= (3.9285981330000,\ 1.6544784563269,\ 0.0734194613434,\ \ 0.1400883421876), \end{aligned}$$

2. For $h = 5 \cdot 10^{-2}$, transfer orbit on Fig. 28 center (red curve):

$$\begin{aligned} \hat{t}_f &= 1.529347472081999, \\ \hat{x}_0 &= (-0.1218428559320,\ 0.0000000000000,\ 0.0000000000000,\ -3.0009696938455), \\ \hat{p}_0 &= (3.9217580218250,\ 1.6961685952114,\ 0.0750545446749,\ \ 0.1396207935397), \end{aligned}$$

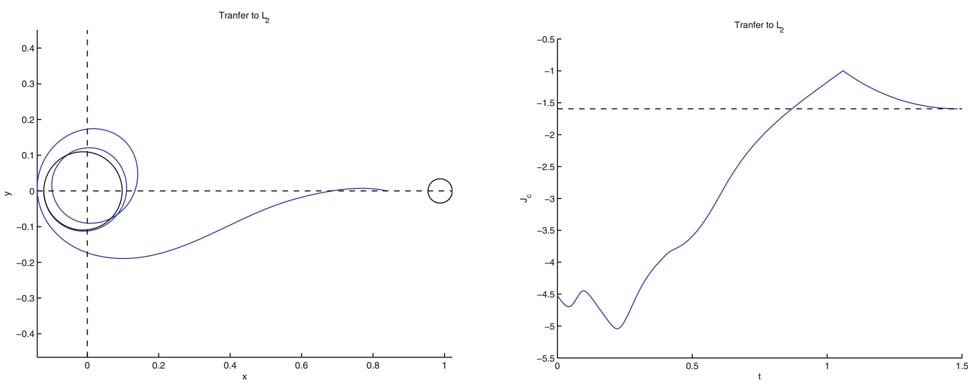

Fig. 27 Transfer orbit from GEO to L_1 that we use as initial condition for the GEO to MO transfer problem ($\varepsilon = 10$N). *Left* $\{XY\}$ projection of the trajectory, *Right* J_c variation

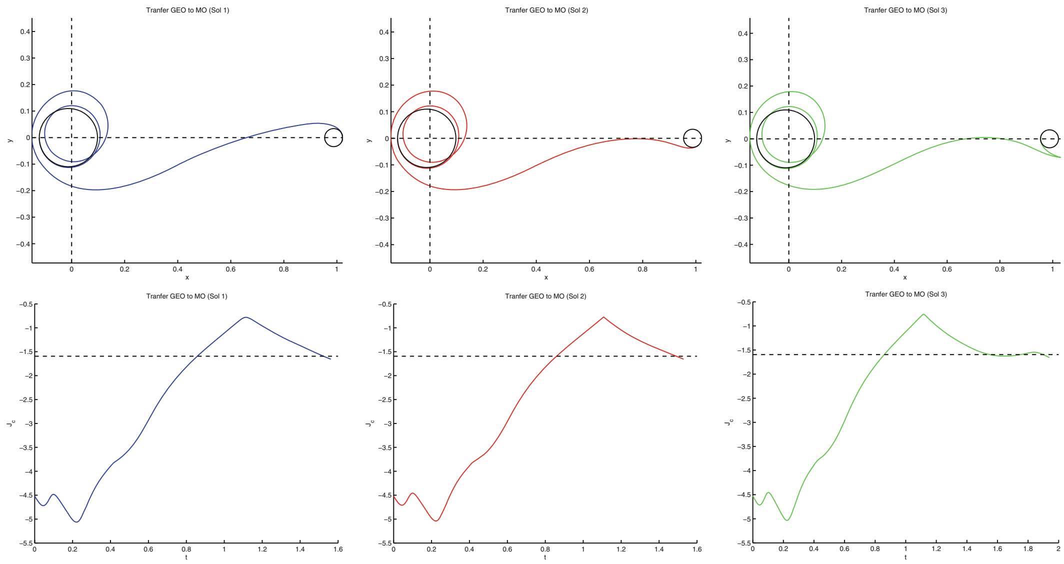

Fig. 28 Transfer orbits form GEO to MO. Three different solutions found from the initial orbit from Fig. 27. *Top*: $\{XY\}$ projection of the trajectory, *Bottom* J_c variation

3. For $h = 10^{-1}$, transfer orbit on Fig. 28 right (green curve):

$$\begin{aligned}
\hat{t}_f &= 1.939506458073425, \\
\hat{x}_0 &= (-0.1218428559320,\ 0.0000000000000,\ 0.0000000000000, -3.0009696938455), \\
\hat{p}_0 &= (3.9733475979444,\ 1.7003282465180,\ 0.0751188225176,\ \ 0.1431121866550),
\end{aligned}$$

Note that for all transfer orbits in Fig. 28 the first phase of the transfer trajectory (orbiting around the Earth) is the same. The difference is seen on the second part, where we find two orbits that arrives to the Moon following a clockwise sense around the Moon (blue and green orbits) and another orbit following an anticlockwise sense (red orbit). Although we find two orbits that arrive to the Moon in a clockwise sense, there is a big difference in the transfer time, the green orbit taking much more time than the blue one. Moreover, the green orbit starts by approaching the Moon with an anticlockwise orbit, then a cusp occurs (the velocity in the moving frame vanishes) and the end of the trajectory winds again clockwise around the target. Finally, if we look at the control law that produces these three transfer orbits (Fig. 29) we see how these one is very similar to the first part of the transfer while a big difference appears when we approach the L_1 neighborhood. There we see how, different ways to decelerate the growth in energy produce different outputs (i.e. transfer orbits). To fix notation, from now on we will call: $\mathscr{C}_1$ the transfer trajectories that arrive to the MO in a clockwise sense, (identified throughout this section by the color blue); $\mathscr{C}_2$ the transfer trajectories that arrive to MO anti-clockwise (identified by the color red); finally $\mathscr{C}_3$ transfer orbits similar to orbit 3 (green), possibly with one cusp before capture by the Moon.

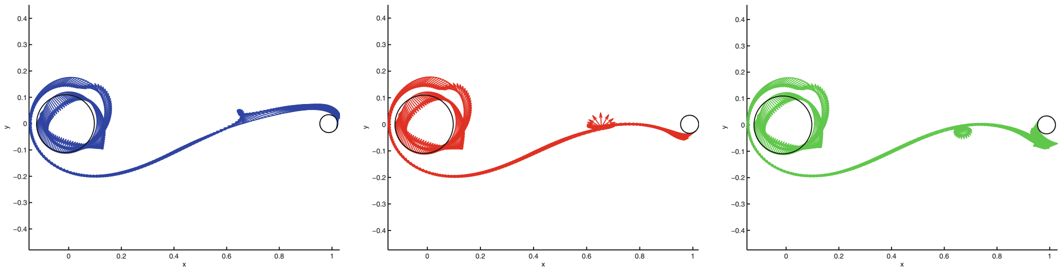

Fig. 29 Control Law for the transfer orbits form GEO to MO. Three different solutions found from the initial orbit from Fig. 27

3.1.1 Homotopy w.r.t. θ_0

Here we have taken the three local minimum time transfer trajectories that appear in Fig. 28 (type $\mathscr{C}_1$, $\mathscr{C}_2$ and $\mathscr{C}_3$), and as in Sect. 2, we have done an homotopy with respect to the initial position on the GEO orbit, θ_0. All three initial orbits are for $\varepsilon = 10$N and $\theta_0 = \pi$, we recall that the initial position on the GEO orbit is given by:

$$x_0 = (r_0 \cos\theta_0 - \mu, r_0 \sin\theta_0, -v_0 \cos\theta_0, v_0 \sin\theta_0).$$

To do this homotopy we proceed as we did in Sect. 2 and compute (if possible) the homotopic path for $\theta = \pi \mapsto 21\pi$ and $\theta = \pi \mapsto -21\pi$, taking small intervals of size 2π to increase the precision. In Figs. 30, 31 and 32 we see the projection of these curves in the θ_0 versus t_f space. The points in black on the 3 curves are the local minima of these curves, and will be candidates for local minimum time transfer trajectories when the initial condition on the GEO orbit is not fixed (Sect. 3.2). The initial conditions for these local minima are summarized in Tables 27, 28 and 29.

As we can see, the behavior of these three curves has similarities to the results for the GEO to L_1 transfer for $\varepsilon = 10$. Notice how as θ_0 increases so does the transfer time, t_f, and as θ_0 decreases t_f decreases up to a certain value θ_0^*, there t_f will start to increase drastically for small variations of θ_0 up to some point where the

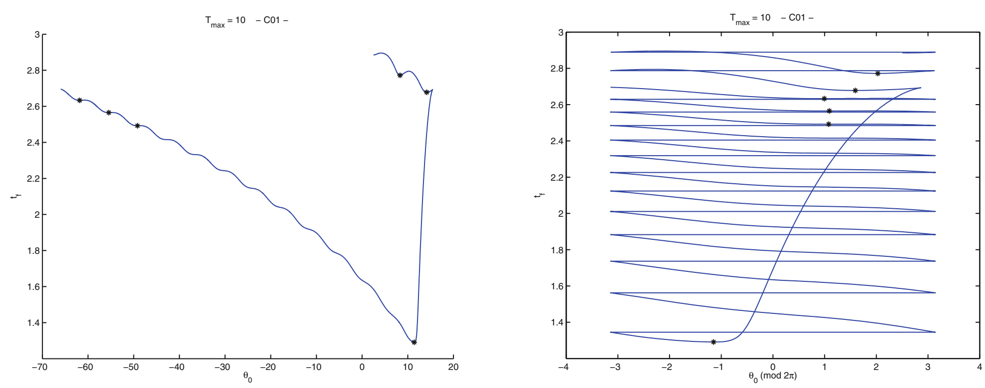

Fig. 30 For $\varepsilon = 10$N: projection of the homotopic path θ_0 versus t_f (*left*) $\theta_0 (\text{mod } 2\pi)$ versus t_f (*right*) for GEO to MO transfer trajectories of type $\mathscr{C}_1$

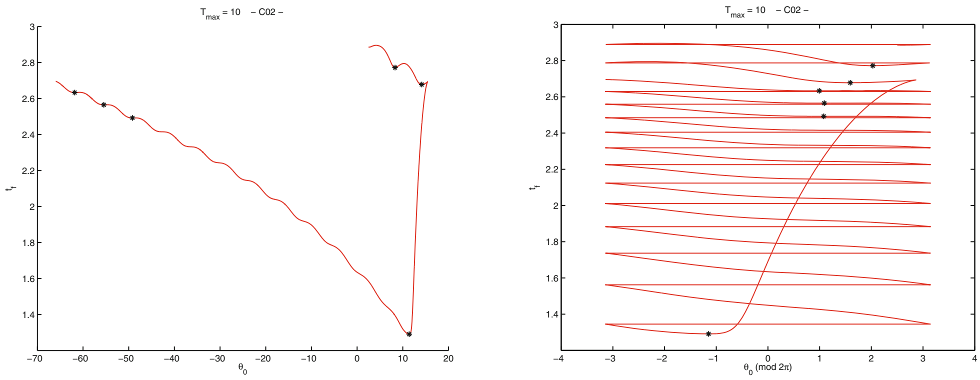

Fig. 31 For $\varepsilon = 10$N: projection of the homotopic path θ_0 versus t_f (*left*) $\theta_0(\text{mod } 2\pi)$ versus t_f (*right*) for GEO to MO transfer trajectories of type $\mathscr{C}_2$

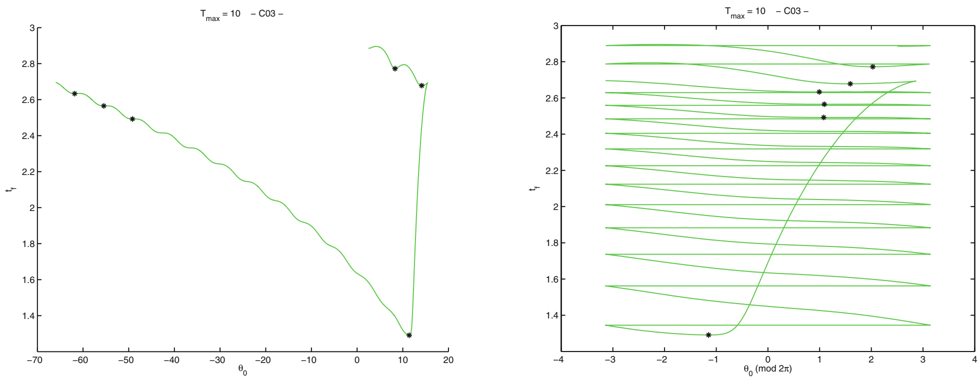

Fig. 32 For $\varepsilon = 10$: projection of the homotopic path θ_0 versus t_f (*left*) $\theta_0(\text{mod } 2\pi)$ versus t_f (*right*) for GEO to MO transfer trajectories of type $\mathscr{C}_3$

homotopic curve has a turning point. The only difference between the three curves is that for a given θ_0^* the minimum transfer time is different for the three kind of trajectories. In Fig. 39 we can see the three homotopic paths on the same figure, and we can appreciate how in terms of transfer time $\mathscr{C}_1$ is always below $\mathscr{C}_2$, which is always below $\mathscr{C}_3$. For each of the three homotopic curves, in Tables 15, 16, 17, 18, 19, 20, 21, 22 and 23 we have the initial conditions $\{t_f, x_0, p_0\}$ for the local minima for $\theta_0 = \pi, 0, \pi/2$ and $3\pi/2$. In Figs. 33, 35 and 37 we have the transfer trajectories from the three homotopic curves for different initial conditions for $\theta_0(\text{ mod } 2\pi) = 0$. As we can see, for each class, the trajectories along the homotopic path remain of the same class, i.e. the insertion sense on the MO remains always the same for all the orbits on the curve. Moreover, as we can see for each class we also find two type of trajectories, that we can call $\mathscr{T}_1$ and $\mathscr{T}_2$. Type $\mathscr{T}_1$ are trajectories that in the first phase spiral around the Earth to gain J_c and then go directly towards the Moon, passing close to L_1. Type $\mathscr{T}_2$ are trajectories that do some turns around the Earth and then do a large excursion before heading towards the Moon. In Figs. 34, 36 and 38 we show the variation of J_c along time for the trajectories that we find in Figs. 33, 35 and 37 respectively. As we can see, for type $\mathscr{T}_1$ trajectories $J_c(t)$ decreases and

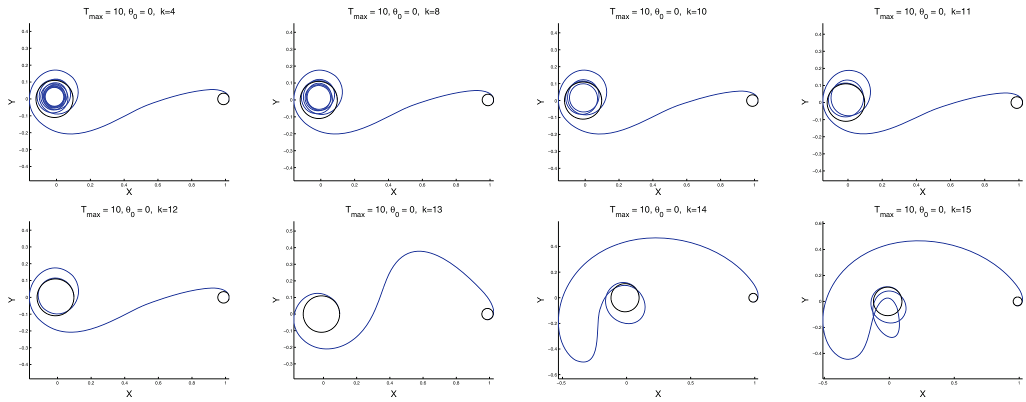

Fig. 33 For class $\mathscr{C}_1$: Transfer trajectories for $\varepsilon = 10$N and $\theta_0 = 0$ fixed. The initial condition on the GEO orbit is $x_0 = (-r_0 - \mu, 0, 0, v_0)$

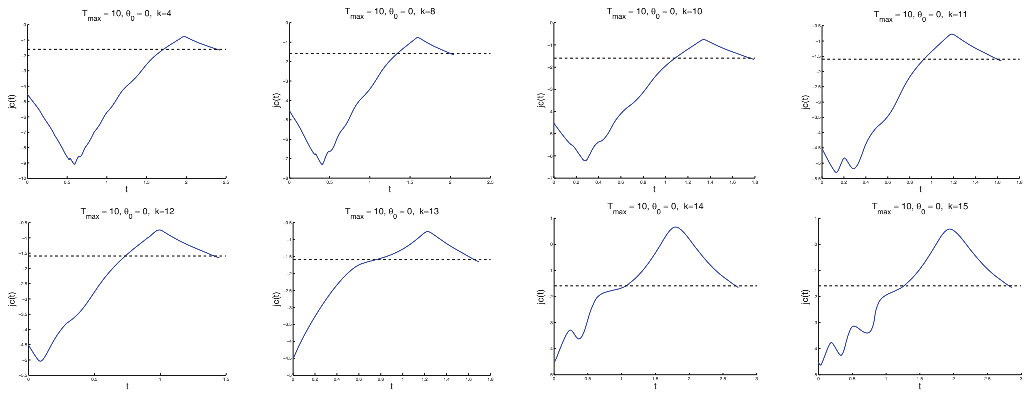

Fig. 34 For class $\mathscr{C}_1$: Variation of J_c for $\varepsilon = 10$N and $\theta_0 = 0$ fixed. The initial condition on the GEO orbit is $x_0 = (-r_0 - \mu, 0, 0, v_0)$

gains energy while they spiral around the Earth and when $J_c(t)$ is slightly larger than $J_c(L_1)$ this one starts to decreases to meet J_c of the MO. On the other hand, for the type $\mathscr{T}_2$ trajectories, $J_c(t)$ will reach much larger values than $J_c(L_1)$ before decreasing to get to the MO. We recall that the main difference between the behavior of the three classes of transfer trajectories $\mathscr{C}_1$ (blue), $\mathscr{C}_2$ (red) and $\mathscr{C}_3$ (green) is the transfer time. As we can see in Fig. 39 for a fixed θ_0, the transfer time for class $\mathscr{C}_2$ orbits is always less than for class $\mathscr{C}_1$ and class $\mathscr{C}_3$. But there are three cases where these curves intersect each other. Hence, we have trajectories of a different class with the same transfer time (i.e. cost function). It might be interesting to study in more detail these intersections as we have two different classes of strategies with the same cost. In Fig. 40 we have the transfer trajectories and the energy variations of the trajectories corresponding to the 3 intersections that we see in Fig. 39, from left to right $\mathscr{C}_1 \cap \mathscr{C}_2$, $\mathscr{C}_1 \cap \mathscr{C}_3$ and $\mathscr{C}_2 \cap \mathscr{C}_3$. As before the color of the orbit is related to its class ($\mathscr{C}_1$ are in blue, $\mathscr{C}_2$ are in red and $\mathscr{C}_3$ are in green).

Finally, we have done a small exploration on different characteristics for the minimum time−transfer trajectories that appear in Figs. 30, 31 and 32, where for each orbit we have computed the maximal value for J_c along the orbit, the norm of

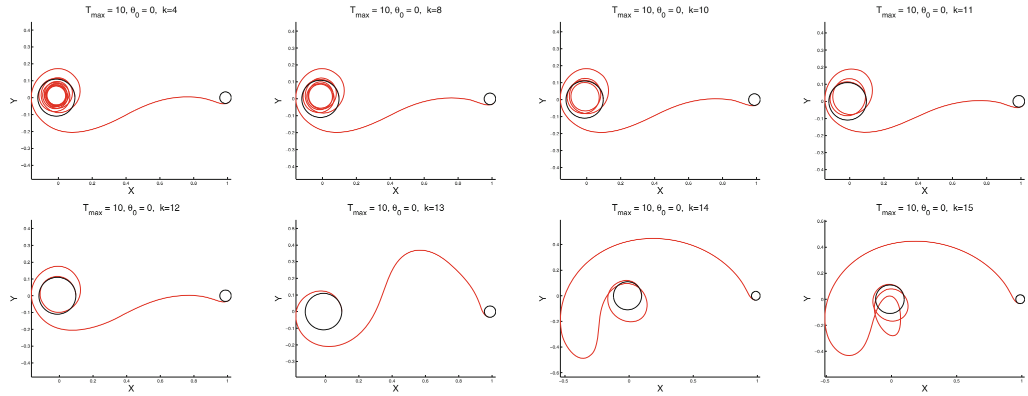

Fig. 35 For class $\mathscr{C}_2$: Transfer trajectories for $\varepsilon = 10$N and $\theta_0 = 0$ fixed. The initial condition on the GEO orbit is $x_0 = (-r_0 - \mu, 0, 0, v_0)$

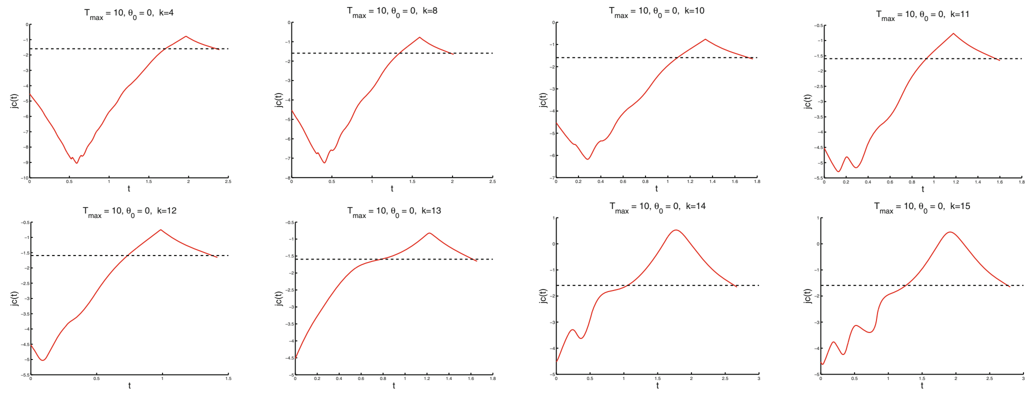

Fig. 36 For class $\mathscr{C}_2$: Variation of J_c for $\varepsilon = 10$N and $\theta_0 = 0$ fixed. The initial condition on the GEO orbit is $x_0 = (-r_0 - \mu, 0, 0, v_0)$

the adjoint vector at t_0, $|p(t_0)|$, and the number of turns the trajectory gives around the Earth before the trajectory goes towards the Moon. These results are summarized in Figs. 41, 42 and 43 for class $\mathscr{C}_1$, $\mathscr{C}_2$ and $\mathscr{C}_3$ respectively, where we can see a similar behavior as the GEO to L_1 transfer.

3.1.2 Homotopy w.r.t. ε

Given the fact that the transfer time for class $\mathscr{C}_3$ (green) is larger than the transfer time for the other two classes of orbits, from now on we will focus only on the classes $\mathscr{C}_1$ and $\mathscr{C}_2$. We recall that we can distinguish these two classes by the sense of insertion on a Moon orbit (blue = clockwise, red = anticlockwise). In this section we have taken the different solutions for $\varepsilon = 10$N and a fixed initial condition: θ_0 mod $(2\pi) = 0$ and π. The initial conditions are summarized in Tables 15 and 16 for class $\mathscr{C}_1$ and Tables 19 and 20 for class $\mathscr{C}_2$. For each of the initial conditions we have performed a homotopy with respect to ε from 10N to 1N. In Fig. 44 and 45 we summarize the results for class $\mathscr{C}_1$ and class $\mathscr{C}_2$ respectively. As we can see, at a first sight, in both cases the behavior is similar to the one found for GEO to L_1 transfer

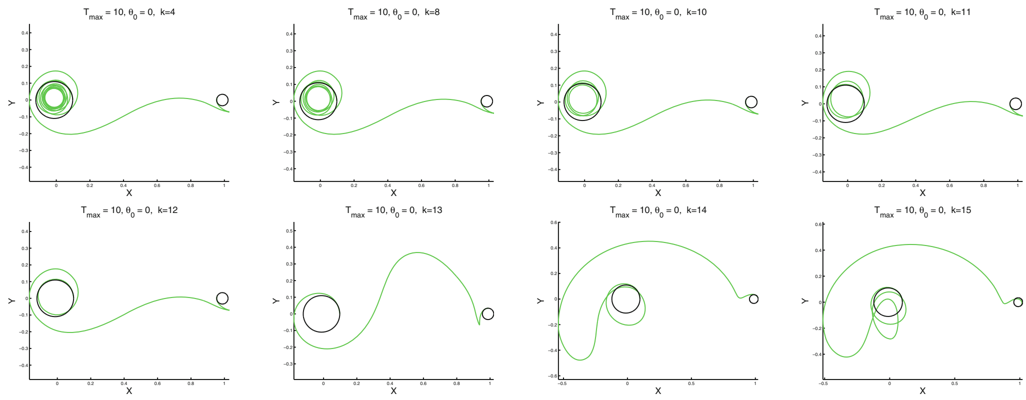

Fig. 37 For class $\mathscr{C}_3$: Transfer trajectories for $\varepsilon = 10$N and $\theta_0 = 0$ fixed. The initial condition on the GEO orbit is $x_0 = (-r_0 - \mu, 0, 0, v_0)$

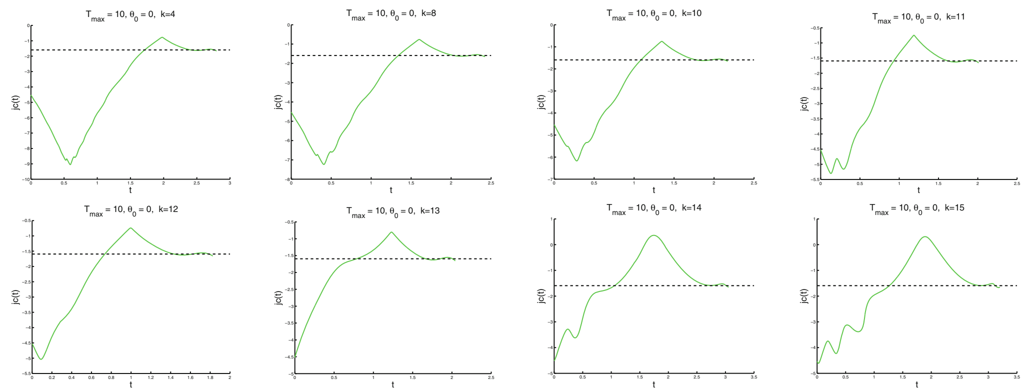

Fig. 38 For class $\mathscr{C}_3$: Variation of J_c for $\varepsilon = 10$N and $\theta_0 = 0$ fixed. The initial condition on the GEO orbit is $x_0 = (-r_0 - \mu, 0, 0, v_0)$

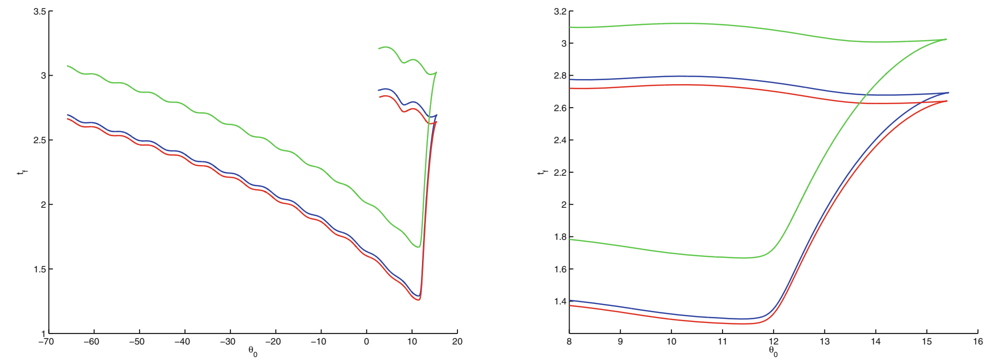

Fig. 39 For $\varepsilon = 10$N: homotopic path θ_0 versus t_f for $\mathscr{C}_1$ (*blue*), $\mathscr{C}_2$ (*red*) and $\mathscr{C}_3$ (*green*)

trajectories (Sect. 2). So in both cases, as ε decreases the transfer time, t_f, increases. In some cases, at some point the slope of $\varepsilon(t_f)$ experiences a drastic change and t_f increases very quickly for small variations of ε. Then at some point the homotopic curve has a turning point and ε grows, not being able to find solutions for lower values of ε. Nevertheless, there are other curves where ε decreases with no problem reaching $\varepsilon = 1$N.

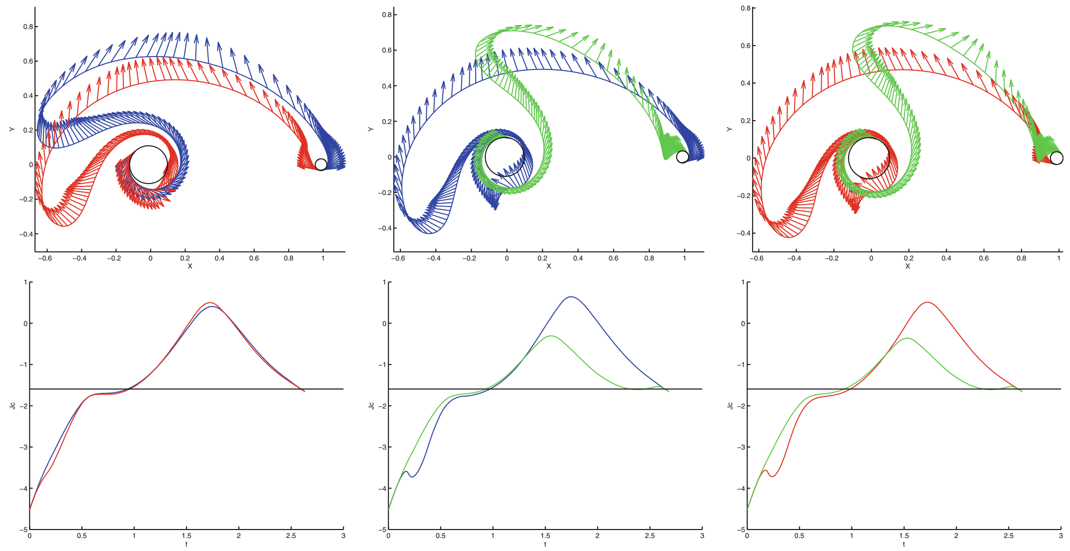

Fig. 40 Transfer trajectories of the intersections between the homotopic path in Fig. 39. *Top plots* transfer trajectories and the associated control law; *Bottom plots* variation of J_c w.r.t. time. From *left* to *right* $\mathscr{C}_1 \cap \mathscr{C}_2$, $\mathscr{C}_1 \cap \mathscr{C}_3$ and $\mathscr{C}_2 \cap \mathscr{C}_3$. The color of the curves is associated to the class, *blue* for class $\mathscr{C}_1$, *red* for class $\mathscr{C}_2$ and *green* for class $\mathscr{C}_3$

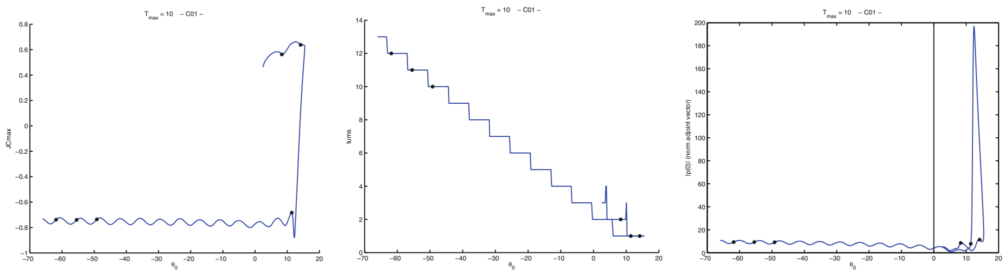

Fig. 41 For class $\mathscr{C}_1$ and $\varepsilon = 10\text{N}$ from *left* to *right* θ_0 versus $\max_{t\in[t_0:t_f]}(J_c(t))$, θ_0 versus N_{ET} and θ_0 versus $|p(t_0)|$

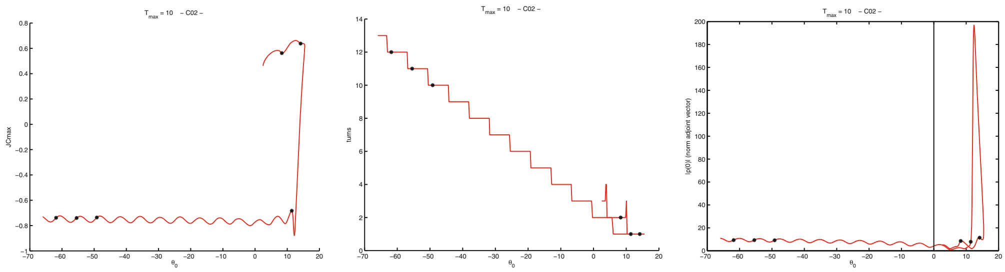

Fig. 42 For class $\mathscr{C}_2$ and $\varepsilon = 10\text{N}$ from *left* to *right* θ_0 versus $\max_{t\in[t_0:t_f]}(J_c(t))$, θ_0 versus N_{ET} and θ_0 versus $|p(t_0)|$

The main difference between the two class of orbits, appears in the region where $\varepsilon \in [1 : 2]$. While for class $\mathscr{C}_1$ the behavior is as we have mentioned, for class $\mathscr{C}_2$ the homotopic path experiences turning points and self-intersections, finding for some of these curves cut points for a fixed θ_0. In Fig. 46 we have zoomed these area for both class of orbits and $\theta_0 = 0$, but the same phenomena is observed for $\theta_0 = \pi$. In Figs. 47

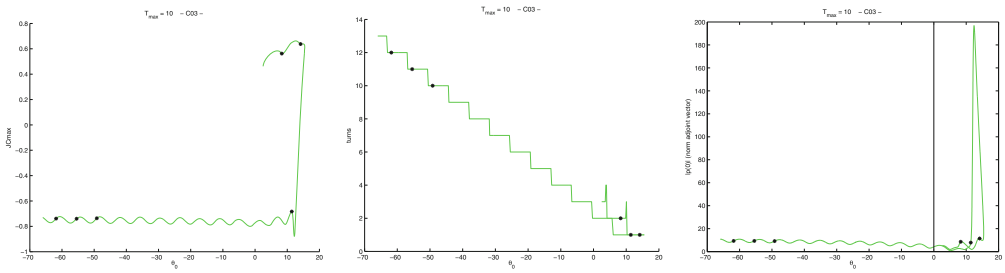

Fig. 43 For class $\mathscr{C}_3$ and $\varepsilon = 10$N from *left* to *right* θ_0 versus $\max_{t\in[t_0:t_f]}(J_c(t))$, θ_0 versus N_{ET} and θ_0 versus $|p(t_0)|$

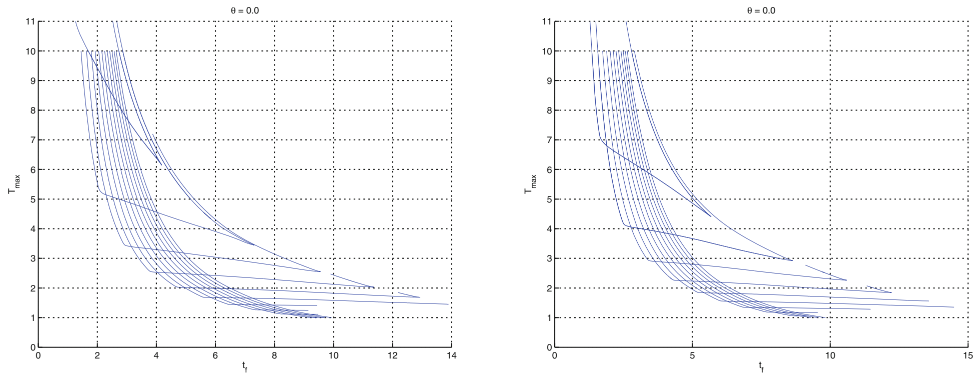

Fig. 44 For class $\mathscr{C}_1$: Homotopy with respect to ε for θ_0 fixed, $\theta_0 = 0$ (*left*), $\theta_0 = \pi$ (*right*)

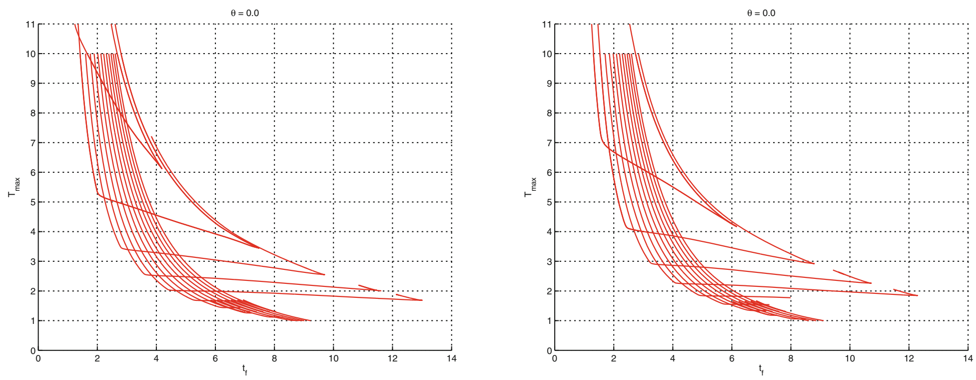

Fig. 45 For class $\mathscr{C}_2$: Homotopy with respect to ε for θ_0 fixed, $\theta_0 = 0$ (*left*), $\theta_0 = \pi$ (*right*)

and 49 we show the type of solutions that we find along one of the homotopic curves of Figs. 44 and 45 respectively, for $\theta_0 = 0$ fixed, and varying ε. The plots correspond to the homotopy path starting by: $\theta_0 = 0$ and $k = 12$ from Table 16 for the class $\mathscr{C}_1$, and $\theta_0 = 0$ and $k = 12$ from Table 20 for the class $\mathscr{C}_2$. Both cases correspond to homotopic paths where $\varepsilon(t_f)$ experiences two drastic changes. As we can see the trajectories remain within their class along the homotopic path. We also notice that on the first part of the path, the trajectories are of type $\mathscr{T}_1$. While when the slope of the homotopic curve changes, the trajectories start to do big excursions before going towards the Moon, i.e. type $\mathscr{T}_2$ trajectories appear. In Figs. 48 and 50, we show the variation of J_c along time for the trajectories plotted in Figs. 47 and 49 respectively (Tables 24, 25 and 26).

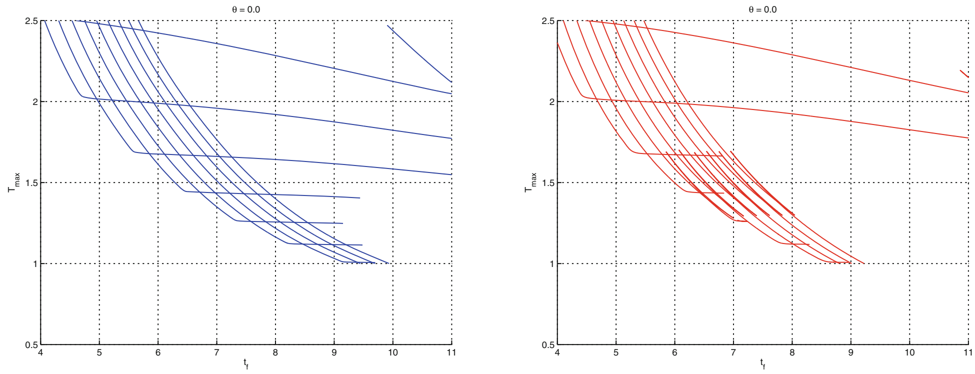

Fig. 46 For class $\mathscr{C}_1$ (*left*) and $\mathscr{C}_2$ (*right*): homotopy with respect to ε for $\theta_0 = 0$ fixed. Zoom for $\varepsilon \in [1:2]$

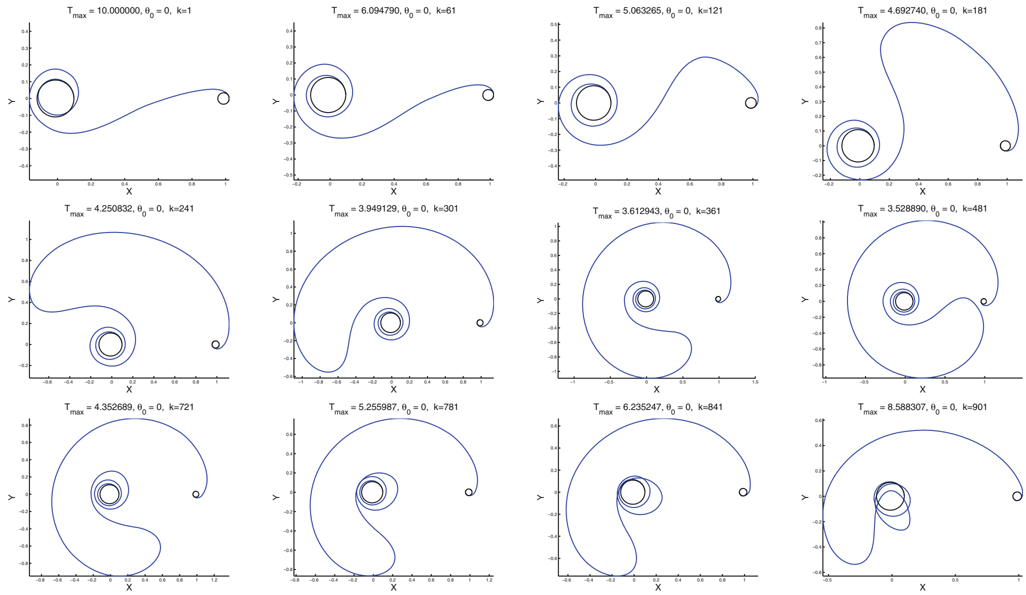

Fig. 47 For class $\mathscr{C}_1$: Transfer trajectories from GEO to MO for θ_0 fixed and varying ε. Here $\theta_0 = 0$ and all the orbits belong to the homotopic curve generated by $k = 12$ from Table 16 when we use ε as the homotopy parameter

3.2 Free Initial Point on a GEO

In this section we summarize the results for a minimum-time transfer from a GEO to a MO, where the position on the GEO orbit is left free. Hence, the Boundary Conditions are:

$$x(t_0) \in \mathscr{M}_0, \quad p(t_0) \perp T_{x(t_0)}\mathscr{M}_0, \quad x(t_f) \in \mathscr{M}_1, \quad p(t_f) \perp T_{x(t_f)}\mathscr{M}_1, \quad h(t_f) = 0, \tag{9}$$

where $\mathscr{M}_0$ represents the GEO orbit, and $\mathscr{M}_1$ the MO. The first two Boundary Conditions are written as,

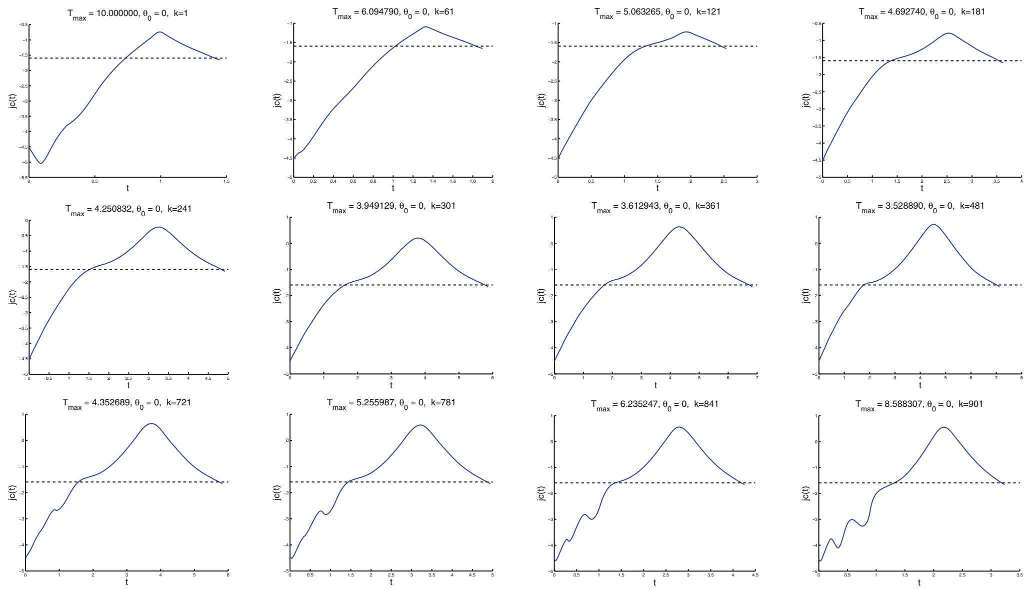

Fig. 48 For class $\mathscr{C}_1$: Variation of the Jacobi constant along time for a transfer trajectories from GEO to MO for θ_0 fixed and varying ε. Here $\theta_0 = 0$ and all the orbits belong to the homotopic curve generated by $k = 12$ from Table 16 when we use ε as the homotopy parameter

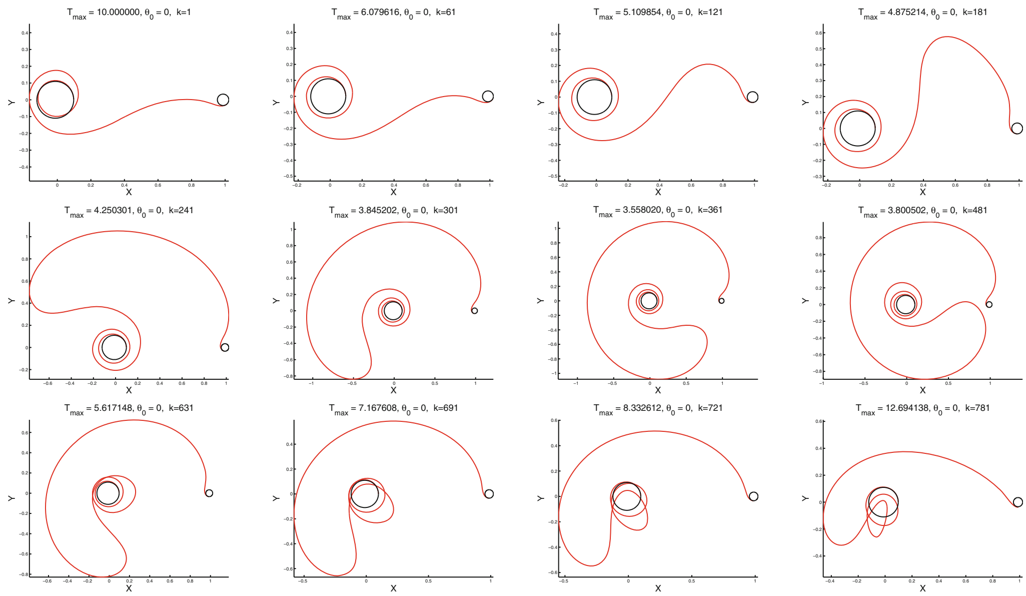

Fig. 49 For class $\mathscr{C}_2$: Transfer trajectories from GEO to MO for θ_0 fixed and varying ε. Here $\theta_0 = 0$ and all the orbits belong to the homotopic curve generated by $k = 12$ from Table 20 when we use ε as the homotopy parameter

$$\begin{aligned}(x_0+\mu)^2 + y_0^2 - r_0^2 &= 0,\\ \dot{x}_0^2 + \dot{y}_0^2 - v_0^2 &= 0,\\ (x_0+\mu)\dot{x}_0 + y_0\dot{y}_0 &= 0,\\ (x_0+\mu)p_{y0} - y_0 p_{x0} + \dot{x}_0 p_{\dot{y}0} - \dot{y}_0 p_{\dot{x}0} &= 0,\end{aligned} \tag{10}$$

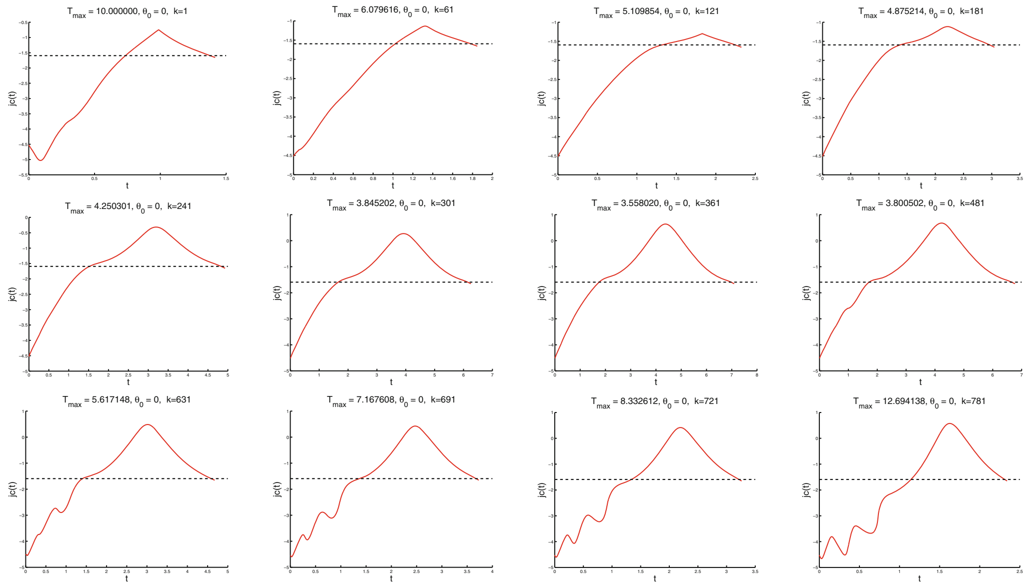

Fig. 50 For class $\mathscr{C}_2$: Variation of the Jacobi constant along time for a transfer trajectories from GEO to MO for θ_0 fixed and varying ε. Here $\theta_0 = 0$ and all the orbits belong to the homotopic curve generated by $k = 12$ from Table 20 when we use ε as the homotopy parameter

where $x(t_0) = (x_0, y_0, \dot{x}_0, \dot{y}_0)$ are the coordinates of the spacecraft and $p(t_0) = (p_{x0}, p_{y0}, p_{\dot{x}0}, p_{\dot{y}0})$ is the adjoint vector, both evaluated at $t = t_0$. While the second two:

$$\begin{aligned} (x_f + \mu - 1)^2 + y_f^2 - r_1^2 &= 0, \\ \dot{x}_f^2 + \dot{y}_f^2 - v_1^2 &= 0, \\ (x_f + \mu - 1)\dot{x}_f + y_f \dot{y}_f &= 0, \\ (x_f + \mu - 1) p_{yf} - y_f p_{xf} + \dot{x}_f p_{\dot{y}_f} - \dot{y}_f p_{\dot{x}_f} &= 0, \end{aligned} \tag{11}$$

where $x(t_f) = (x_f, y_f, \dot{x}_f, \dot{y}_f)$ are the coordinates of the spacecraft and $p(t_f) = (p_{xf}, p_{yf}, p_{\dot{x}f}, p_{\dot{y}f})$ is the adjoint vector, both evaluated at $t = t_f$. Moreover, r_0 is the radius of the GEO orbit, r_1 is the radius of the arrival Moon orbit and $v_0 = \sqrt{(1-\mu)/r_0}$, $v_1 = \sqrt{\mu/r_1}$ the corresponding velocities on the GEO and the arrival MO so that the orbits are circular at first order. We recall that all the solutions found in the previous section, for a fixed initial condition on the GEO orbit, are not necessarily solutions of this problem. Only the local minima in the homotopic paths in Figs. 30, 31 and 32 are good initial guesses to find the local minima of this new problem. The values for $x(t_0)$, $p(t_0)$ are summarized in Tables 27, 28 and 29 for classes $\mathscr{C}_1$, $\mathscr{C}_2$ and $\mathscr{C}_3$ respectively and $\varepsilon = 10$N. In this section we have taken some of the local minima of the homotopic curve for $\varepsilon = 10$N and class $\mathscr{C}_1$ and $\mathscr{C}_2$, and performed homotopies with respect to the thrust magnitude $\varepsilon \in [1 : 10]$. For both class of transfer orbits we have taken as initial condition the local minima numbers 5, 6 and 7 in Tables 27 and 28. On the left hand side of Fig. 51 we can these homotopic paths. As usual, the curve in blue represents the solution for class $\mathscr{C}_1$ transfer orbits and the curve in red the solutions for class $\mathscr{C}_2$ transfer orbits. Notice that the red curve is always

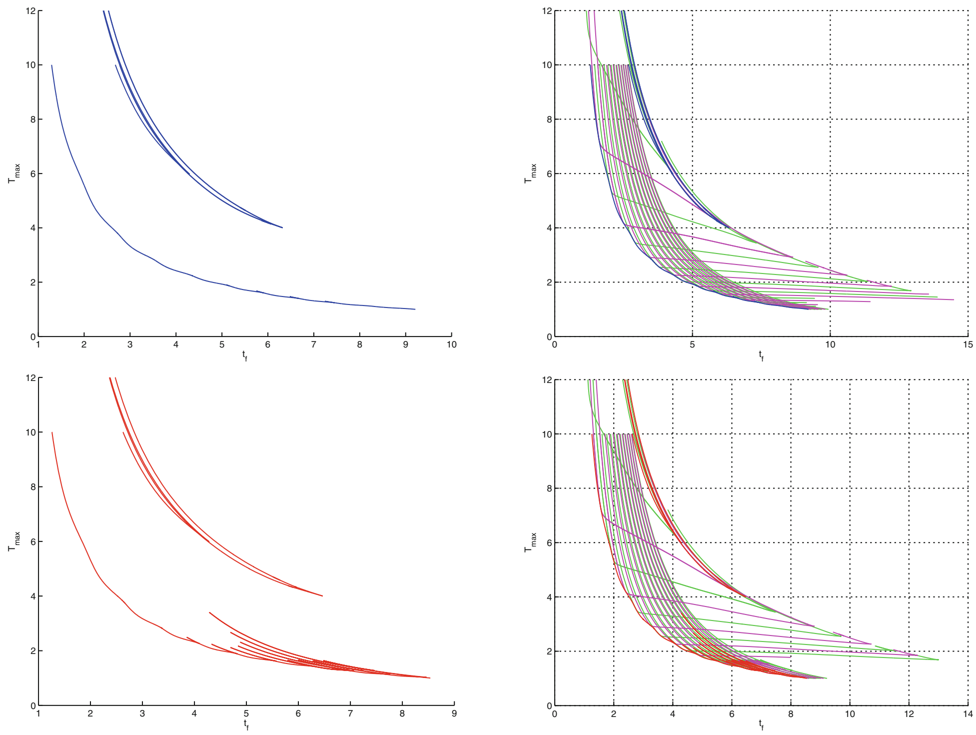

Fig. 51 Homotopy w.r.t. ε for transfers orbit from GEO to MO. *Left* Local minimum for θ_0 free. *Right* Comparison between the local minima for θ_0 free and θ_0 fixed. *Top* results for class $\mathscr{C}_1$, θ_0 free (*blue line*) and θ_0 fixed (*green* and *magenta lines*). *Bottom* results for class $\mathscr{C}_2$, θ_0 free (*red line*) and θ_0 fixed (*green* and *magenta lines*)

bellow the blue curve, hence, the class $\mathscr{C}_2$ transfer trajectories are always better than the class $\mathscr{C}_1$ ones. Also notice that the red curve presents a more complex structure for $\varepsilon \in [1:3]$N. It can be seen that, as it happened for the GEO to L_1 transfer, all the solutions generated by the local minima number 5 are $\mathscr{T}_1$ type transfer orbits, while solutions generated by local minima number 6 and 7 are type $\mathscr{T}_2$ transfer orbits. Moreover, when we let θ_0 free these two type of solutions do not connect if we compute the homotopic paths varying ε. On the right hand side of Fig. 51 we compare for both class of trajectories, $\mathscr{C}_1$ (top) and $\mathscr{C}_2$ (bottom), the solutions for θ_0 free and θ_0 fixed. As we can see, in both cases, the curve for θ_0 free is always below the curves for θ_0 fixed. In Figs. 52 and 53 we have zoomed different areas of these two curves for comparisons, class $\mathscr{C}_1$ and $\mathscr{C}_2$ respectively. In both cases, the curves for θ_0 free present self-intersections, i.e. cut point candidates. Although the structure for $\mathscr{C}_2$ is much more complex presenting different kind of self-intersections. In the next section we will study in more detail these phenomena.

3.3 Cut Points

As we can appreciate in Figs. 52 and 53, for both classes ($\mathscr{C}_1$ and $\mathscr{C}_2$) the homotopic paths for the GEO to MO transfer with θ_0 free have several turning points and the

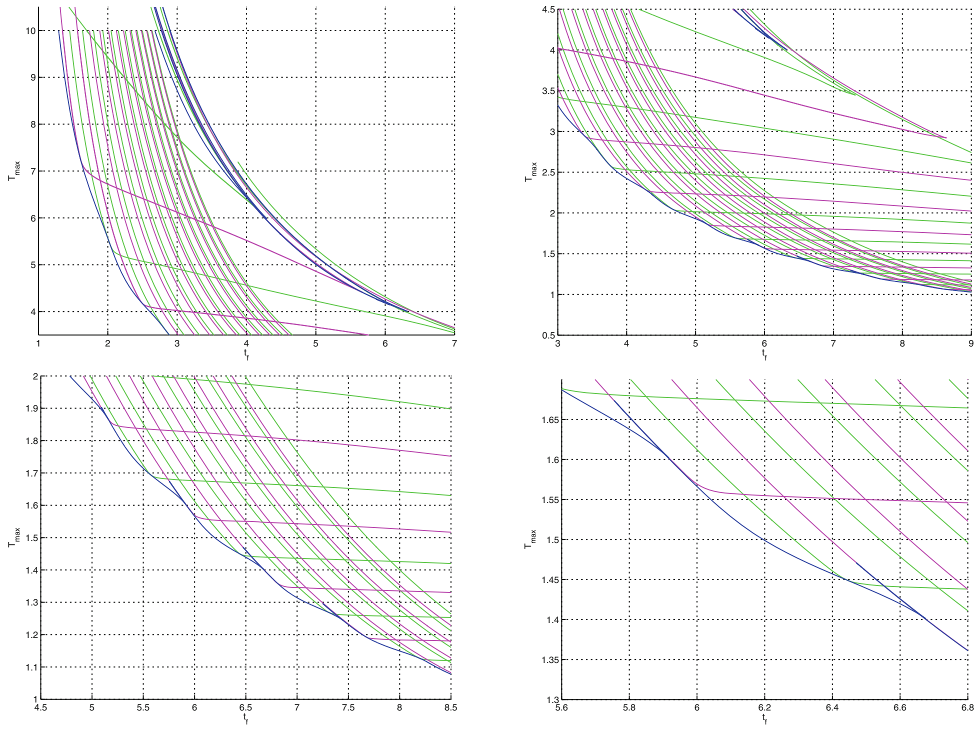

Fig. 52 For class $\mathscr{C}_1$: zoomed regions of the comparison between the local minima for θ_0 free (*blue line*) versus θ_0 fixed (*green* and *magenta lines*)

path self-intersects several times. These intersections are cut point candidates. As in Sect. 2.3, we call the couple $\{(x_0, p_0), (x_1, p_1)\}$ a cut point, if they are two different initial conditions such that for the same ε they generate two different local optimal transfer orbits from GEO to MO with the same transfer time t_f^*. We find these initial conditions on the self-intersections on the projection of homotopic path ε versus t_f, Figs. 52 and 53. To fix notation, (x_0, p_0) is the first point on the homotopic path that reaches (ε, t_f) and (x_1, p_1) is the second point on the same curve that reaches (ε, t_f). In Tables 30 and 31 we summarize all the cut points that we have found for $\varepsilon \in [1, 10]$N for class $\mathscr{C}_1$ and $\mathscr{C}_2$ respectively. All these points have been computed by refining the intersections found in Figs. 52 and 53. Finally in Figs. 54 and 55 we plot different projections of the homotopic path for the two class of orbits, and we have highlighted in green the regions close to the different cut points.

We do the same analysis as in Sect. 2.3. First we have taken both solutions (x_0, p_0) and (x_1, p_1) and compute the transfer trajectory, the variation of $J_c(t)$, the control law $\mathbf{u}(t)$ and $(H_1(t), H_2(t))$. Second we have integrated both trajectories backward and forward in time on $[-t_f, 2t_f]$, where t_f is the transfer time. We have also taken the solutions in the neighborhood of the cut point and checked the variation of different parameters. We recall, that as we did in Sect. 2.3, if ε^*, t_f^* are the thrust magnitude and the minimum transfer time for the cut point, we consider a solution to be in the cut neighborhood if $t_f \in [t_f^* - 0.15 : t_f^* + 0.15]$. In the Appendix "Summary of the cut points on the GEO to MO transfer" we have the plots summarizing this analysis for all the cut points. In this section we will only plot some of them and discuss

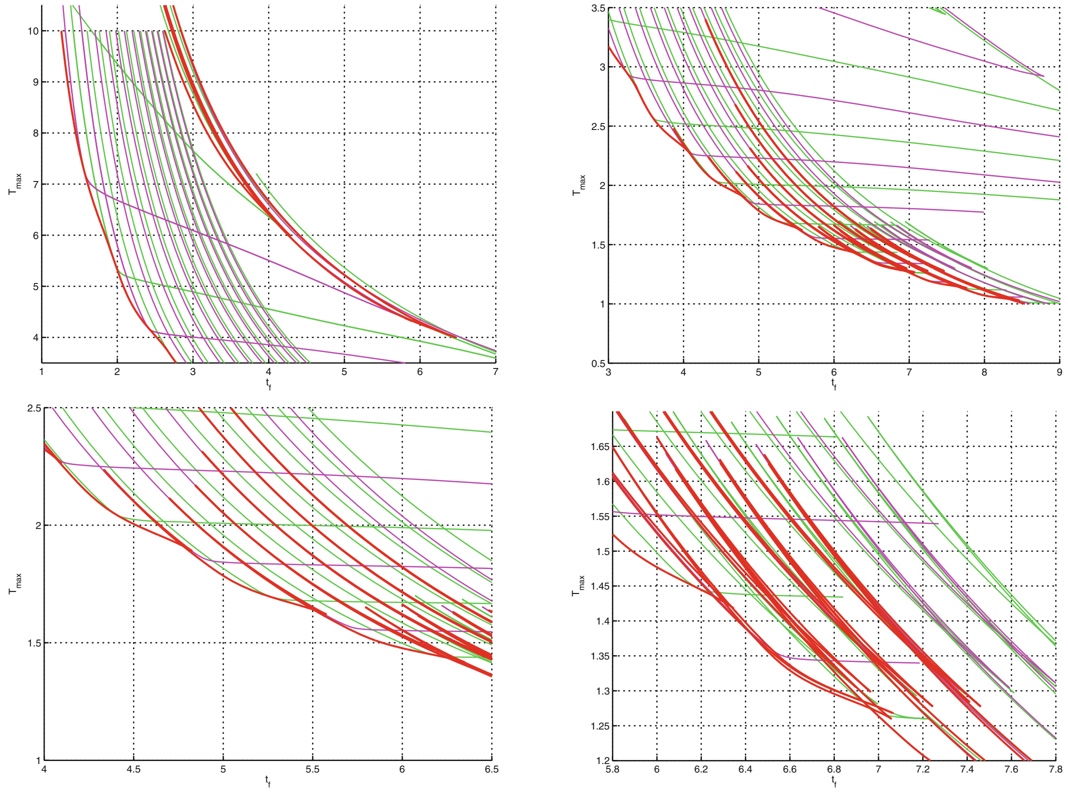

Fig. 53 For class $\mathscr{C}_2$: zoomed regions of the comparison between the local minima for θ_0 free (*red line*) versus θ_0 fixed (*green* and *magenta lines*)

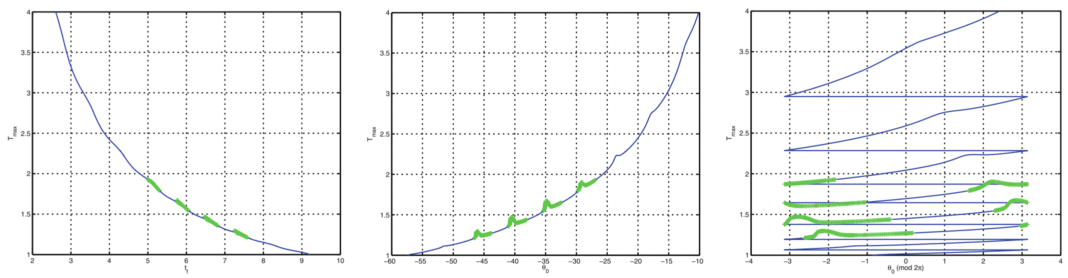

Fig. 54 Homotopy of the local minima of class $\mathscr{C}_1$, for the GEO to MO control problem. *Left* ε versus t_f, *Center* ε versus θ_0, *Right* ε versus θ_0 mod 2π

the most relevant results. In the case of class $\mathscr{C}_1$ orbits (Table 30) all the cut points are of the same kind and present, qualitatively, a similar behavior. This is why here we only show the results for the cut point number 3. This cut point corresponds to $\varepsilon^* \approx 1.6073723$ and $t_f^* \approx 5.9023179$ (see Table 30). On the left hand side of Fig. 56 we have the homotopic curve and highlighted in green the region that we want to study. On the right hand side of the Fig. we have 4 subplots, one is a zoom of the cut point region showing t_f versus ε, the other is the same zoom but plotting θ_0 versus ε. The two subplots on the bottom show θ_0 versus N_{ET} and θ_0 versus N_{ZH}, being N_{ET} the number of turns around the Earth before $J_c(t) > J_c(L_1)$ and N_{ZH} the number of times $|(H_1(t), H_2(t))|$ is close to zero.

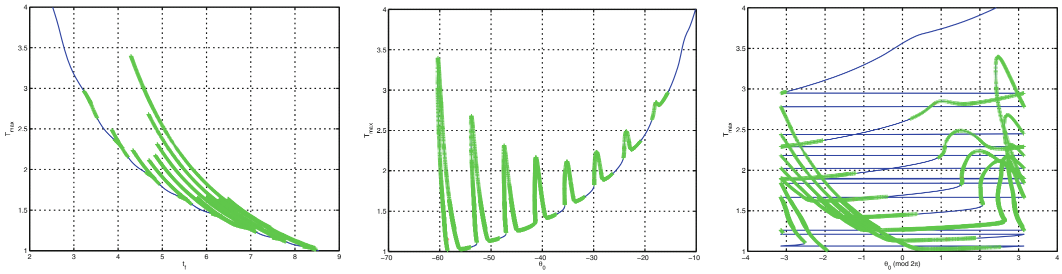

Fig. 55 Homotopy of the local minima of class $\mathscr{C}_2$, for the GEO to MO control problem. *Left* ε versus t_f, *Center* ε versus θ_0, *Right* ε versus θ_0 mod 2π

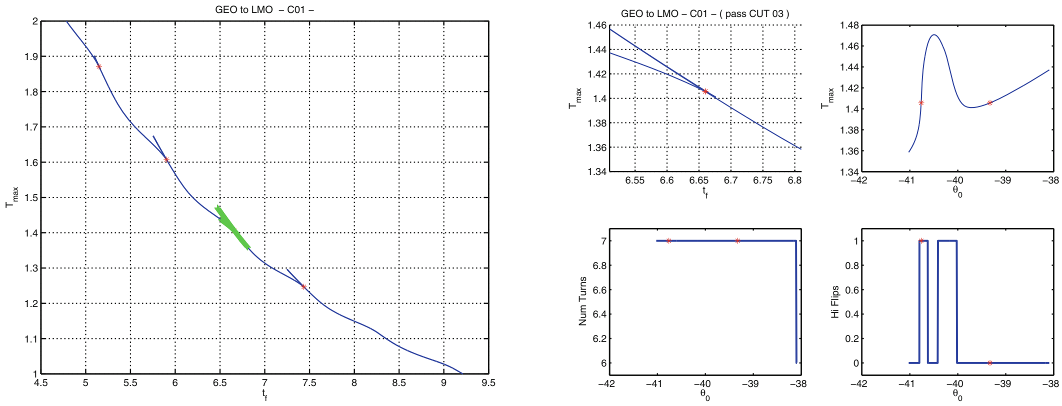

Fig. 56 $\mathscr{C}_1$ cut point n^o 3: *Left* t_f versus ε homotopic curve with highlight of the cut passage in *green*; *Right* versus analysis of the cut passage: (*top-left* subplot) t_f versus ε zoom, (*top-right* subplot) θ_0 versus ε, (*bottom-left* subplot) θ_0 versus N_{ET}, (*bottom-right* subplot) θ_0 versus N_{ZH}. *Red* points are values corresponding the each cut point

In Fig. 57 we plot different aspects of both cut transfer trajectories. In all the plots, the curves in blue correspond to the first cup point (x_0, p_0) and the curves in red correspond to the second cut point (x_1, p_1). The three plots on the top show, from left to right: the $\{x, y\}$ projection of the transfer trajectory, the $\{\dot{x}, \dot{y}\}$ projection of the transfer trajectory and $J_c(t)$ along the transfer trajectory. The three plots on the bottom show, from left to right: the $\{x, y\}$ projection of the transfer trajectory and the control law $\mathbf{u}(t)$, the projection (H_1, H_2) and the variation of $|(H_1, H_2)|$ along the transfer trajectory. As we can see, the main difference between both trajectories appears on the control law at the beginning of the transfer, where the second cut point (red curve) experiences a drastic change.

In Fig. 58 we plot the integration backward in time ($t \in [-t_f : 0]$) and forward in time ($t \in [0 : 2t_f]$) for both transfer trajectories and the variation of J_c for each of the trajectories. As we can see, when we integrate backwards in time, we have a similar behaviors to the one experienced by the different cut points in the GEO to L_1 transfer problem. We have that the first cut points spirals away form the Earth (red curve) while the second cut points spirals towards the Earth (blue curve). This is also reflected on the behavior of $J_c(t)$ where in the first case will start to grow, while in the second case this one will decrease. Moreover, this behavior is repeated for all the cut points of class $\mathscr{C}_1$. If we look at the behavior of the two trajectories for $t \in [0 : 2t_f]$, it is true that there is a difference between the two trajectories. But as we can see in

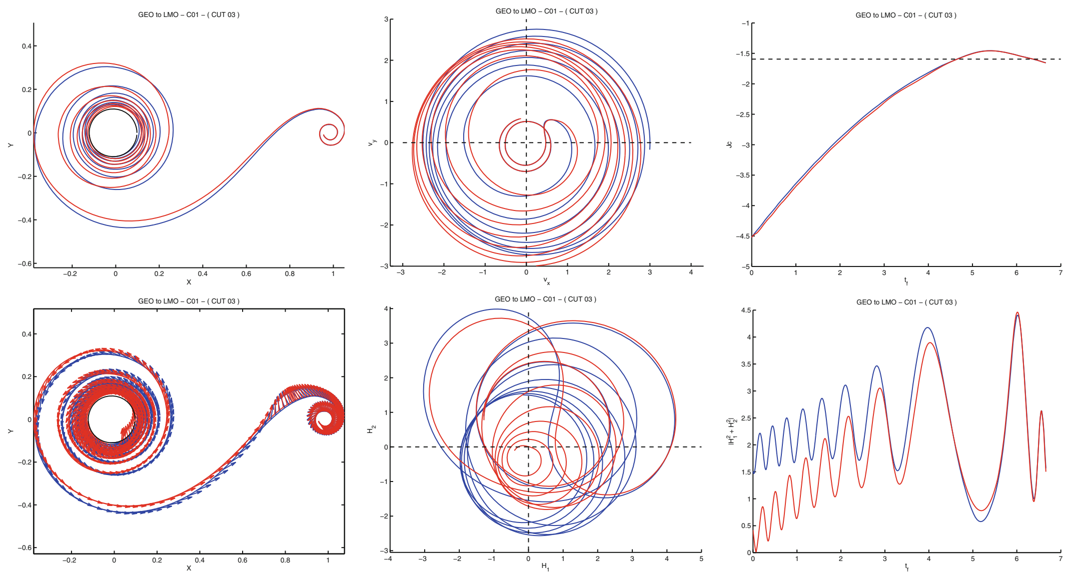

Fig. 57 $\mathscr{C}_1$ cut point n^o 3: *blue* orbits correspond to the first cut value and *red* orbits to the second cut value. *Top-Left* $\{XY\}$ projection of the transfer trajectory, *Top-Center* $\{\dot{X}\dot{Y}\}$ projection of the transfer trajectory, *Top-Right* t versus J_c (energy variation along the transfer trajectory), *Bottom-Left* control along the trajectory, *Bottom-Center* H_1 versus H_2, *Bottom-Right* t versus $|(H_1, H_2)|$

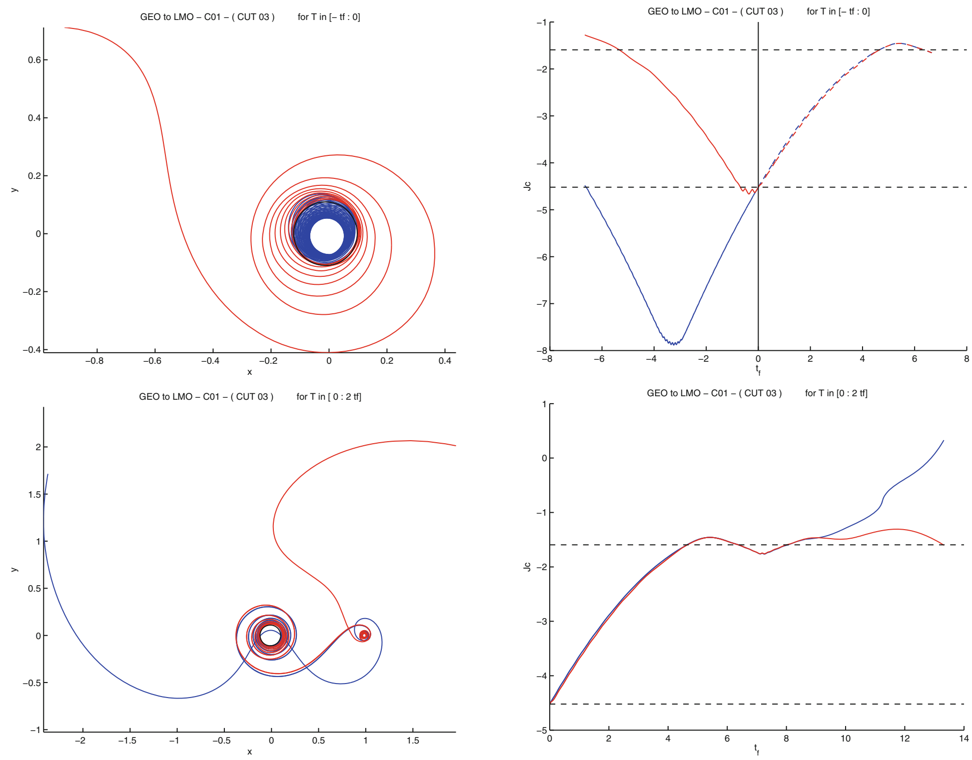

Fig. 58 $\mathscr{C}_1$ cut point n^o 3: *Left* optimal solutions for $t \in [-t_f, 0]$ ($\{XY\}$ projection and J_c variation), *Right* optimal solutions for $t \in [0, 2t_f]$ ($\{XY\}$ projection and J_c variation)

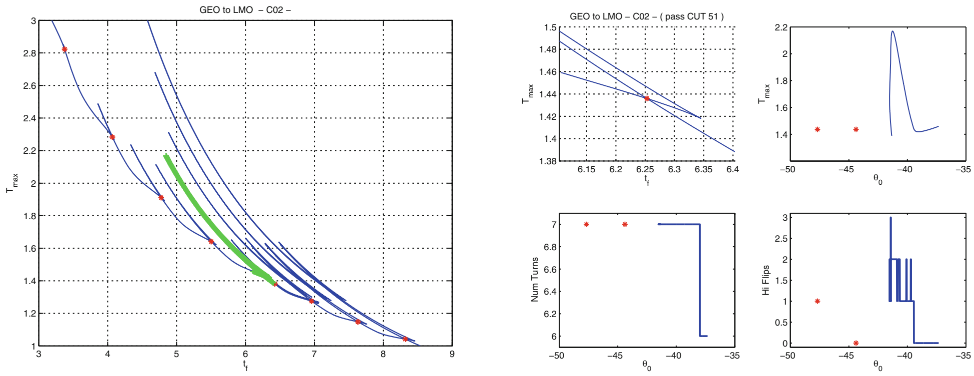

Fig. 59 $\mathscr{C}_2$ cut point n^o 5: *Left* t_f versus ε homotopic curve with highlight of the cut passage in *green*; *Right* analysis of the cut passage: (*top-left* subplot) t_f versus ε zoom, (*top-right* subplot) θ_0 versus ε, (*bottom-left* subplot) θ_0 versus N_{ET}, (*bottom-right* subplot) θ_0 versus N_{ZH}. *Red* points are values corresponding the each cut point

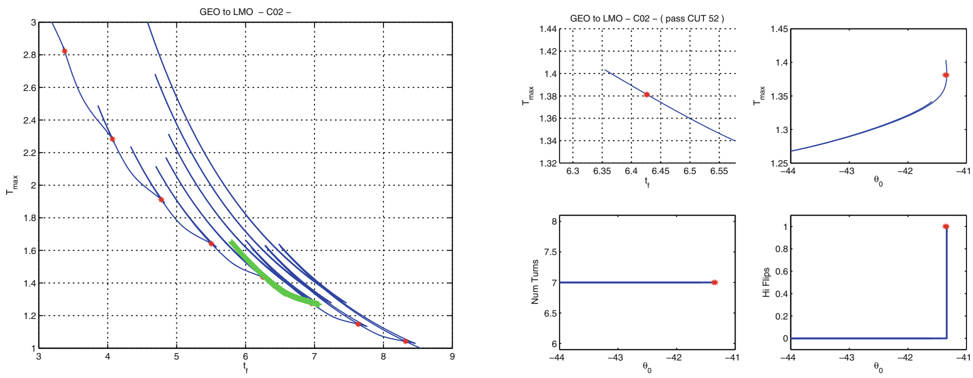

Fig. 60 $\mathscr{C}_2$ cut point n^o 6: *Left* t_f versus ε homotopic curve with highlight of the cut passage in *green*; *Right* analysis of the cut passage: (*top-left* subplot) t_f versus ε zoom, (*top-right* subplot) θ_0 versus ε, (*bottom-left* subplot) θ_0 versus N_{ET}, (*bottom-right* subplot) θ_0 versus N_{ZH}. *Red* points are values corresponding the each cut point

Appendix "Summary of the cut points on the GEO to MO transfer", this behavior does not show a distinctive pattern between the four cut points of class $\mathscr{C}_1$. On the other hand, not all the cut points of class $\mathscr{C}_2$ (Table 31) experience a similar behavior. As the plots in Appendix "Summary of the cut points on the GEO to MO transfer" show, we have cut point number 1, 2, 3, 4, 5, 8 and 9 that present a similar behavior and cut points 6 and 7 that show another. Here we show the results for cut point 5 and cut point number 6 and we will briefly comment on their main differences. A more extensive study on these two kinds of cut points should be done in detail. In Figs. 59 and 60 we plot the behavior of the trajectories close to the cut point for cut point number 5 and 6 respectively. Where we have the on the right hand side the variation of N_{ET} and N_{ZH} for the different solutions.

In Figs. 61 and 62 we see the behavior of the two transfer trajectories for cut point number 5 and 6 respectively. As before, red is assigned to the first cut point (x_0, p_0) and blue to the second one (x_1, p_1). On the top we have, from left to right, the $\{x, y\}$

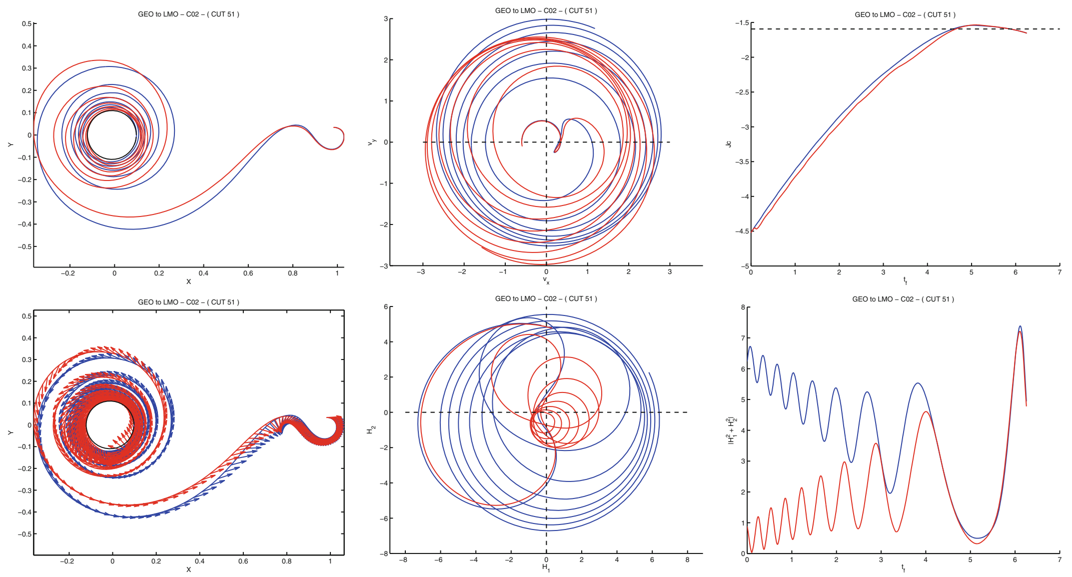

Fig. 61 $\mathscr{C}_2$ cut point n^o 5: *blue* orbits correspond to the first cut value and *red* orbits to the second cut value. *Top-Left* $\{XY\}$ projection of the transfer trajectory, *Top-Center* $\{\dot{X}\dot{Y}\}$ projection of the transfer trajectory, *Top-Right* t versus J_c (energy variation along the transfer trajectory), *Bottom-Left* control along the trajectory, *Bottom-Center* H_1 versus H_2, *Bottom-Right* t versus $|(H_1, H_2)|$

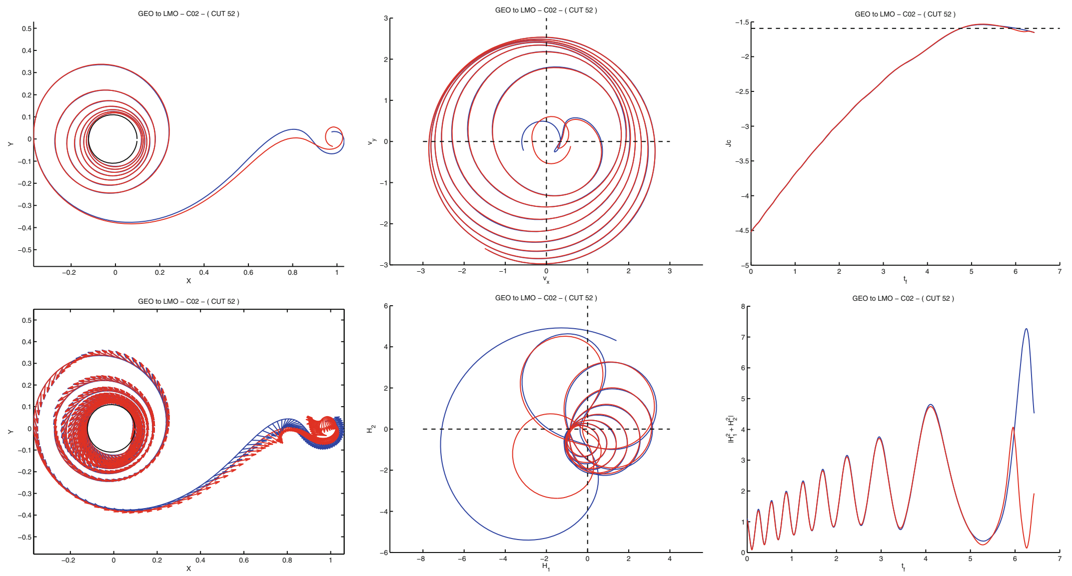

Fig. 62 $\mathscr{C}_2$ cut point n^o 6: *blue* orbits correspond to the first cut value and *red* orbits to the second cut value. *Top-Left* $\{XY\}$ projection of the transfer trajectory, *Top-Center* $\{\dot{X}\dot{Y}\}$ projection of the transfer trajectory, *Top-Right* t versus J_c (energy variation along the transfer trajectory), *Bottom-Left* control along the trajectory, *Bottom-Center* H_1 versus H_2, *Bottom-Right* t versus $|(H_1, H_2)|$

projection, the $\{\dot{x}, \dot{y}\}$ projection and the variation of $J_c(t)$. On the bottom we have, from left to right, the $\{x, y\}$ projection and the control law $\mathbf{u}(t)$, (H_1, H_2) projection and the variation of $|(H_1, H_2)|$ along time. As we can see, for cut point number 5, the main difference between the two cut trajectories is seen at the beginning of the orbit, where again we see a drastic change on the orientation of **u**. Which can be related to $|(H_1, H_2)|$ passing close to zero for one of the two trajectories. On the other hand, for cut point number 6, the main difference between the two cut trajectories appears at the end of the transfer, during the insertion to the Moon orbit. Where we can see how the arrival point on the Moon orbit is very different for the two trajectories (i.e. this is not the case in cut point number 5). Moreover, the control law is very different at the end of the transfer, and the second cut point (red curve) experiences a drastic change on its orientation.

Finally, in Figs. 63 and 64 we show for cut point number 5 and 6 respectively, the behavior of the transfer trajectories when we integrate backward in time $t \in [-t_f : 0]$ and forward in time $t \in [0 : 2t_f]$. As we can see, in the case of cut point number 5, the difference between the two cut point appears when we look at the behavior of the trajectories backward in time. Where we find similar results to the ones we have already observed. While if we look at the behavior of the transfer trajectories forward in time for cut point number 5 both are qualitatively the same. On the contrary, if we look at the behavior of cut point number 6 backward in time, both trajectories have a similar behavior, they both spiral away from the Earth and $J_c(t)$ increases. But if we look at their behavior forward in time we do see different behaviors between them.

To summarize, we can say that for class $\mathscr{C}_1$ transfer orbits, the cut points present a similar behavior to the cut points that we found when we studied the GEO to L_1 minimum-time transfer problem. Where the main difference between the two cut points is found at the beginning of the transfer trajectory. On the other hand, for the

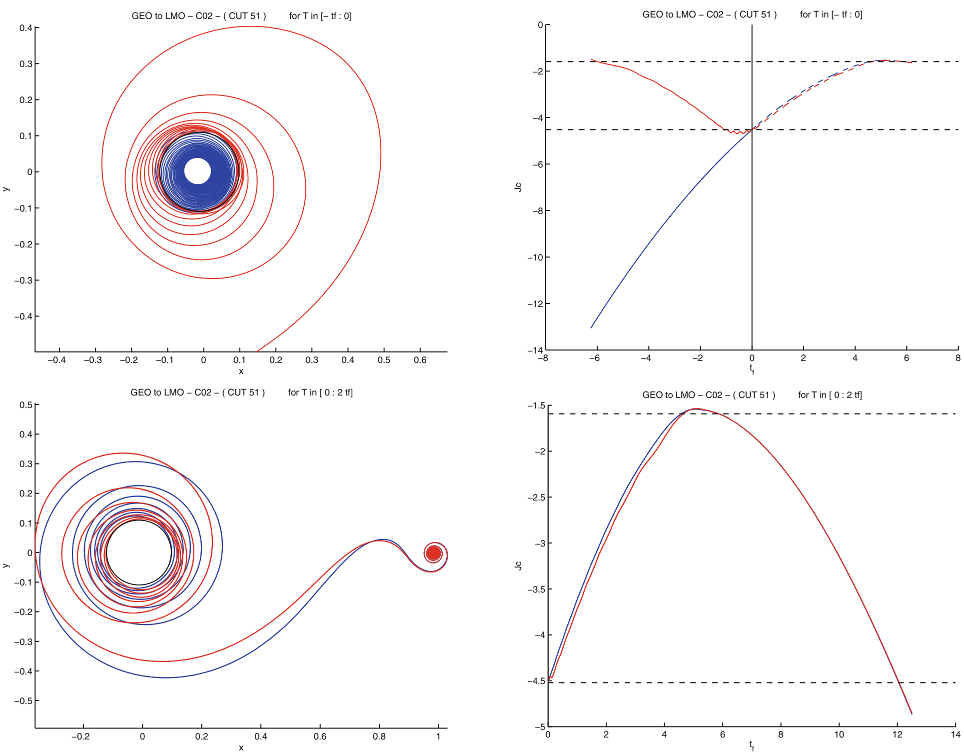

Fig. 63 $\mathscr{C}_2$ cut point n^o 5: *Top* optimal solutions for $t \in [-t_f, 0]$ (XY projection and J_c variation), *Bottom* optimal solutions for $t \in [0, 2t_f]$ (XY projection and J_c variation)

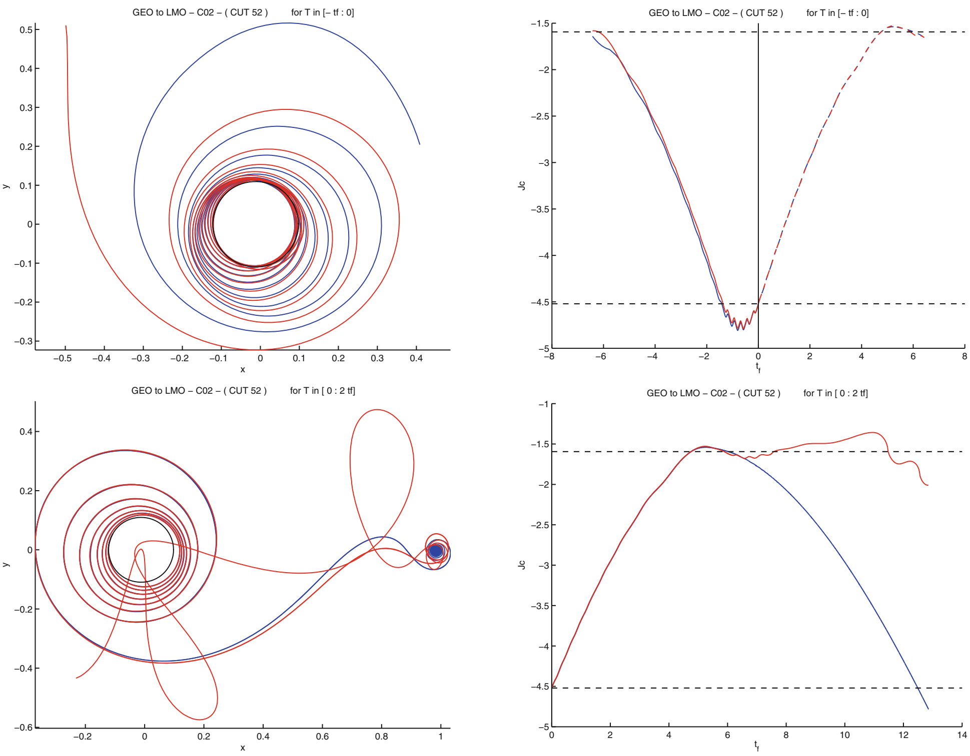

Fig. 64 $\mathscr{C}_2$ cut point n^o 6: *Top* optimal solutions for $t \in [-t_f, 0]$ (XY projection and J_c variation), *Bottom* optimal solutions for $t \in [0, 2t_f]$ (XY projection and J_c variation)

class $\mathscr{C}_2$ transfer orbits, the cut point structure is more complex. There are many type of self-intersections and type of cut behavior. We find many cut points where the behavior shows similarities with the cut points for class $\mathscr{C}_1$. But we also find two cut points where the difference between the two transfer trajectories appears in the second phase of the transfer, i.e. when we get to the Moon orbit. This is probably because we enter this orbit in an anti-clock wise sense and the structure of the L_1 to Moon orbit has a similar behavior. Further studies in this direction should be done in order to draw further conclusions.

3.4 Homotopy w.r.t r_1

Here we have considered the minimum time solutions found for $\varepsilon = 1$N and θ_0 free found in Sect. 3.2. The trajectories of the transfer orbit for both classes are in Fig. 65. We recall that the blue orbit corresponds to class $\mathscr{C}_1$ and the red orbit corresponds to class $\mathscr{C}_2$. In this section we will perform homotopies of these solutions with respect to r_1 the size of the arrival orbit, to find transfer trajectories to a circular orbit closer to the Moon. To be more specific, we have considered a transfer from GEO to circular MO where the position on the departure and arrival orbits is not fixed. We recall that the boundary conditions of these problem are written as:

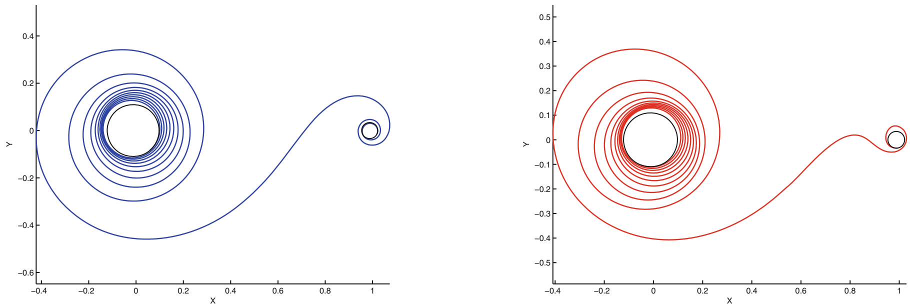

Fig. 65 Minimum-time transfer trajectories of class $\mathscr{C}_1$ (*left*) and class $\mathscr{C}_2$ (*right*), for $\varepsilon = 1N$, and θ_0 free

$$
\begin{aligned}
(x_0+\mu)^2 + y_0^2 - r_0^2 &= 0,\\
\dot{x}_0^2 + \dot{y}_0^2 - v_0^2 &= 0,\\
(x_0+\mu)\dot{x}_0 + y_0\dot{y}_0 &= 0,\\
(x_0+\mu)p_{y0} - y_0 p_{x0} + \dot{x}_0 p_{\dot{y}0} - \dot{y}_0 p_{\dot{x}0} &= 0,\\
(x_f+\mu-1)^2 + y_f^2 - r_1^2 &= 0,\\
\dot{x}_f^2 + \dot{y}_f^2 - v_1^2 &= 0,\\
(x_f+\mu-1)\dot{x}_f + y_f\dot{y}_f &= 0,\\
(x_f+\mu-1)p_{yf} - y_f p_{xf} + \dot{x}_f p_{\dot{y}_f} - \dot{y}_f p_{\dot{x}_f} &= 0.
\end{aligned}
\tag{12}
$$

We recall that $x(t_0) = (x_0, y_0, \dot{x}_0, \dot{y}_0)$ and $x(t_f) = (x_f, y_f, \dot{x}_f, \dot{y}_f)$ are the coordinates of the spacecraft at $t = t_0$ and t_f respectively; $p(t_0) = (p_{x0}, p_{y0}, p_{\dot{x}0}, p_{\dot{y}0})$ and $p(t_f) = (p_{xf}, p_{yf}, p_{\dot{x}f}, p_{\dot{y}f})$ are the coordinates of the adjoint vector at $t = t_0$ and t_f respectively; r_0 is the radius of the GEO, r_1 the radius of the MO, and $v_0 = \sqrt{(1-\mu)/r_0}$, $v_1 = \sqrt{\mu/r_1}$ the corresponding velocities such that these orbits are circular using the two-body problem approximation. In this work we have used $r_0 = 0.109689855932071$ for the GEO orbit and $r_1 = 0.034$ for the MO, which corresponds to $r_0 \approx 42,164$ km and $r_1 \approx 13,069.6$ km (we recall that $r_M = 1,737.10$ km). We have performed an homotopy with respect to r_1, from 0.034 to 0.015 ($r_1 = 0.015$ corresponds to a MO of radius $\approx 5,766$ km). To perform this homotopy we have also used the package `hampath`.

In Fig. 66 we show the homotopic curve found by varying r_1, showing the projection t_f versus r_f. The blue curve corresponds to the path found for class $\mathscr{C}_1$ transfer orbits and the red curve to the path for class $\mathscr{C}_2$. Notice that for class $\mathscr{C}_1$ the curve decreases slowly having larger transfer times for smaller r_1 as expected. On the other hand, for class $\mathscr{C}_2$ orbits the curve presents a more complex structure. It is still true that the transfer time increases as r_1 gets smaller, but we find several self-intersections. Having cut points and different local minimum solutions for the same r_1. A more detailed study on the structure of these "cut" points should be done. Moreover, notice that the transfer time for class $\mathscr{C}_2$ is always smaller that the one for class $\mathscr{C}_1$ orbits. In Fig. 67 we plot the two minimum-time transfer trajectories found for $\varepsilon = 1$N and $r_1 = 0.015$, each orbit corresponds to one class. For both orbits we have also plotted the variation of J_c with respect to time. Notice that now $J_c(t_f)$ is

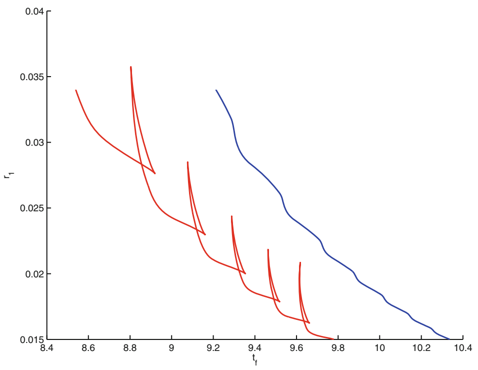

Fig. 66 Homotopic path w.r.t. $r_1 \in [0.034 : 0.015]$, for $\varepsilon = 1N$ (t_f vs. r_1). In *blue* solutions for class $\mathscr{C}_1$ and in *red* solutions for class $\mathscr{C}_2$

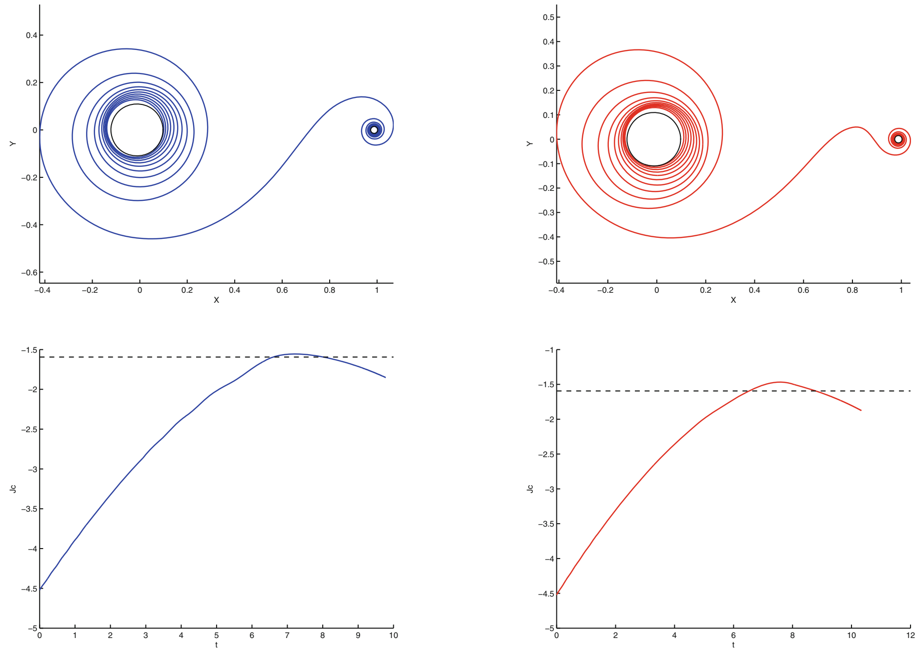

Fig. 67 *Top* $\{XY\}$ projection of minimum-time transfer trajectories for $\varepsilon = 1$N and $r_1 = 0.015$. *Bottom* variation of J_c along the transfer trajectories. *Left* (and *blue curves*) class $\mathscr{C}_1$ trajectories, *Right* (and *red curves*) class $\mathscr{C}_2$ trajectories

much smaller than $J_c(L_1)$. We can also see that in both cases, the transfer trajectory is split in three phases. A first phase where the orbit spirals around the Earth and gains J_c, a second phase where the orbit goes from the vicinity of the Earth to the vicinity of the Moon, and a third phase where the orbit spirals towards the Moon and J_c decreases. The difference between the two class of orbits would happen in the second phase where the orbit chooses different kind of paths and control laws to reach the Moon orbit.

Finally, in Fig. 68 we show the X, Y, J_c projection of different transfer trajectories for $\varepsilon = 1$N. On the left hand side we have the two transfer orbits for $r_1 = 0.034$ and on the right hand side the two transfer orbits for $r_1 = 0.015$. Here we can see clearly

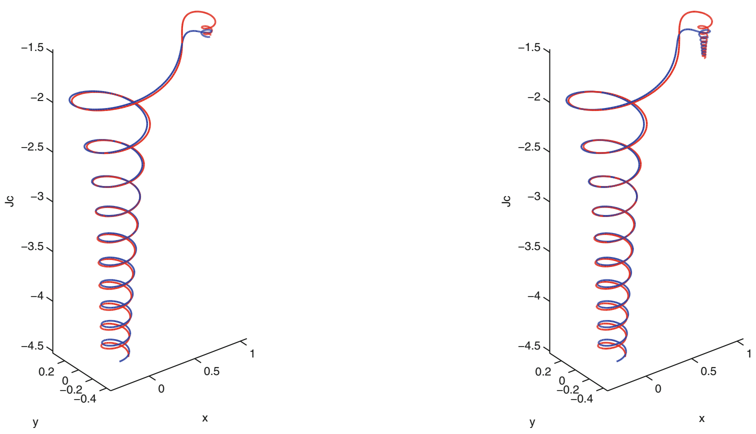

Fig. 68 $\{XYJ_c\}$ projection of minimum-time transfer trajectories for $\varepsilon = 1$N, for trajectories of class $\mathscr{C}_1$ (*blue*) and class $\mathscr{C}_2$ (*red*). *Left* $r_1 = 0.034$ and *Right* $r_1 = 0.015$

the structure of the transfer orbit, how J_c increases and decreases spiraling around one of the primaries. The difference between the two plots can be seen in $J_c(t_f)$ that will vary from one problem to the other. This plot suggests that one might be able to describe the strategies in terms of $J_c(t_0)$ and $J_c(t_f)$.

4 Conclusion

The detailed numerical study conducted in Sects. 2 and 3 illustrates two features of the three−body problem that are obviously due to the particular topology of the two-body problem (as explained in the introduction, for typical boundary conditions the controllability analysis of [5] entails that one can view the problem as two 2BP coupled by an L_1 target): (i) For a given level of thrust, a homotopy in the covering of the angle defining the initial position on the initial orbit allows to unfold and connect local minima associated to different rotation numbers; in particular, local minima of different types (some with many revolutions around the primary, some with large excursions—both clearly not globally minimizing) are indeed connected. (ii) The systematic study of these local minima for fixed thrust level allows to confirm numerically that, when leaving the position free on the initial orbit (here the geostationary one for all tests) and using a homotopy on the level of thrust, one actually follows a path of (at least seemingly) global optimizers for some time. When the thrust is decreased sufficiently, one has to add an extra turn around the initial primary at some point (and possibly around the target one as well), which could result in a bifurcation of the path, or even lead to a discontinuity, that is to the requirement to jump to another branch. It turns that the relevant phenomenon, at least for what is observable in the current computations, is a classic swallowtail singularity [1]: No

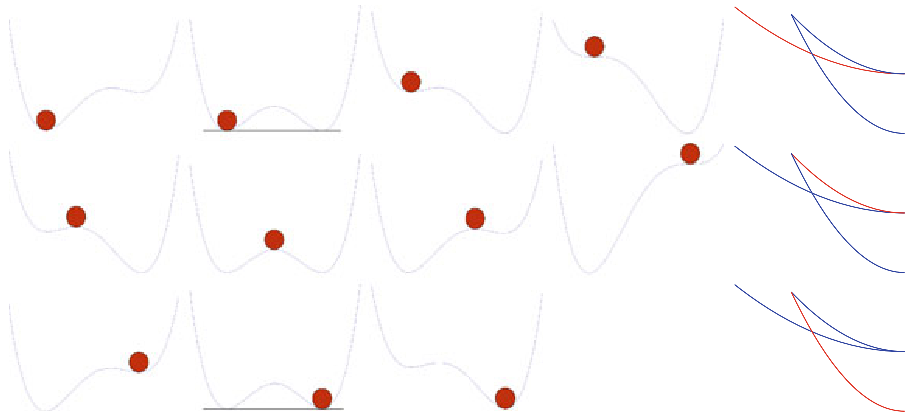

Fig. 69 Swallowtail singularity. On the first line, the global minimum is changed into a local one (passing through a configuration with two equal global minima, corresponding to the first crossing of the self intersection on the rightmost graph), then into a critical point which is neither a local minimum or maximum (corresponding to the first cusp or turning point on the path). On the second line, a branch of local maxima is described, up to another critical point (second cusp or turning point). On the last line of subplots, local then global maxima are retrieved (passing now through a configuration with two equal global minima corresponding to the second crossing of the self intersection on the rightmost graph). All three rightmost subplots are schematic views of these three connected branches of the (t_f, ε)-path. In this optimal control setting, turning points are associated with conjugate points while self-intersections correspond to cut points.

discontinuity is encountered, and the path connects the (apparently) global solutions for, say, ε_1 and ε_2 $(< \varepsilon_1)$ by going through a branch of global then local minima (change at a first cut point), a first turning point (which is also a conjugate point—see the analysis in [5]—and is neither a local minimum or maximum), a branch of local maxima, a second turning point (again a conjugate point), a branch of local then global maxima (change at a second cut point with same cost as the previous one). See Fig. 69 for a schematic picture. The rest of the picture consists of connecting in the (t_f, ε)-space such swallowtail singularities to form the global path (see, e.g., Fig. 21). The typical cut-like point encountered in these situations correspond to very similar though different control strategies; in particular, the two extremals may have the same rotation numbers (see Fig. 22). But there is actually of wealth of extremals corresponding to various structures of the control, and we are far from understanding the global picture at this stage. (See for instance Fig. 40 illustrating three different strategies for the same problem, possibly living on different branches of the (t_f, ε)-homotopy.)

5 Tables for GEO to L_1 Transfer Problem

Table 3 Cut Points for GEO to L_1 minimum-time transfer problem

N^o	t_f	ε (N)	(x_0, p_0)
1	3.2044271	2.8177314	x0 = (−4.3004036e−02 1.0526195e−01 −2.8798280e+00 −8.4404363e−01) p0 = (−8.0686913e+00 1.8446666e+01 −6.1769698e−01 −8.3732696e−02)
	3.2044218	2.8177314	x1 = (7.7386132e−02 6.3360936e−02 −1.7334716e+00 2.4496725e+00) p1 = (5.7983831e+00 8.0411480e+00 −1.3156893e−01 3.8933850e−01)
2	3.8375203	2.2761716	x0 = (−1.2063951e−01 1.6203154e−02 −4.4329690e−01 −2.9680477e+00) p0 = (−4.4671254e+01 5.8135647e+00 −2.4592639e−01 −1.4365076e+00)
	3.8375175	2.2761716	x1 = (5.2514551e−02 8.8600069e−02 −2.4239810e+00 1.7692189e+00) p1 = (4.3721245e+00 1.1331595e+01 −3.5478899e−01 4.0145337e−01)
3	4.4722368	1.9042420	x0 = (−8.7103192e−02 −8.0089532e−02 2.1911439e+00 −2.0505383e+00) p0 = (−5.5133744e+01 −5.7358673e+01 1.9780637e+00 −1.7979208e+00)
	4.4722337	1.9042420	x1 = (6.9733651e−03 1.0800947e−01 −2.9549967e+00 5.2327211e−01) p1 = (−6.5935699e−01 1.4254660e+01 −6.0595336e−01 2.2366696e−01)
4	5.1076234	1.6346218	x0 = (1.8465131e−03 −1.0879282e−01 2.9764280e+00 3.8300820e−01) p0 = (1.2560860e+01 −1.2124635e+02 4.1425055e+00 6.4421919e−01)
	5.1076249	1.6346218	x1 = (−4.7448985e−02 1.0385595e−01 −2.8413617e+00 −9.6565156e−01) p1 = (−8.1438007e+00 1.4247984e+01 −7.4247922e−01 −1.3165896e−01)
5	5.7431841	1.4309308	x0 = (7.7334294e−02 −6.3434128e−02 1.7354740e+00 2.4482543e+00) p0 = (1.3695137e+02 −1.0313743e+02 3.3137469e+00 4.9871067e+00)
	5.7431642	1.4309308	x1 = (−9.5138164e−02 7.1730935e−02 −1.9624637e+00 −2.2703646e+00) p1 = (−1.5939313e+01 9.6554337e+00 −6.4632581e−01 −5.7341753e−01)
6	6.3789344	1.2718365	x0 = (9.5773675e−02 1.9588193e−02 −5.3590712e−01 2.9527314e+00) p0 = (2.2901189e+02 3.4599146e+01 −1.7065479e+00 7.9999291e+00)
	6.3789252	1.2718365	x1 = (−1.2039301e−01 1.7775384e−02 −4.8631103e−01 −2.9613039e+00) p1 = (−2.0965394e+01 2.8593691e−01 −2.6964121e−01 −9.3925785e−01)
7	7.0149950	1.1442218	x0 = (5.1158197e−02 8.9574309e−02 −2.4506349e+00 1.7321108e+00) p0 = (1.8011622e+02 2.3963981e+02 −8.8959222e+00 5.8951334e+00)
	7.0149569	1.1442218	x1 = (−1.1314330e−01 −4.2811500e−02 1.1712661e+00 −2.7629612e+00) p1 = (−2.0185746e+01 −1.1936458e+01 3.2074658e−01 −1.0480066e+00)

Results obtained from Fig. 18

Table 4 Initial conditions for minimum-time transfer orbits for $\varepsilon = 10$N and $\theta_0 = 0$ (fixed)

k	t_f	p_0
1	2.5599110579	(−8.10302600967e+00, 3.02060685402e−01, 7.51746305081e−03, −2.72282719406e−01)
2	2.4917687101	(−7.99512361116e+00, 3.62833827849e−01, 9.87071526042e−03, −2.70747978337e−01)
3	2.4189259511	(−7.77134183976e+00, 4.70243193749e−01, 1.38944882768e−02, −2.63770704241e−01)
4	2.3422687228	(−7.61830506790e+00, 5.25624650131e−01, 1.59953031798e−02, −2.60958013110e−01)
5	2.2591797538	(−7.35595976228e+00, 6.30264231036e−01, 1.98961901745e−02, −2.53456263812e−01)
6	2.1709334950	(−7.11929765212e+00, 6.79535789150e−01, 2.16728858950e−02, −2.48023436490e−01)
7	2.0733748800	(−6.78411359981e+00, 7.70584361967e−01, 2.49883101080e−02, −2.38936843908e−01)
8	1.9682235824	(−6.37730302696e+00, 8.14920691231e−01, 2.63907417363e−02, −2.27864801770e−01)

(continued)

Table 4 (continued)

k	t_f	p_0
9	1.8483950863	(−5.88075426291e+00, 8.70998413743e−01, 2.81742195599e−02, −2.14116786836e−01)
10	1.7156981531	(−5.06426694761e+00, 9.19001172403e−01, 2.92798458710e−02, −1.89107342495e−01)
11	1.5565271364	(−4.11188635118e+00, 8.96978816242e−01, 2.74753371581e−02, −1.59911895051e−01)
12	1.3726059062	(−1.28979835829e+00, 1.13483961580e+00, 3.40752669425e−02, −6.71095824899e−02)
13	1.6797923278	(2.06357664128e+02, 4.43098626559e+00, 3.96574729885e−01, 7.29822417118e+00)
14	2.7126920399	(3.46017661782e+00, −2.74792593807e+00, −1.17714841093e−01, 3.75634764455e−02)
15	2.8397955185	(−2.03473423827e+00, −2.51445819123e+00, −1.05824599138e−01, −1.77547444466e−01)

Here, $x_0 = (9.7536855, 0.00, 0.00, 3.0009696)$

Table 5 Initial conditions for minimum-time transfer orbits for $\varepsilon = 10$N and $\theta_0 = \pi/2$ (fixed)

k	t_f	p_0
1	2.5572956763	(−2.44641634194e−01, −1.01506238330e+01, 4.12858647068e−01, 9.76331017638e−03)
2	2.4886728553	(−1.89607461766e−01, −1.00207778997e+01, 4.08352174314e−01, 7.44373886471e−03)
3	2.4160055626	(−1.58685283710e−01, −9.88623604487e+00, 4.05766385543e−01, 6.13888229610e−03)
4	2.3384047229	(−9.13707083469e−02, −9.68400986037e+00, 3.98201189251e−01, 3.23659167759e−03)
5	2.2550784768	(−4.14972187431e−02, −9.48955468735e+00, 3.93446236657e−01, 1.11399808019e−03)
6	2.1651688933	(3.84033740410e−02, −9.16568566700e+00, 3.80989948634e−01, −2.44111301378e−03)
7	2.0665590453	(1.14827639931e−01, −8.85889814521e+00, 3.71852942749e−01, −5.75137698271e−03)
8	1.9585116066	(2.08588953344e−01, −8.30708874791e+00, 3.50763039836e−01, −1.01280325044e−02)
9	1.8359151993	(3.21190272472e−01, −7.76041413477e+00, 3.31853813310e−01, −1.51754873201e−02)
10	1.6977423611	(4.38111145210e−01, −6.68069683079e+00, 2.92026306333e−01, −2.10584817444e−02)
11	1.5315914535	(5.95238470964e−01, −5.50225170504e+00, 2.47157039202e−01, −2.86754751281e−02)
12	1.3337000522	(8.41013821159e−01, −2.36998678661e+00, 1.40666039253e−01, −4.16602092444e−02)
13	2.4460134134	(−3.41756924766e+00, 9.30607903262e+01, −3.30975784324e+00, 2.28357418848e−01)
14	2.6648851780	(1.04603325391e+00, 1.15237952755e+01, −5.20036306956e−01, −3.77212192660e−02)
15	2.7603423501	(2.59359121331e+00, 6.50388228992e+00, −3.36307995906e−01, −1.04272573878e−01)

Here, $x_0 = (-0.0121530, 0.10968985, -3.000969693, 0.00)$

Table 6 Initial conditions for minimum-time transfer orbits for $\varepsilon = 10$N and $\theta_0 = \pi$ (fixed)

k	t_f	p_0
1	2.5527521947	(1.06375513461e+01, 1.47617758655e+00, 5.76423437473e−02, 4.26278852503e−01)
2	2.4822720399	(1.04148331743e+01, 1.51294121857e+00, 5.94360744304e−02, 4.15282668813e−01)
3	2.4076155799	(1.01096843737e+01, 1.56726510132e+00, 6.19943495282e−02, 4.01904923185e−01)
4	2.3275603558	(9.79781572723e+00, 1.59332432531e+00, 6.34927961111e−02, 3.86869947665e−01)
5	2.2416129890	(9.40007362986e+00, 1.65348347180e+00, 6.64030056517e−02, 3.69487185012e−01)
6	2.1483459356	(8.93393057118e+00, 1.66987158824e+00, 6.77164579804e−02, 3.48137299904e−01)
7	2.0461306463	(8.40135607228e+00, 1.72740096089e+00, 7.07069439315e−02, 3.24679976788e−01)
8	1.9331012440	(7.61364755861e+00, 1.74635539983e+00, 7.24930725671e−02, 2.91092295102e−01)
9	1.8052056817	(6.83154051800e+00, 1.76666004320e+00, 7.43502285645e−02, 2.56569966663e−01)
10	1.6583042568	(5.29715773055e+00, 1.81736951791e+00, 7.81883129707e−02, 1.94875672822e−01)
11	1.4833856840	(3.83493364971e+00, 1.72669505097e+00, 7.64256922974e−02, 1.32959769935e−01)
12	1.2663896517	(−6.72434494581e−01, 1.82222989708e+00, 8.21403775003e−02, −4.33956185640e−02)
13	2.7731212505	(−6.53927977825e+00, −3.06988032726e+00, −1.17632989071e−01, −2.73303542519e−01)
14	2.8708627397	(−4.21419866917e+00, −3.15031550790e+00, −1.19145737733e−01, −2.14919176388e−01)

Here, $x_0 = (-0.1218428559, 0.00, 0.00, -3.00096969)$

Table 7 Initial conditions for minimum-time transfer orbits for $\varepsilon = 10$N and $\theta_0 = -\pi/2$ (fixed)

k	t_f	p_0
1	2.5907703198	(−1.61091775746e+00, 8.96037592684e+00, −3.04417077032e−01, 6.67655131141e−02)
2	2.5224151691	(−1.55066132206e+00, 8.65746432330e+00, −2.90472826121e−01, 6.48366258398e−02)
3	2.4501991195	(−1.47912650562e+00, 8.34215239832e+00, −2.75824570744e−01, 6.24872471641e−02)
4	2.3732312047	(−1.38995583017e+00, 7.99971550025e+00, −2.60564073245e−01, 5.94653100445e−02)
5	2.2909754645	(−1.31509971463e+00, 7.55737613122e+00, −2.40862906381e−01, 5.71424148173e−02)
6	2.2024783905	(−1.18473581289e+00, 7.17707239902e+00, −2.24753134059e−01, 5.25318628076e−02)
7	2.1060684965	(−1.09371385568e+00, 6.54755398598e+00, −1.97864122169e−01, 4.97973648749e−02)
8	2.0011242565	(−9.22196318408e−01, 6.07973280392e+00, −1.79300208002e−01, 4.36502684663e−02)
9	1.8831711949	(−7.94589175887e−01, 5.15470225726e+00, −1.41779328238e−01, 3.98082008222e−02)
10	1.7521393123	(−5.80577218930e−01, 4.42683184881e+00, −1.14541558497e−01, 3.22645112679e−02)
11	1.5971627494	(−3.91234096149e−01, 2.89940049164e+00, −5.62359857709e−02, 2.66110707927e−02)
12	1.4178043955	(−7.38577985007e−02, 1.04802410397e+00, 1.11883639221e−02, 1.54629906135e−02)
13	1.2200224705	(6.62105764118e−01, −4.51174644544e+00, 2.10821364039e−01, −1.97873327616e−02)
14	2.7726988590	(1.56502812470e+00, −2.70258668378e+00, −2.67064625097e−03, −5.02608779760e−02)
15	2.8760265384	(1.98895030587e+00, 6.05889722576e−01, −1.29117271405e−01, −7.01041330191e−02)

Here, $x_0 = (-0.012153, -0.10968985, 3.0009696, 0.00)$

Table 8 Initial conditions for minimum-time transfer orbits for $\varepsilon = 1$N and $\theta_0 = 0$ (fixed)

k	t_f	p_0
1	1.1734093510e+01	(−5.00293794181e+01, −8.92810787059e+00, −3.59642774825e−01, −1.86911263217e+00)
2	1.1552149062e+01	(−4.64542148014e+01, −8.85541434942e+00, −3.57354266774e−01, −1.68458131918e+00)
3	1.1366823527e+01	(−4.27162042580e+01, −8.50085033910e+00, −3.43959041446e−01, −1.49382338146e+00)
4	1.1178437340e+01	(−3.90281882445e+01, −7.78774378223e+00, −3.16398638411e−01, −1.30767766999e+00)
5	1.0987120064e+01	(−3.51231910879e+01, −6.81437528378e+00, −2.78577923093e−01, −1.11807707778e+00)
6	1.0793552884e+01	(−3.14356984450e+01, −5.56528120994e+00, −2.29828878667e−01, −9.43717166154e−01)
7	1.0597583348e+01	(−2.79786185901e+01, −4.07511367761e+00, −1.71505714926e−01, −7.88549733091e−01)
8	1.0399786390e+01	(−2.46548436680e+01, −2.46000281169e+00, −1.08203666943e−01, −6.47556492294e−01)
9	1.0200113173e+01	(−2.19410610646e+01, −7.51713433563e−01, −4.10953162593e−02, −5.43897525038e−01)
10	9.9985467473e+00	(−1.93444226096e+01, 9.50690537301e−01, 2.58472323136e−02, −4.54373346619e−01)
11	9.7951297247e+00	(−1.73746355786e+01, 2.54951122509e+00, 8.88514567696e−02, −4.02551176887e−01)
12	9.5893495406e+00	(−1.55102319471e+01, 4.03093493029e+00, 1.47292632024e−01, −3.63484827095e−01)
13	9.3811110629e+00	(−1.41307893780e+01, 5.24777692114e+00, 1.95387270812e−01, −3.53693100684e−01)
14	9.1697915366e+00	(−1.24787976530e+01, 6.30173897074e+00, 2.37044906641e−01, −3.40124616465e−01)
15	8.9564212414e+00	(−9.96070518965e+00, 7.14686809501e+00, 2.70390736552e−01, −3.01555539885e−01)
16	8.7418485088e+00	(−6.83558281878e+00, 7.74226722168e+00, 2.93836955496e−01, −2.47118606219e−01)
17	8.5274300169e+00	(−2.87799323127e+00, 8.02137698122e+00, 3.04743143954e−01, −1.67260037676e−01)
18	8.3147860737e+00	(2.35469713546e+00, 7.93462860048e+00, 3.01178035452e−01, −4.34661909985e−02)
19	8.1065871814e+00	(9.08133786760e+00, 7.45204156306e+00, 2.82147510584e−01, 1.35684066835e−01)

Here, $x_0 = (9.7536855, 0.00, 0.00, 3.0009696)$

Table 9 Initial conditions for minimum-time transfer orbits for $\varepsilon = 1\text{N}$ and $\theta_0 = \pi/2$ (fixed)

k	t_f	p_0
1	1.1617836482e+01	(−5.86265374666e−01, −3.55563514170e+01, 1.05337756761e+00, 1.33730970732e−02)
2	1.1448706422e+01	(−1.95081480500e+00, −3.38390778413e+01, 1.00258679684e+00, 6.71037566339e−02)
3	1.1278103045e+01	(−3.20864825547e+00, −3.26693195566e+01, 9.81204357826e−01, 1.16722579010e−01)
4	1.1106156553e+01	(−4.35464384443e+00, −3.14871164620e+01, 9.65464703194e−01, 1.61949064207e−01)
5	1.0932241536e+01	(−5.31187787666e+00, −3.08348948035e+01, 9.76384410476e−01, 1.99807373235e−01)
6	1.0756369590e+01	(−6.10327738038e+00, −3.00934747065e+01, 9.88636669326e−01, 2.31120029517e−01)
7	1.0577724397e+01	(−6.66192909273e+00, −2.97815306058e+01, 1.02109064306e+00, 2.53299344487e−01)
8	1.0396252516e+01	(−7.00372755398e+00, −2.93378374216e+01, 1.05145175237e+00, 2.66902151015e−01)
9	1.0210946491e+01	(−7.11002130272e+00, −2.91066374962e+01, 1.09142290415e+00, 2.71227569949e−01)
10	1.0021678797e+01	(−6.95232923626e+00, −2.87290157156e+01, 1.12625828544e+00, 2.65104252329e−01)
11	9.8273162387e+00	(−6.57280516945e+00, −2.82964650663e+01, 1.15892547212e+00, 2.50208359620e−01)
12	9.6276234212e+00	(−5.90387876777e+00, −2.76421558052e+01, 1.18053824596e+00, 2.23843275857e−01)
13	9.4214770376e+00	(−5.02818856177e+00, −2.65752199328e+01, 1.18564798030e+00, 1.89258893999e−01)
14	9.2093222798e+00	(−3.92185928576e+00, −2.45693574627e+01, 1.15400456124e+00, 1.45449008253e−01)
15	8.9910694916e+00	(−2.55235178987e+00, −2.15715237005e+01, 1.08180604209e+00, 9.11178102638e−02)
16	8.7671882439e+00	(−9.03453037648e−01, −1.75530736265e+01, 9.65375348447e−01, 2.56172123980e−02)
17	8.5383024028e+00	(1.01520847489e+00, −1.20346776264e+01, 7.83887782000e−01, −5.07298023085e−02)
18	8.3056624144e+00	(3.15812939064e+00, −4.39749794305e+00, 5.11247116113e−01, −1.36177598815e−01)
19	8.0723986254e+00	(5.42827481965e+00, 6.63751133717e+00, 9.73408800576e−02, −2.26732255341e−01)

Here, $x_0 = (-0.0121530, 0.10968985, -3.000969693, 0.00)$

Table 10 Initial conditions for minimum-time transfer orbits for $\varepsilon = 1$N and $\theta_0 = \pi$ (fixed)

k	t_f	p_0
1	1.1646032796e+01	(4.35820317970e+01, −6.97203875251e+00, −2.67592133177e−01, 1.66301217141e+00)
2	1.1485236628e+01	(4.37585430926e+01, −6.69039944005e+00, −2.56610149092e−01, 1.70903376102e+00)
3	1.1321046566e+01	(4.37240293957e+01, −6.25620042964e+00, −2.39574105051e−01, 1.74655569983e+00)
4	1.1152733288e+01	(4.37675745318e+01, −5.62229590496e+00, −2.14649926510e−01, 1.78436089077e+00)
5	1.0980154177e+01	(4.35089211994e+01, −4.82799184320e+00, −1.83347465212e−01, 1.80865451918e+00)
6	1.0802454544e+01	(4.32226530120e+01, −3.84571340396e+00, −1.44603533348e−01, 1.82732965694e+00)
7	1.0619484295e+01	(4.25243806843e+01, −2.70997766117e+00, −9.97386371548e−02, 1.82657605409e+00)
8	1.0430292744e+01	(4.16628910456e+01, −1.40939476929e+00, −4.83235458265e−02, 1.81245666478e+00)
9	1.0234702320e+01	(4.02817932505e+01, 1.81467268683e−02, 8.18204640558e−03, 1.77302515080e+00)
10	1.0031771052e+01	(3.84999672540e+01, 1.54946772480e+00, 6.88626431563e−02, 1.70778591237e+00)
11	9.8212253563e+00	(3.60965807585e+01, 3.15294489415e+00, 1.32484589900e−01, 1.61129767954e+00)
12	9.6024262387e+00	(3.30037280021e+01, 4.73129817551e+00, 1.95230574044e−01, 1.47523999498e+00)
13	9.3749180129e+00	(2.91609229803e+01, 6.27129559125e+00, 2.56569834778e−01, 1.30076781743e+00)
14	9.1390248144e+00	(2.39414709043e+01, 7.67238191823e+00, 3.12601135363e−01, 1.06314010901e+00)
15	8.8950906687e+00	(1.75803390429e+01, 8.84229708176e+00, 3.59632148056e−01, 7.70429590121e−01)
16	8.6444531496e+00	(9.88532815690e+00, 9.64112370784e+00, 3.92074238174e−01, 4.16075141018e−01)
17	8.3893607950e+00	(2.91016617542e−01, 9.91527824166e+00, 4.03440280820e−01, −1.84749248199e−02)
18	8.1349942117e+00	(−1.21682629238e+01, 9.49406823282e+00, 3.85908930770e−01, −5.63637830626e−01)
19	7.8908221594e+00	(−2.81958350894e+01, 8.32334870019e+00, 3.37763204171e−01, −1.23276529113e+00)

Here, $x_0 = (-0.1218428559, 0.00, 0.00, -3.00096969)$

Table 11 Initial conditions for minimum-time transfer orbits for $\varepsilon = 1$N and $\theta_0 = -\pi/2$ (fixed)

k	t_f	p_0
1	1.1836259008e+01	(1.23953384370e−01, 5.58014204190e+01, −2.34355121544e+00, 7.31217010374e−04)
2	1.1668173067e+01	(−1.12637871873e+00, 5.49368632729e+01, −2.31314733956e+00, 5.02034025451e−02)
3	1.1494977738e+01	(−2.43013759564e+00, 5.37800558199e+01, −2.26636836799e+00, 1.01834227745e−01)
4	1.1316444909e+01	(−3.73867482357e+00, 5.21481628093e+01, −2.19301350363e+00, 1.53734809391e−01)
5	1.1132147759e+01	(−5.03123349646e+00, 5.02184792008e+01, −2.10070221912e+00, 2.05060506552e−01)
6	1.0942085363e+01	(−6.24652949505e+00, 4.76050485755e+01, −1.97431837106e+00, 2.53439391801e−01)
7	1.0745912324e+01	(−7.30567854186e+00, 4.47349782782e+01, −1.82838840429e+00, 2.95710475343e−01)
8	1.0543714233e+01	(−8.17915954565e+00, 4.11508108368e+01, −1.64832839207e+00, 3.30754209295e−01)
9	1.0335506711e+01	(−8.76509910607e+00, 3.70540225185e+01, −1.44156444675e+00, 3.54525410401e−01)
10	1.0121474693e+01	(−8.97432560521e+00, 3.27551946459e+01, −1.22143574046e+00, 3.63463384917e−01)
11	9.9019153074e+00	(−8.80015208947e+00, 2.76983915872e+01, −9.71301869386e−01, 3.57354768910e−01)
12	9.6774814837e+00	(−8.16195680841e+00, 2.27577796399e+01, −7.26323848357e−01, 3.32910646341e−01)
13	9.4484234174e+00	(−7.06575685391e+00, 1.75955941388e+01, −4.79250762317e−01, 2.90388230931e−01)
14	9.2155352697e+00	(−5.60762563079e+00, 1.23669861038e+01, −2.38161479064e−01, 2.33535020863e−01)
15	8.9795679223e+00	(−3.77052273681e+00, 7.74479647932e+00, −3.49039253972e−02, 1.61528029972e−01)
16	8.7414772457e+00	(−1.71785807871e+00, 2.03434555631e+00, 1.96943233655e−01, 8.03156792010e−02)
17	8.5052543934e+00	(5.06092325796e−01, −4.46899050442e+00, 4.42579821491e−01, −8.24699078928e−03)
18	8.2741044454e+00	(2.74485776680e+00, −1.16500671006e+01, 6.94421237073e−01, −9.74865696033e−02)
19	8.0516175632e+00	(4.82917625787e+00, −2.00110461836e+01, 9.71050333412e−01, −1.80716555601e−01)
20	7.8468442012e+00	(6.70860143528e+00, −5.23882372324e+01, 2.10673692237e+00, −2.58577208010e−01)

Here, $x_0 = (-0.012153, -0.10968985, 3.0009696, 0.00)$

Table 12 Local minima of the homotopic path θ_0–t_f for θ_0 fixed and $\varepsilon = 10$N

Num.	t_f	(x_0, p_0)
1	2.5559195559	x0 = (6.21066150680e−02, 8.07302549835e−02, −2.20867323166e+00, 2.03164506327e+00) p0 = (−6.66443552579e+00, −6.25173710798e+00, 2.71700855321e−01, −2.16542651328e−01)
2	2.4877948854	x0 = (5.78471160865e−02, 8.44502708426e−02, −2.31044795603e+00, 1.91511079266e+00) p0 = (−6.28986613857e+00, −6.58580267048e+00, 2.84096838074e−01, −2.05132653869e−01)
3	2.4152338141	x0 = (5.89589525192e−02, 8.35161943465e−02, −2.28489285585e+00, 1.94552917010e+00) p0 = (−6.31179701154e+00, −6.36448410888e+00, 2.80093512573e−01, −2.05851412612e−01)
4	2.3383263886	x0 = (4.30199848124e−02, 9.48040413121e−02, −2.59371345157e+00, 1.50946004928e+00) p0 = (−5.01682430960e+00, −7.53159608900e+00, 3.20380424397e−01, −1.63281437222e−01)
5	1.2164636130	x0 = (3.40824580273e−02, −9.94693265805e−02, 2.72134949944e+00, 1.26494111184e+00) p0 = (4.16086874010e+00, −6.01023069117e+00, 2.79810763690e−01, 8.02669222580e−02)
6	2.6648355866	x0 = (−6.43377120172e−03, 1.09540654392e−01, −2.99688773664e+00, 1.56470551902e−01) p0 = (1.84143605513e+00, 1.15160214759e+01, −5.22937010460e−01, −1.80219702492e−02)
7	2.7553318369	x0 = (−5.24985178093e−02, 1.02000508900e−01, −2.79059930716e+00, −1.10380012079e+00) p0 = (−2.83255512265e+00, 8.32582148917e+00, −4.10828349203e−01, −1.79352374657e−01)

Table 13 Local Minima of the homotopic path θ_0-t_f for θ_0 fixed and $\varepsilon = 5$N

Num.	t_f	(x_0, p_0)
1	3.7536181208	x0 = (−1.94215853959e−02, 1.09448764991e−01, −2.99437376388e+00, −1.98858903633e−01) p0 = (−5.82743545042e−01, −1.45939805915e+01, 5.28108712479e−01, 9.17938940083e−02)
2	3.6509835654	x0 = (−1.69972571399e−02, 1.09582834731e−01, −2.99804173504e+00, −1.32532482085e−01) p0 = (−9.53230835340e−01, −1.42854614796e+01, 5.24210432656e−01, 8.11068337560e−02)
3	3.5439391311	x0 = (−1.68414052537e−02, 1.09589613320e−01, −2.99822718828e+00, −1.28268580164e−01) p0 = (−1.00456664254e+00, −1.39836723639e+01, 5.20093415016e−01, 8.08316251597e−02)
4	3.4300586117	x0 = (−2.71066881650e−02, 1.08665779839e−01, −2.97295232347e+00, −4.09113172891e−01) p0 = (3.57976926298e−01, −1.39256054397e+01, 5.21330369402e−01, 1.28696805687e−01)
5	1.9938793490	x0 = (4.57631694913e−02, −9.31535390469e−02, 2.54855788786e+00, 1.58450996175e+00) p0 = (8.68472172157e+00, -1.16744246852e+01, 5.34314865825e−01, 2.79941139278e−01)
6	5.1452276858	x0 = (−8.18646156795e−02, -8.46885779963e−02, 2.31696772525e+00, −1.90721780228e+00) p0 = (−1.46895925996e+01, −1.67744576566e+01, 7.48345214075e−01, −5.83852266304e−01)
7	5.2618852143	x0 = (6.37976388579e−02, −9.67713587949e−02, 2.64753666151e+00, −1.41292916054e+00) p0 = (−9.33069203371e+00, −1.67310113847e+01, 7.85284331298e−01, −4.04362665917e−01)
8	5.3718352579	x0 = (−5.30765714538e−02, −1.01769965950e−01, 2.78429195632e+00, −1.11961490562e+00) p0 = (−7.46146481108e+00, −1.72142885351e+01, 8.46354933519e−01, −3.20501384394e−01)

Table 14 Local Minima of the homotopic path θ_0-t_f for θ_0 fixed and $\varepsilon = 1\text{N}$

Num.	t_f	(x_0, p_0)
1	1.1613772473	x0 = (−4.94521037379e−02, 1.03153484481e−01, −2.82214319740e+00, −1.02045425234e+00) p0 = (9.01995283736e+00, −3.46406158244e+01, 9.87371645985e−01, 4.85208334522e−01)
2	1.1447550943	x0 = (−3.19708106454e−02, 1.07884748127e−01, −2.95158432661e+00, −5.42189144473e−01) p0 = (2.90230260337e+00, −3.41066967680e+01, 9.95854575771e−01, 3.05746057876e−01)
3	1.1278080850	x0 = (−1.51263711042e−02, 1.09649548919e−01, −2.99986694718e+00, −8.13475092700e−02) p0 = (−2.50988487628e+00, −3.28125831403e+01, 9.83895951743e−01, 1.50964707129e−01)
4	1.1105567895	x0 = (2.95705857691e−03, 1.08644146766e−01, −2.97236047116e+00, 4.13391260989e−01) p0 = (−7.69998223257e+00, −3.02620884245e+01, 9.33675575493e−01, −2.24004350034e−03)
5	1.0929544056	x0 = (2.04744264680e−02, 1.04724952106e−01, −2.86513647766e+00, 8.92643327742e−01) p0 = (−1.21596048543e+01, −2.71809934984e+01, 8.71972929361e−01, −1.36697854580e−01)
6	1.0750144861	x0 = (3.83142161995e−02, 9.73905775437e−02, −2.66447766925e+00, 1.38071643052e+00) p0 = (−1.59157802958e+01, −2.29695613710e+01, 7.73993351114e−01, −2.54453250197e−01)
7	1.0566954554	x0 = (5.44818172342e−02, 8.71301649529e−02, −2.38376632206e+00, 1.82304065745e+00) p0 = (−1.86958979730e+01, −1.85218216807e+01, 6.71937688249e−01, −3.48430037725e−01)
8	1.0379987132	x0 = (6.88212850245e−02, 7.39934433897e−02, −2.02436295744e+00, 2.21534957152e+00) p0 = (−2.02518665484e+01, −1.35149987541e+01, 5.52549152903e−01, −4.05199546746e−01)
9	1.0188925627	x0 = (8.03393763200e−02, 5.89663024700e−02, −1.61324021412e+00, 2.53046934823e+00) p0 = (−2.08004284902e+01, −8.77291310702e+00, 4.43835886576e−01, −4.38897740719e−01)
10	9.9936149094	x0 = (8.95455084671e−02, 4.11008259435e−02, −1.12446435452e+00, 2.78233697387e+00) p0 = (−2.00552248948e+01, -3.91048195304e+00, 3.29850374180e−01, −4.36668392516e−01)
11	9.7938762650	x0 = (9.53384673112e−02, 2.18506056371e−02, −5.97803732642e−01, 2.94082468252e+00) p0 = (−1.84286807100e+01, 3.08770987062e−01, 2.33200787107e−01, −4.17738961747e−01)
12	9.5893510522	x0 = (9.75357647120e−02, 4.89297497890e−04, −1.33865337862e−02, 3.00093983950e+00) p0 = (−1.55475035168e+01, 3.99090490857e+00, 1.50081331902e−01, −3.64314206604e−01)
13	9.3800526379	x0 = (9.55661265389e−02, −2.06991372746e−02, 5.66301077909e−01, 2.94705313854e+00) p0 = (−1.21277045301e+01, 6.54661511552e+00, 9.57838813041e−02, −3.03714475156e−01)
14	9.1654637945	x0 = (8.88535253959e−02, −4.27731969234e−02, 1.17021821740e+00, 2.76340523030e+00) p0 = (−7.71976404968e+00, 7.84981751360e+00, 7.58962825540e−02, −2.16097777716e−01)
15	8.9466593775	x0 = (7.66012223247e−02, −6.44558182773e−02, 1.76342612175e+00, 2.42819838839e+00) p0 = (−2.49582677532e+00, 7.08434895345e+00, 1.15517251704e−01, −1.06074141800e−01)
16	8.7241872271	x0 = (5.72812946469e−02, −8.49160952469e−02, 2.32319229695e+00, 1.89963066482e+00) p0 = (2.35166174593e+00, 3.73477013320e+00, 2.26388522820e−01, −1.23043980769e−02)
17	8.4992141171	x0 = (3.14063514616e−02, −1.00669992540e−01, 2.75419813551e+00, 1.19172636803e+00) p0 = (5.39316031292e+00, −2.35824421954e+00, 4.16994199205e−01, 2.06174555327e−02)
18	8.2736157050	x0 = (3.92050344557e−05, −1.09010158391e−01, 2.98237406617e+00, 3.33562638939e−01) p0 = (4.93801945083e+00, −1.09681340969e+01, 6.81788653598e−01, −5.92784509757e−02)
19	8.0504545877	x0 = (−3.23905959857e−02, −1.07806791098e−01, 2.94945152519e+00, −5.53673917369e−01) p0 = (−5.59633476936e−01, −2.08904205668e+01, 9.86344334901e−01, −3.07897514898e−01)
20	7.8363385435	x0 = (−6.50028495259e−02, −9.61184576538e−02, 2.62967414796e+00, −1.44590213383e+00) p0 = (−1.65966613960e+01, −3.56290598456e+01, 1.46688275370e+00, −9.16052717119e−01)

6 Tables from GEO to MO Transfer Problem

Table 15 ($\mathscr{C}_1$ class) Initial conditions for minimum-time transfer orbits for $\varepsilon = 10$N and $\theta_0 = \pi$, $x_0 = (-0.121842, 0.00, 0.00, -3.00096)$

k	t_f	p_0
1	2.6295366742	(1.06192601736e+01, 1.37248310916e+00, 5.35735968598e−02, 4.25981151967e−01)
2	2.5591513809	(1.03908338033e+01, 1.40394233209e+00, 5.51645610936e−02, 4.14831750559e−01)
3	2.4845856122	(1.01139459577e+01, 1.46253515025e+00, 5.78478667723e−02, 4.02851462389e−01)
4	2.4046902936	(9.78964388018e+00, 1.48536195756e+00, 5.92289931606e−02, 3.87549322564e−01)
5	2.3188203948	(9.43753819675e+00, 1.55135836535e+00, 6.23078750780e−02, 3.72156376196e−01)
6	2.2258097799	(8.94542905348e+00, 1.56715282851e+00, 6.36188551329e−02, 3.50206904265e−01)
7	2.1236421514	(8.46157104228e+00, 1.62768549326e+00, 6.66669404664e−02, 3.28774925899e−01)
8	2.0109987788	(7.64680356801e+00, 1.65788540815e+00, 6.89101321311e−02, 2.94809550939e−01)
9	1.8831760208	(6.90929970278e+00, 1.67399427716e+00, 7.05530473416e−02, 2.62079313820e−01)
10	1.7368384045	(5.39899067667e+00, 1.74013293816e+00, 7.49642789303e−02, 2.01920571395e−01)
11	1.5620914595	(3.92859812720e+00, 1.65447845805e+00, 7.34194614218e−02, 1.40088341785e−01)
12	1.3450368533	(−1.07601143153e−01, 1.77014236738e+00, 8.04240137313e−02, −1.74291709898e−02)
13	2.7874623764	(−6.49469099937e+00, −2.98006923087e+00, −1.14119319520e−01, −2.75907575312e−01)
14	2.8890843383	(−4.08758212257e+00, −2.98692269111e+00, −1.12596624508e−01, −2.15040713745e−01)

7 Summary of the Cut Points on the GEO to L_1 Transfer

In this Appendix we summarize the results for the all the CUT points that we have found for the GEO to L_1 transfer problem. The initial conditions for the CUT points are summarized in Table 3. For each pair of cut points we have done the same analysis. First for each cut point we have computed the transfer trajectory, the energy variation along the trajectory ($J_c(t)$), the control along the trajectory and also the variation of

Table 16 ($\mathscr{C}_1$ class) Initial conditions for minimum-time transfer orbits for $\varepsilon = 10$N and $\theta_0 = 0$, $x_0 = (0.0975368, 0.00, 0.00, 3.00096)$

k	t_f	p_0
1	2.6382335901	(−8.15469444647e+00, 1.70467856003e−01, 2.36653029038e−03, −2.73809684344e−01)
2	2.5701583528	(−8.02693895139e+00, 2.42252173754e−01, 5.11383610870e−03, −2.71042424433e−01)
3	2.4971963201	(−7.80352301218e+00, 3.38330092208e−01, 8.68257649872e−03, −2.63922213562e−01)
4	2.4206053972	(−7.62548760869e+00, 4.10629220864e−01, 1.14039103010e−02, −2.59643712704e−01)
5	2.3373895493	(−7.36482326796e+00, 5.01793409601e−01, 1.47652984972e−02, −2.52022253778e−01)
6	2.2491972124	(−7.09747508042e+00, 5.76972246145e−01, 1.75119377896e−02, −2.44905008216e−01)
7	2.1515314965	(−6.76586878979e+00, 6.50789920666e−01, 2.01398087796e−02, −2.35723176492e−01)
8	2.0463772193	(−6.32305321005e+00, 7.36876168589e−01, 2.31369509217e−02, −2.22847227010e−01)
9	1.9265529833	(−5.83277580845e+00, 7.67061071412e−01, 2.38895759600e−02, −2.09001197960e−01)
10	1.7936072565	(−4.97749858940e+00, 8.76114686754e−01, 2.73632618304e−02, −1.82379844772e−01)
11	1.6348670072	(−4.03983916332e+00, 8.17496491769e−01, 2.41026868298e−02, −1.53093741527e−01)
12	1.4489820024	(−1.21477895977e+00, 1.08381100292e+00, 3.18058539495e−02, −5.93687133649e−02)
13	1.6913726515	(1.92911022593e+02, 4.09909700389e+00, 3.68559661513e−01, 6.83488813468e+00)
14	2.7288387842	(3.09692369616e+00, −2.60108464159e+00, −1.12213330995e−01, 2.17133715663e−02)
15	2.8589830417	(−2.22653391549e+00, −2.36994535022e+00, −9.99958635019e−02, −1.85205984442e−01)

$H_{1,2}$. Moreover, for each cut solution we have integrated both optimal solutions back and forward in time ($t \in [-t_f, 2t_t]$, where t_f is the transfer time). Finally, for the solutions on the homotopic curve close to them ($t_f^* \in [t_f - 0.15 : t_f + 0.15]$), for each solutions we have computed some distinctive parameters of the transfer orbits, trying to characterize their passage. In the plots that we will see, the number of turns around the Earth, and the number of times that $|(H_1, H_2)|$ comes close to zero (in particular $|(H_1, H_2)| < 0.05$).

In Fig. 70 we show the homotopic curve t_f versus ε and the same curve plotting θ_0 versus ε, where θ_0 in the angle that parameterizes the initial condition on the departure GEO orbit. In both plots we have highlighted in green the solutions close to the CUT pair, which are the solutions that we have analyzed. Figures 71, 72 and

Table 17 ($\mathscr{C}_1$ class) Initial conditions for minimum-time transfer orbits for $\varepsilon = 10$N and $\theta_0 = \pi/2$, $x_0 = (-0.012153, 0.109689, -3.00096, 0.00)$

k	t_f	p_0
1	2.6338132940	(−2.58170927519e−01, −1.00417479238e+01, 4.05017074760e−01, 1.00460710975e−02)
2	2.5653207218	(−2.07888498661e−01, −9.89425530106e+00, 3.99790676407e−01, 7.89106089518e−03)
3	2.4924927065	(−1.85843554959e−01, −9.77354474323e+00, 3.97814405932e−01, 6.95648216568e−03)
4	2.4150831353	(−1.25626071521e−01, −9.55623627017e+00, 3.89793003207e−01, 4.31969409249e−03)
5	2.3315729003	(−8.39820060625e−02, −9.37472183474e+00, 3.85532601096e−01, 2.53783657098e−03)
6	2.2419382962	(−1.31487906225e−02, −9.04030262447e+00, 3.73024539442e−01, −6.61312444426e−04)
7	2.1431311332	(5.52757105262e−02, −8.74409478565e+00, 3.64176114835e−01, −3.64700523503e−03)
8	2.0354632450	(1.38587221198e−01, −8.18964778994e+00, 3.43706754821e−01, −7.59222655671e−03)
9	1.9127093077	(2.42801592628e−01, −7.64937021577e+00, 3.24724323237e−01, −1.23124693731e−02)
10	1.7749732845	(3.49911359159e−01, −6.58187830265e+00, 2.86744744526e−01, −1.77517569581e−02)
11	1.6089306960	(4.95907841498e−01, −5.40397217878e+00, 2.41166917636e−01, −2.49571014357e−02)
12	1.4102828725	(7.23053068198e−01, −2.59378036965e+00, 1.46469675587e−01, −3.68627889085e−02)
13	2.4479531178	(−3.38396896021e+00, 9.49237142101e+01, −3.37779371321e+00, 2.29212476015e−01)
14	2.6779763301	(1.19830766801e+00, 1.13780127873e+01, −5.12382210052e−01, −4.39638576402e−02)
15	2.7791837819	(2.81655473172e+00, 5.61007167226e+00, −2.93511162565e−01, −1.14270102398e−01)

73 summarize the results for the first cut point. Similarly, Figs. 74, 75 and 76 for the second cut point, Figs. 77, 78 and 79 for the third cut point, Figs. 80, 81 and 82 for the forth cut point, Figs. 83, 84 and 85 for the fifth cut point, Figs. 86, 87 and 88 for the sixth cut point, and finally Figs. 89, 90 and 91 for the seventh cut point.

Table 18 ($\mathscr{C}_1$ class) Initial conditions for minimum-time transfer orbits for $\varepsilon = 10$N and $\theta_0 = 3\pi/2$, $x_0 = (-0.012153, -1.096898, 3.000969, 0.00)$

k	t_f	p_0
1	2.6690810760	(−1.60148685709e+00, 9.08946766361e+00, −3.13300481199e−01, 6.61185213214e−02)
2	2.6008623676	(−1.54788345969e+00, 8.80209189253e+00, −2.99932270379e−01, 6.44329166721e−02)
3	2.5287091355	(−1.48776605296e+00, 8.47773003663e+00, −2.85028133227e−01, 6.25395502059e−02)
4	2.4519026572	(−1.40500394555e+00, 8.15666769590e+00, −2.70463857125e−01, 5.97473478092e−02)
5	2.3697031266	(−1.34275441268e+00, 7.70451974629e+00, −2.50533464519e−01, 5.79263564017e−02)
6	2.2813887573	(−1.22186934790e+00, 7.34625820586e+00, −2.34873041588e−01, 5.36733452623e−02)
7	2.1850625115	(−1.14306384179e+00, 6.70918812205e+00, −2.08000594543e−01, 5.14177402740e−02)
8	2.0802601077	(−9.84194129457e−01, 6.25065652108e+00, −1.89113692261e−01, 4.57761908262e−02)
9	1.9625235243	(−8.70139276974e−01, 5.33149659787e+00, −1.52203685456e−01, 4.24464538424e−02)
10	1.8314874695	(−6.71790327170e−01, 4.57367060157e+00, −1.22999765824e−01, 3.55761395655e−02)
11	1.6770533301	(−4.99447542856e−01, 3.10421985352e+00, −6.71298805584e−02, 3.05143051338e−02)
12	1.4969723177	(−2.11266620451e−01, 1.19696152516e+00, 3.54958676405e−03, 2.08238576227e−02)
13	1.2945503501	(5.15688868736e−01, −4.36713996233e+00, 2.05263933984e−01, −1.38119494149e−02)
14	2.7873443220	(1.63345406733e+00, −2.65524823134e+00, −6.44278753506e−04, −5.30504819040e−02)
15	2.8935039376	(2.05298326674e+00, 6.37332707982e−01, −1.25355445474e−01, −7.25661087416e−02)

Table 19 ($\mathscr{C}_2$ class) Initial conditions for minimum-time transfer orbits for $\varepsilon = 10$N and $\theta_0 = \pi$, $x_0 = (-0.121842, 0.00, 0.00, -3.00096)$

k	t_f	p_0
1	2.5980387359	(1.06435287264e+01, 1.38139088237e+00, 5.38698217696e−02, 4.27687562930e−01)
2	2.5276171200	(1.04197332870e+01, 1.41679263649e+00, 5.56093693046e−02, 4.16741367382e−01)
3	2.4530424463	(1.01354110133e+01, 1.47583141615e+00, 5.83202062677e−02, 4.04443207658e−01)
4	2.3730813733	(9.81815625576e+00, 1.50226355964e+00, 5.98360979453e−02, 3.89358210983e−01)
5	2.2872021224	(9.45271738688e+00, 1.56932212509e+00, 6.29723565050e−02, 3.73464035481e−01)
6	2.1940824150	(8.97261257687e+00, 1.58768227806e+00, 6.43744566344e−02, 3.51814760713e−01)
7	2.0918861292	(8.47506952249e+00, 1.65281951424e+00, 6.76178742737e−02, 3.29905135280e−01)
8	1.9790911917	(7.67374927169e+00, 1.67928450120e+00, 6.97076840290e−02, 2.96143235096e−01)
9	1.8511363857	(6.91696727321e+00, 1.70718186065e+00, 7.18325734637e−02, 2.62736457777e−01)
10	1.7045623193	(5.39278478726e+00, 1.77172229454e+00, 7.62018032334e−02, 2.01790101767e−01)
11	1.5293474752	(3.92175802120e+00, 1.69616859547e+00, 7.50545446867e−02, 1.39620793489e−01)
12	1.3121055642	(−4.07540989225e−01, 1.82698024096e+00, 8.24995437375e−02, −2.93268907749e−02)
13	2.7349672541	(−6.44652936791e+00, −3.03741643602e+00, −1.16238481485e−01, −2.70092491562e−01)
14	2.8348007566	(−4.08335716722e+00, −3.09857369694e+00, −1.16936332793e−01, −2.10233821136e−01)

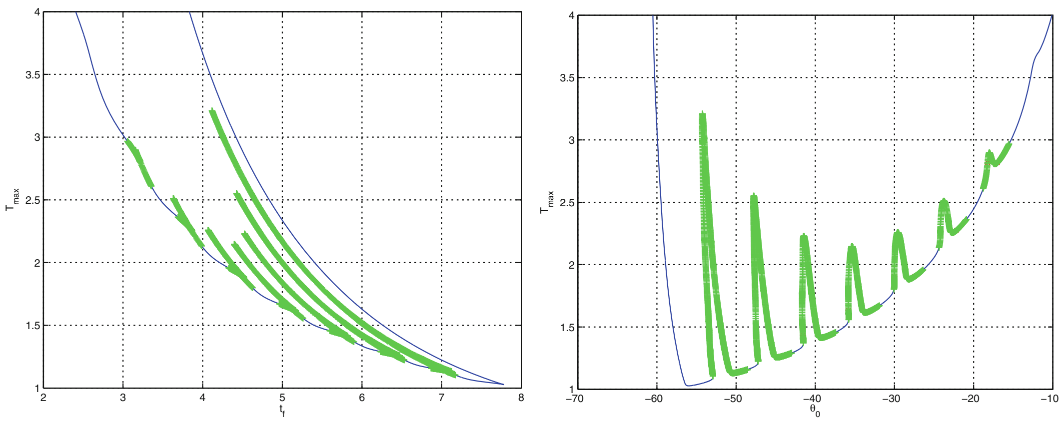

Fig. 70 For the GEO to L_1 control problem, homotopic curve for $\varepsilon \in [1:10]$N. *Left* t_f (transfer time) versus ε projection. *Right* θ_0 (angle defining the initial position on the departure orbit) versus ε

Table 20 ($\mathscr{C}_2$ class) Initial conditions for minimum-time transfer orbits for $\varepsilon = 10$N and $\theta_0 = 0$, $x_0 = (0.0975368, 0.00, 0.00, 3.00096)$

k	t_f	p_0
1	2.6061700198	(−8.10712545558e+00, 1.89540042126e−01, 3.02951748274e−03, −2.70993641088e−01)
2	2.5380201140	(−7.98832817545e+00, 2.59775949334e−01, 5.73286770389e−03, −2.68755580138e−01)
3	2.4650494180	(−7.75538520280e+00, 3.62884468178e−01, 9.56534705873e−03, −2.61182580565e−01)
4	2.3883796279	(−7.58970803264e+00, 4.31241026849e−01, 1.21532458177e−02, −2.57593525824e−01)
5	2.3051381815	(−7.31720208022e+00, 5.32166005246e−01, 1.58845821085e−02, −2.49451562603e−01)
6	2.2168668949	(−7.06641305915e+00, 5.99411681487e−01, 1.83454693321e−02, −2.43199556855e−01)
7	2.1191349339	(−6.71997726657e+00, 6.87257241108e−01, 2.15107998020e−02, −2.33438167469e−01)
8	2.0139211293	(−6.29894313030e+00, 7.57106564979e−01, 2.38986154068e−02, −2.21599131661e−01)
9	1.8939163357	(−5.78936380987e+00, 8.09971284648e−01, 2.55311678798e−02, −2.07142760589e−01)
10	1.7610136117	(−4.96411319056e+00, 8.97635598020e−01, 2.81969305386e−02, −1.81740722662e−01)
11	1.6017081412	(−3.99249110713e+00, 8.68838412584e−01, 2.60957559015e−02, −1.51674639469e−01)
12	1.4167921654	(−1.11120743455e+00, 1.13046941869e+00, 3.35818304486e−02, −5.59741017211e−02)
13	1.6556450929	(1.90041169951e+02, 4.11177240588e+00, 3.65721183952e−01, 6.73092385668e+00)
14	2.6740283644	(3.36137910646e+00, −2.72778518065e+00, −1.16970922525e−01, 3.45243380243e−02)
15	2.8030960157	(−2.11859368374e+00, −2.49178961344e+00, −1.04892810539e−01, −1.79419042463e−01)

Table 21 ($\mathscr{C}_2$ class) Initial conditions for minimum-time transfer orbits for $\varepsilon = 10$N and $\theta_0 = \pi/2$, $x_0 = (-0.012153, 0.109689, -3.00096, 0.00)$

k	t_f	p_0
1	2.6019829845	(−2.84425571457e−01, −1.00404237110e+01, 4.05458442869e−01, 1.10979295268e−02)
2	2.5334348861	(−2.32569565646e−01, −9.89968792431e+00, 4.00560274651e−01, 8.89110982802e−03)
3	2.4606436274	(−2.10541872966e−01, −9.77638734159e+00, 3.98549565013e−01, 7.95603536659e−03)
4	2.3831582744	(−1.47706167233e−01, −9.56627413895e+00, 3.90837330674e−01, 5.22553690464e−03)
5	2.2996872805	(−1.06156499893e−01, −9.38234623244e+00, 3.86599531240e−01, 3.44800514348e−03)
6	2.2099469387	(−3.14884828915e−02, −9.05530130469e+00, 3.74338881818e−01, 1.05119003627e−04)
7	2.1111698233	(3.71188462151e−02, −8.75716517386e+00, 3.65618710498e−01, −2.88387786486e−03)
8	2.0033553989	(1.25544557986e−01, −8.20997380954e+00, 3.45244907817e−01, −7.02816735224e−03)
9	1.8805738016	(2.31302088017e−01, −7.66818254447e+00, 3.26583609500e−01, −1.17992930350e−02)
10	1.7426682066	(3.43556047009e−01, −6.60492748194e+00, 2.88284900044e−01, −1.74520049392e−02)
11	1.5763097264	(4.97275584574e−01, −5.42450563786e+00, 2.43378420465e−01, −2.49405258515e−02)
12	1.3781347238	(7.28625942842e−01, −2.47538707912e+00, 1.43995244406e−01, −3.71575252603e−02)
13	2.4048352258	(−3.39252896456e+00, 9.36495680309e+01, −3.33176058888e+00, 2.28072959760e−01)
14	2.6257251580	(1.05189499044e+00, 1.14191299701e+01, −5.15529286934e−01, −3.80961922524e−02)
15	2.7236432248	(2.60098969942e+00, 6.24273168138e+00, −3.24847143004e−01, −1.04909522361e−01)

Table 22 ($\mathscr{C}_2$ class) Initial conditions for minimum-time transfer orbits for $\varepsilon = 10$N and $\theta_0 = 3\pi/2$, $x_0 = (-0.012153, -1.096898, 3.000969, 0.00)$

k	t_f	p_0
1	2.6374327060	$(-1.62857972444\text{e}{+}00, 9.08391575714\text{e}{+}00, -3.12602494846\text{e}{-}01, 6.72031001922\text{e}{-}02)$
2	2.5691569872	$(-1.57643427418\text{e}{+}00, 8.78702892946\text{e}{+}00, -2.98800874499\text{e}{-}01, 6.55880396062\text{e}{-}02)$
3	2.4969636719	$(-1.51162908577\text{e}{+}00, 8.46917014342\text{e}{+}00, -2.84073535582\text{e}{-}01, 6.35051396988\text{e}{-}02)$
4	2.4200699217	$(-1.43149645719\text{e}{+}00, 8.13260148526\text{e}{+}00, -2.68828877698\text{e}{-}01, 6.08371578637\text{e}{-}02)$
5	2.3378362689	$(-1.36493857285\text{e}{+}00, 7.68625412066\text{e}{+}00, -2.49019602217\text{e}{-}01, 5.88430641217\text{e}{-}02)$
6	2.2493898782	$(-1.24390573655\text{e}{+}00, 7.31082683074\text{e}{+}00, -2.32688325847\text{e}{-}01, 5.46051794303\text{e}{-}02)$
7	2.1530090828	$(-1.16282817958\text{e}{+}00, 6.67343179150\text{e}{+}00, -2.05563880726\text{e}{-}01, 5.22675189137\text{e}{-}02)$
8	2.0480368975	$(-1.00003739357\text{e}{+}00, 6.20872801454\text{e}{+}00, -1.86460126643\text{e}{-}01, 4.64792293390\text{e}{-}02)$
9	1.9301495747	$(-8.83664790191\text{e}{-}01, 5.26814185126\text{e}{+}00, -1.48387158771\text{e}{-}01, 4.30927981545\text{e}{-}02)$
10	1.7989149784	$(-6.76316263624\text{e}{-}01, 4.52955863451\text{e}{+}00, -1.20054957255\text{e}{-}01, 3.58431970542\text{e}{-}02)$
11	1.6440341344	$(-4.97450251574\text{e}{-}01, 2.98177731120\text{e}{+}00, -6.06185355582\text{e}{-}02, 3.06225341296\text{e}{-}02)$
12	1.4638781887	$(-1.91345523973\text{e}{-}01, 1.13707535911\text{e}{+}00, 7.19728539102\text{e}{-}03, 2.00319879174\text{e}{-}02)$
13	1.2629462369	$(5.27114903375\text{e}{-}01, -4.53699320696\text{e}{+}00, 2.12661485766\text{e}{-}01, -1.45016746772\text{e}{-}02)$
14	2.7339401945	$(1.55300153992\text{e}{+}00, -2.64703138256\text{e}{+}00, -3.90733403113\text{e}{-}03, -4.97729160780\text{e}{-}02)$
15	2.8391341334	$(1.96486277754\text{e}{+}00, 6.95609002372\text{e}{-}01, -1.31187447456\text{e}{-}01, -6.91977913949\text{e}{-}02)$

Table 23 ($\mathscr{C}_3$ class) Initial conditions for minimum-time transfer orbits for $\varepsilon = 10$N and $\theta_0 = \pi$, $x_0 = (-0121842, 0.00, 0.00, -3.00096)$

k	t_f	p_0
1	3.0079434320	(1.06644572264e+01, 1.35187551484e+00, 5.26512270100e−02, 4.29500793828e−01)
2	2.9375415112	(1.04434578826e+01, 1.38953138641e+00, 5.44744339982e−02, 4.18722639089e−01)
3	2.8630041962	(1.01618362339e+01, 1.45007088633e+00, 5.72390673417e−02, 4.06603688803e−01)
4	2.7830629302	(9.84764443081e+00, 1.47895907175e+00, 5.88472004949e−02, 3.91667351531e−01)
5	2.6972242903	(9.48496629685e+00, 1.54853782815e+00, 6.20765991896e−02, 3.75979183483e−01)
6	2.6041287654	(9.00869563804e+00, 1.56903828964e+00, 6.35588503243e−02, 3.54472174794e−01)
7	2.5019691384	(8.51291261627e+00, 1.63845183385e+00, 6.69650951886e−02, 3.32749964057e−01)
8	2.3892198510	(7.71967340255e+00, 1.66527871957e+00, 6.90619941530e−02, 2.99253127735e−01)
9	2.2612723039	(6.96040246349e+00, 1.70115071916e+00, 7.14998649587e−02, 2.65876126446e−01)
10	2.1147973125	(5.44320887379e+00, 1.76777958465e+00, 7.59453383727e−02, 2.05235264592e−01)
11	1.9395064592	(3.97334759818e+00, 1.70032824652e+00, 7.51188225176e−02, 1.43112186670e−01)
12	1.7223793899	(−3.49402376257e−01, 1.84952575418e+00, 8.34028988787e−02, −2.52900821308e−02)
13	3.1156574206	(−6.51510558872e+00, −3.08751946862e+00, −1.18263364650e−01, −2.70782400660e−01)
14	3.2127569407	(−4.21028083233e+00, −3.19576818179e+00, −1.20901762188e−01, −2.12539884711e−01)

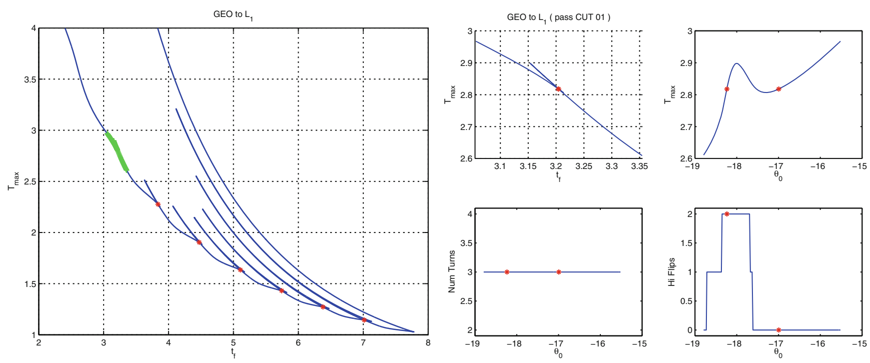

Fig. 71 For cut point n^o 1: (*left*) t_f versus ε homotopic curve with highlight of the cut passage in *green*; (*right*) analysis of the cut passage: (*top-left* subplot) t_f versus ε zoom, (*top-right* subplot) θ_0 versus ε, (*bottom-left* subplot) θ_0 versus num. turns around the Earth, (*bottom-right* subplot) θ_0 versus the number of times $|(H_1, H_2)|$ passes close to zero. *Red* points are values corresponding the each cut point

Table 24 ($\mathscr{C}_3$ class) Initial conditions for minimum-time transfer orbits for $\varepsilon = 10$N and $\theta_0 = 0$, $x_0 = (0.0975368, 0.00, 0.00, 3.00096)$

k	t_f	p_0
1	3.0160686346	(−8.07952473541e+00, 1.56009762355e−01, 1.63190503522e−03, −2.68719969249e−01)
2	2.9478762607	(−7.96124497160e+00, 2.28947488502e−01, 4.44172318728e−03, −2.66486754726e−01)
3	2.8748808644	(−7.72016520272e+00, 3.34226564842e−01, 8.34507374051e−03, −2.58467672325e−01)
4	2.7981671236	(−7.55602926960e+00, 4.05394083101e−01, 1.10454479194e−02, −2.54931109877e−01)
5	2.7148931246	(−7.27415717237e+00, 5.09903199832e−01, 1.49025953133e−02, −2.46306617667e−01)
6	2.6265776367	(−7.02615679895e+00, 5.80035014991e−01, 1.74807801082e−02, −2.40158650743e−01)
7	2.5288032793	(−6.66921179529e+00, 6.73203679187e−01, 2.08407300183e−02, −2.29902094968e−01)
8	2.4235482061	(−6.25292923064e+00, 7.45932195898e−01, 2.33480462145e−02, −2.18236701100e−01)
9	2.3034863018	(−5.73159256933e+00, 8.06189964121e−01, 2.52583831813e−02, −2.03303437857e−01)
10	2.1710299861	(−4.91544276746e+00, 8.96489918177e−01, 2.80205574326e−02, −1.78204644826e−01)
11	2.0111660933	(−3.92900285748e+00, 8.77250871764e−01, 2.63023408558e−02, −1.47666820427e−01)
12	1.8264984515	(−1.00305568125e+00, 1.15297499904e+00, 3.43275408112e−02, −5.02059871398e−02)
13	2.0431049217	(1.86578177364e+02, 4.08561828326e+00, 3.60755982581e−01, 6.60857596413e+00)
14	3.0540126835	(3.61881934098e+00, −2.81462056517e+00, −1.20190778166e−01, 4.54101687908e−02)
15	3.2018637194	(−1.96637660380e+00, −2.60107142593e+00, −1.09312588413e−01, −1.72944354724e−01)

Table 25 ($\mathscr{C}_3$ class) Initial conditions for minimum-time transfer orbits for $\varepsilon = 10\text{N}$ and $\theta_0 = \pi/2$, $x_0 = (-0.012153, 0.109689, -3.00096, 0.00)$

k	t_f	p_0
1	3.0114201851	(−3.17790993078e−01, −9.99620628532e+00, 4.02877878386e−01, 1.23338642431e−02)
2	2.9428784342	(−2.66437255556e−01, −9.85807299220e+00, 3.98162529647e−01, 1.01525525586e−02)
3	2.8700856406	(−2.47561176375e−01, −9.73541452344e+00, 3.96250079704e−01, 9.34509289696e−03)
4	2.7926111380	(−1.84912105298e−01, −9.52892872608e+00, 3.88770128141e−01, 6.62912797585e−03)
5	2.7091438748	(−1.46456526906e−01, −9.34583623592e+00, 3.84664090025e−01, 4.97786212278e−03)
6	2.6194200750	(−7.15636845081e−02, −9.02376276247e+00, 3.72690032847e−01, 1.63487427495e−03)
7	2.5206527435	(−5.76199475645e−03, −8.72666992070e+00, 3.64151059255e−01, −1.23792031755e−03)
8	2.4128647384	(8.32099513855e−02, −8.18644238539e+00, 3.44124212000e−01, −5.39328168163e−03)
9	2.2900952639	(1.87090924654e−01, −7.64565340599e+00, 3.25712424499e−01, −1.00831811499e−02)
10	2.1522470577	(2.99246181934e−01, −6.59424327083e+00, 2.87877672276e−01, −1.57184440223e−02)
11	1.9858762347	(4.53674686372e−01, −5.41187749151e+00, 2.43244220883e−01, −2.32284106856e−02)
12	1.7880235904	(6.80299038636e−01, −2.46145430043e+00, 1.44255335142e−01, −3.52558523439e−02)
13	2.7896443361	(−3.41374362314e+00, 9.32731850142e+01, −3.31755914190e+00, 2.28456530459e−01)
14	3.0074529459	(9.87115821527e−01, 1.15185661024e+01, −5.20294817745e−01, −3.53915049620e−02)
15	3.1016075052	(2.46829014099e+00, 6.81961761072e+00, −3.51739669061e−01, −9.88979615343e−02)

Table 26 ($\mathscr{C}_3$ class) Initial conditions for minimum-time transfer orbits for $\varepsilon = 10$N and $\theta_0 = 3\pi/2$, $x_0 = (-0.012153, -1.096898, 3.000969, 0.00)$

k	t_f	p_0
1	3.0477620262	(−1.65436243883e+00, 9.13015536385e+00, −3.15423464048e−01, 6.81362816051e−02)
2	2.9795368970	(−1.60623443630e+00, 8.83016269889e+00, −3.01446202255e−01, 6.66677453622e−02)
3	2.9073039428	(−1.54133345202e+00, 8.51559503544e+00, −2.86806843906e−01, 6.45849249114e−02)
4	2.8304040772	(−1.46607509242e+00, 8.17299095306e+00, −2.71226012966e−01, 6.21184798314e−02)
5	2.7481886105	(−1.39982960612e+00, 7.73048160814e+00, −2.51533856789e−01, 6.01327857674e−02)
6	2.6597101749	(−1.28312320054e+00, 7.34735121468e+00, −2.34755001038e−01, 5.60784042063e−02)
7	2.5633588116	(−1.20420297838e+00, 6.70973715294e+00, −2.07551473300e−01, 5.38271396019e−02)
8	2.4583262887	(−1.04355838469e+00, 6.24074714632e+00, −1.88118009827e−01, 4.81332584817e−02)
9	2.3404678233	(−9.30788833999e−01, 5.29153019869e+00, −1.49557187330e−01, 4.49012589544e−02)
10	2.2091494228	(−7.23352672817e−01, 4.55685507376e+00, −1.21226959607e−01, 3.76477925265e−02)
11	2.0542769577	(−5.48043592799e−01, 2.98526534387e+00, −6.05924194202e−02, 3.25919877337e−02)
12	1.8739945514	(−2.41372435293e−01, 1.16542210106e+00, 6.40892432862e−03, 2.19566013991e−02)
13	1.6724924789	(4.78305672369e−01, −4.56845039900e+00, 2.15049807592e−01, −1.26469413261e−02)
14	3.1147430656	(1.52316731297e+00, −2.69581657727e+00, −4.16727729788e−03, −4.85564981134e−02)
15	3.2177755237	(1.94272857430e+00, 6.29139383819e−01, −1.31608874036e−01, −6.83226668898e−02)

Table 27 ($\mathscr{C}_1$ class) Local Minima of the homotopic path θ_0-t_f for θ_0 fixed and $\varepsilon = 10$N

Num.	t_f	(x_0, p_0)
1	2.6344109813	x0 = (−6.61692049717e−02, 9.54678694392e−02, −2.61187491303e+00, −1.47781207951e+00) p0 = (5.40200904069e+00, −9.04436482091e+00, 3.81168153429e−01, 2.05269577680e−01)
2	2.5654788135	x0 = (−4.52828715879e−02, 1.04567089008e−01, −2.86081755165e+00, −9.06389563114e−01) p0 = (3.15983116724e+00, −9.70188823099e+00, 3.98877317690e−01, 1.23233133448e−01)
3	2.4925251859	x0 = (−2.95411256412e−02, 1.08302897416e−01, −2.96302433931e+00, −4.75716169365e−01) p0 = (1.54563324437e+00, −9.81613709586e+00, 4.01898104211e−01, 6.56372972600e−02)
4	2.7946382317	x0 = (−8.62590901998e−02, −8.08712057808e−02, 2.21252945945e+00, −2.02744482549e+00) p0 = (−6.36693882796e−01, −4.91318631097e+00, 7.08068709438e−03, −1.47732494031e−01)
5	2.8956929200	x0 = (−7.16101551794e−02, −9.21776070570e−02, 2.52185767661e+00, −1.62666929644e+00) p0 = (2.02907798275e+00, −2.75514593814e+00, −6.83047057606e−02, −9.50712106843e−02)

Table 28 ($\mathscr{C}_2$ class) Local Minima of the homotopic path θ_0-t_f for θ_0 fixed and $\varepsilon = 10\text{N}$

Num.	t_f	(x_0, p_0)
1	2.6027273646	x0 = (−7.08353877411e−02, 9.26727676532e−02, −2.53540461703e+00, −1.60547268183e+00) p0 = (5.89933290763e+00, −8.78036555972e+00, 3.73602572575e−01, 2.24143289427e−01)
2	2.5336945761	x0 = (−5.28636779641e−02, 1.01855315024e−01, −2.78662699434e+00, −1.11379042071e+00) p0 = (3.94605260276e+00, −9.49349757966e+00, 3.93894887009e−01, 1.51870763055e−01)
3	2.4607414965	x0 = (−3.58852334423e−02, 1.07091762478e−01, −2.92988928582e+00, −6.49282586092e−01) p0 = (2.17392046524e+00, −9.75993925757e+00, 4.01617069536e−01, 8.86090945569e−02)
4	2.7418546856	x0 = (−8.84246217632e−02, −7.88321267809e−02, 2.15674294911e+00, −3.08669091108e+00) p0 = (−7.80575217720e−01, −4.91458653148e+00, 2.36855239340e−03, −1.47525204726e−01)
5	2.8414849743	x0 = (−7.36542225280e−02, −9.08265606530e−02, 2.48489483006e+00, −1.68259228141e+00) p0 = (1.96421647292e+00, −2.81151922798e+00, −7.22948807464e−02, −9.24617336107e−02)

Table 29 ($\mathscr{C}_3$ class) Local Minima of the homotopic path θ_0-t_f for θ_0 fixed and $\varepsilon = 10$N

Num.	t_f	(x_0, p_0)
1	3.0122653352	x0 = (−7.37384179257e−02, 9.07694926321e−02, −2.48333352432e+00, −1.68489575638e+00) p0 = (6.16866446074e+00, −8.59208825496e+00, 3.66245485321e−01, 2.36096512184e−01)
2	2.9431966623	x0 = (−5.61856226705e−02, 1.00463887224e−01, −2.74855936609e+00, −1.20467444370e+00) p0 = (4.25079407550e+00, −9.36060260305e+00, 3.88696084246e−01, 1.64942973814e−01)
3	2.8702232457	x0 = (−4.13981576422e−02, 1.05719370263e−01, −2.89234244604e+00, −8.00108916456e−01) p0 = (2.69474357150e+00, −9.64529876802e+00, 3.97577540129e−01, 1.09009754379e−01)
4	3.1227565037	x0 = (−8.86205667692e−02, −7.86420740187e−02, 2.15154335636e+00, −2.09205170785e+00) p0 = (−8.17719507113e−01, −4.95440837383e+00, 1.50403834833e−03, −1.47673574600e−01)
5	3.2201514889	x0 = (−7.20630362335e−02, −9.18839067611e−02, 2.51382242413e+00, −1.63905952438e+00) p0 = (2.00055655527e+00, −2.78413963830e+00, −7.43272782471e−02, −9.10311210657e−02)

Table 30 Cut Points for GEO to MO minimum-time transfer problem for $\mathscr{C}_1$

N^o	t_f	ε (N)	(x_0, p_0)
1	5.1488625	1.8710653	x0 = (−1.2183420e−01 1.3776662e−03 −3.7691130e−02 −3.0007330e+00) p0 = (−2.4853749e+01 −2.5590439e+00 −1.1469955e−e−01 −7.7640343e−01)
	5.1488623	1.8710653	x1 = (−6.4010619e−02 9.6657394e−02 −2.6444187e+00 −1.4187560e+00) p1 = (−7.6598810e+00 6.5174405e+00 −3.8985884e−01 −5.6991497e−02)
2	5.9023179	1.6073723	x0 = (−8.6446318e−02 −8.0699240e−02 2.2078247e+00 −2.0325671e+00) p0 = (−2.3664669e+01 −2.9201326e+01 8.2641553e−01 −8.7846091e−01)
	5.9023450	1.6073723	x1 = (−1.0690133e−01 5.5268597e−02 −1.5120759e+00 −2.5921894e+00) p1 = (−1.0303101e+01 1.6834274e+00 −3.1756083e−01 −2.7329434e−01)
3	6.6599800	1.4056522	x0 = (−1.8408681e−02 −1.0951133e−01 2.9960854e+00 −1.7114719e−01) p0 = (−5.0074394e−01 −4.6582515e+01 1.5038084e+00 −1.6486206e−01)
	6.6600036	1.4056522	x1 = (−1.2149790e−01 −8.6923162e−03 2.3781030e−01 −2.9915323e+00) p1 = (−9.4498793e+00 −4.5941257e+00 −1.0821845e−01 −4.0563385e−01)
4	7.4356086	1.2469239	x0 = (4.1469228e−02 −9.5689713e−02 2.6179443e+00 1.4670334e+00) p0 = (2.4346187e+01 −3.8413717e+01 1.3257393e+00 6.3983535e−01)
	7.4356173	1.2469239	x1 = (−8.7964292e−02 −7.9274917e−02 2.1688571e+00 −2.0740969e+00) p1 = (−3.6145240e+00 −9.4918222e+00 1.6199661e−01 −3.5458440e−01)

Results obtained from Fig. 52

Table 31 Cut Points for GEO to MO minimum-time transfer problem for $\mathscr{C}_2$

N^o	t_f	ε (N)	(x_0, p_0)
1	3.3752853	2.8226511	x0 = (−3.7663428e−02 1.0668216e−01 −2.9186830e+00 −6.9793164e−01) p0 = (−6.6375288e+00 1.5464483e+01 −5.2361131e−01 −1.7763009e−02)
	3.3752836	2.8226511	x1 = (6.1715222e−02 8.1088534e−02 −2.2184753e+00 2.0209371e+00) p1 = (3.6609960e+00 8.9031244e+00 −1.9029376e−01 3.3598070e−01)
2	4.0676620	2.2832275	x0 = (−1.2136523e−01 1.0225081e−02 −2.7974471e−01 −2.9879026e+00) p0 = (−4.1968548e+01 2.8323241e+00 −1.6608360e−01 −1.3456351e+00)
	4.0676607	2.2832275	x1 = (3.8446702e−02 9.7321810e−02 −2.6625963e+00 1.3843411e+00) p1 = (2.4323326e+00 1.1587609e+01 −3.9450109e−01 3.3641398e−01)
3	4.7758028	1.9114577	x0 = (−7.6851323e−02 −8.8577601e−02 2.4233663e+00 −1.7700607e+00) p0 = (−4.7402787e+01 −6.3131982e+01 2.1643608e+00 −1.5337171e+00)
	4.7757718	1.9114577	x1 = (−7.9147362e−03 1.0960795e−01 −2.9987287e+00 1.1595330e−01) p1 = (−2.6027323e+00 1.3934522e+01 −6.2536775e−01 1.3900950e−01)
4	5.5026835	1.6412384	x0 = (2.1204286e−02 −1.0449477e−01 2.8588389e+00 9.1261133e−01) p0 = (3.5025550e+01 −1.2059407e+02 4.0860053e+00 1.4312241e+00)
	5.5027193	1.6412384	x1 = (−6.1645451e−02 9.7889539e−02 −2.6781286e+00 −1.3540481e+00) p1 = (−1.0123795e+01 1.3145099e+01 −7.2436101e−01 −2.3911818e−01)
5a	6.2531152	1.4359703	x0 = (8.8714814e−02 −4.3099288e−02 1.1791396e+00 2.7596103e+00) p0 = (1.6152834e+02 −7.4842600e+01 2.2694695e+00 5.8095787e+00)
	6.2531294	1.4359703	x1 = (−1.0551390e−01 5.7581311e−02 −1.5753487e+00 −2.5542309e+00) p1 = (−1.7636018e+01 7.2559327e+00 −5.5642890e−01 −6.8757051e−01)

(continued)

Table 31 (continued)

N^o	t_f	ε (N)	(x_0, p_0)
5b	6.4271669	1.3811556	x0 = (−1.0866349e−01 5.2130500e−02 −1.4262217e+00 −2.6403997e+00) p0 = (−2.2795619e+01 9.1266774e+00 −6.1238761e−01 −9.1810499e−01)
	6.4255029	1.3811556	x1 = (−1.0722281e−01 5.4713762e−02 −1.4968963e+00 −2.6009845e+00) p1 = (−2.1556926e+01 9.0788639e+00 −6.1268640e−01 −8.5326763e−01)
6	6.9610479	1.2748062	x0 = (9.3095263e−02 3.0897695e−02 −8.4532016e−01 2.8794536e+00) p0 = (2.1996284e+02 5.7639512e+01 −2.4939350e+00 7.6317637e+00)
	6.9602231	1.2748062	x1 = (−1.2181767e−01 2.3504855e−03 −6.4306181e−02 −3.0002806e+00) p1 = (−2.0563120e+01 −2.6910797e+00 −1.3495182e−01 −9.5548578e−01)
7	7.6312547	1.1477254	x0 = (3.3347528e−02 9.9807647e−02 −2.7306055e+00 1.2448344e+00) p0 = (1.3464477e+02 2.7341686e+02 −1.0034451e+01 4.2090529e+00)
	7.6360553	1.1477254	x1 = (−1.0627936e−01 −5.6321337e−02 1.5408774e+00 −2.5751730e+00) p1 = (−1.8271336e+01 −1.4562037e+01 4.5974795e−01 −9.9004366e−01)
8	8.3208073	1.0419705	x0 = (−4.5399318e−02 1.0453012e−01 −2.8598062e+00 −9.0957538e−01) p0 = (−1.0240946e+02 3.5758771e+02 −1.2592360e+01 −4.4189365e+00)
	8.3210727	1.0419705	x1 = (−6.0626095e−02 −9.8398290e−02 2.6920474e+00 −1.3261599e+00) p1 = (−8.8941099e+00 −2.5008323e+01 1.0588586e+00 −6.4682426e−01)

Results obtained from Fig. 53

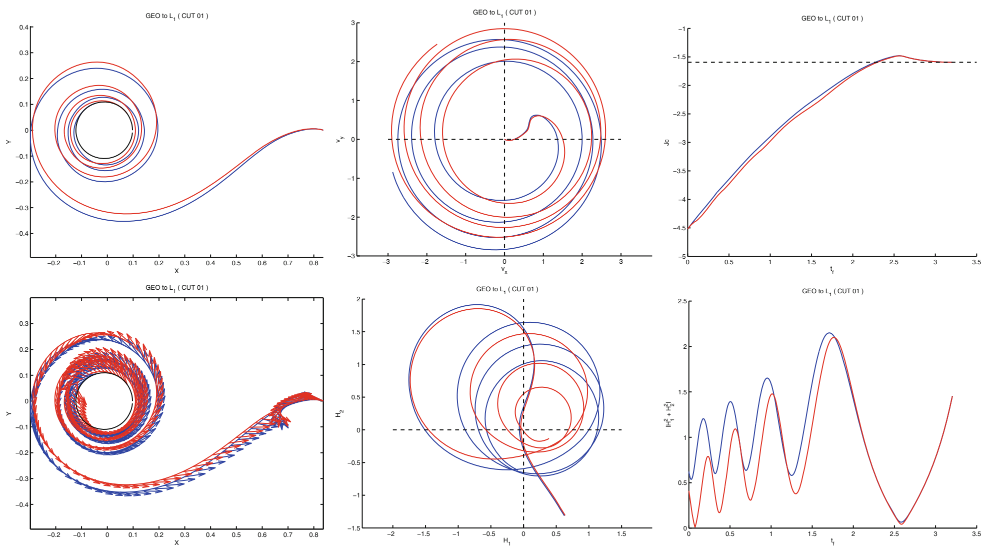

Fig. 72 For cut point n^o 1, *blue* orbits correspond to the first cut value and *red* orbits to the second cut value. (*top-left*) $\{XY\}$ projection of the transfer trajectory, (*top-center*) $\{V_x V_y\}$ projection of the transfer trajectory, (*top-right*) t versus J_c (energy variation along the transfer trajectory), (*bottom-left*) control along the trajectory, (*bottom-center*) H_1 versus H_2, (*bottom-right*) t versus $|(H_1, H_2)|$

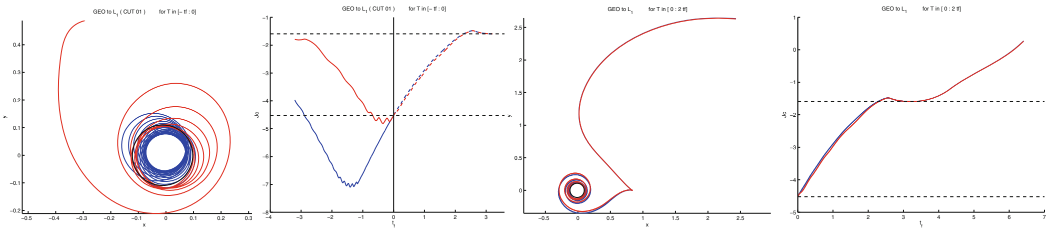

Fig. 73 For cut point n^o 1, (*left*) optimal solutions for $t \in [-t_f, 0]$ (XY projection and J_c variation), (*right*) optimal solutions for $t \in [0, 2t_f]$ (XY projection and J_c variation)

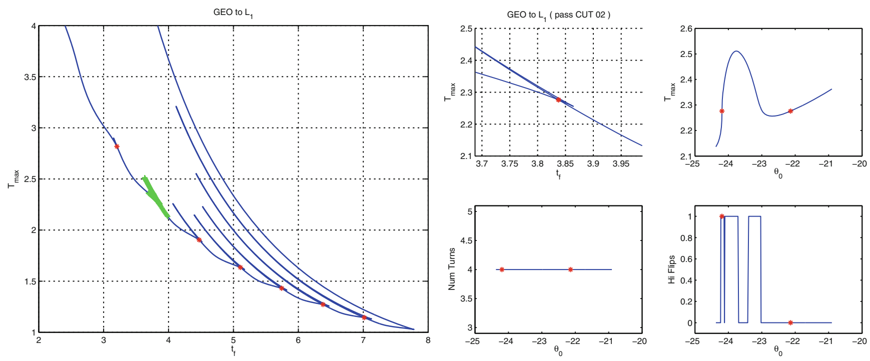

Fig. 74 For cut point n^o 2: (*left*) t_f versus ε homotopic curve with highlight of the cut passage in *green*; (*right*) analysis of the cut passage: (*top-left* subplot) t_f versus ε zoom, (*top-right* subplot) θ_0 versus ε, (*bottom-left* subplot) θ_0 versus num. turns around the Earth, (*bottom-right* subplot) θ_0 versus the number of times $|(H_1, H_2)|$ passes close to zero. *Red points* are values corresponding the each cut point

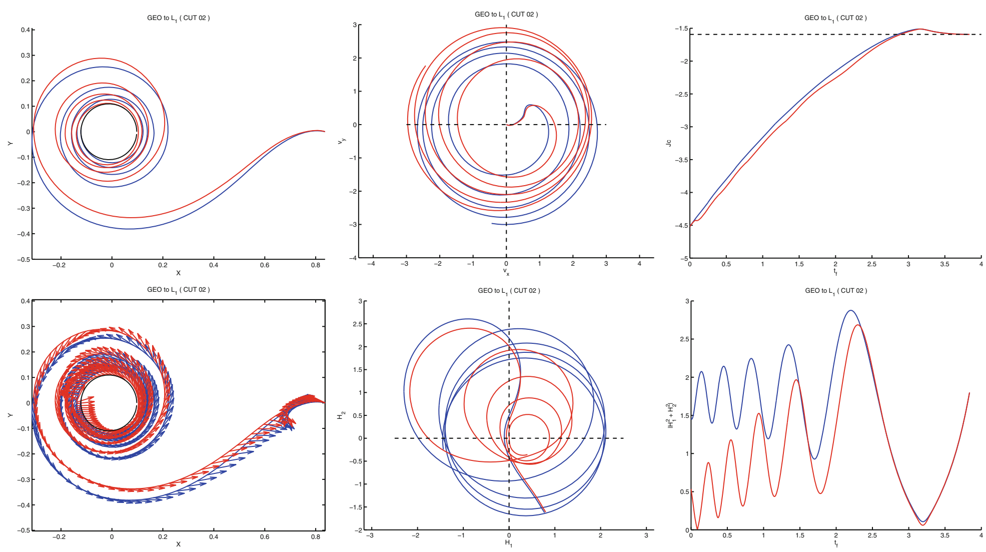

Fig. 75 For cut point n^o 2, *blue* orbits correspond to the first cut value and *red* orbits to the second cut value (*top-left*) $\{XY\}$ projection of the transfer trajectory, (*top-center*) $\{V_x V_y\}$ projection of the transfer trajectory, (*top-right*) t versus J_c (energy variation along the transfer trajectory), (*bottom-left*) control along the trajectory, (*bottom-center*) H_1 versus H_2, (*bottom-right*) t versus $|(H_1, H_2)|$

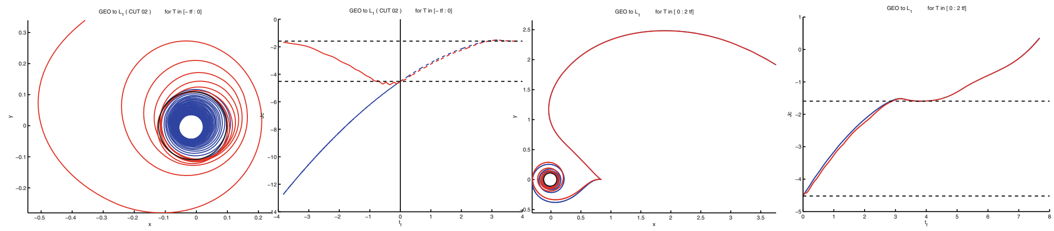

Fig. 76 For cut point n^o 2, (*left*) optimal solutions for $t \in [-t_f, 0]$ (XY projection and J_c variation), (*right*) optimal solutions for $t \in [0, 2t_f]$ (XY projection and J_c variation)

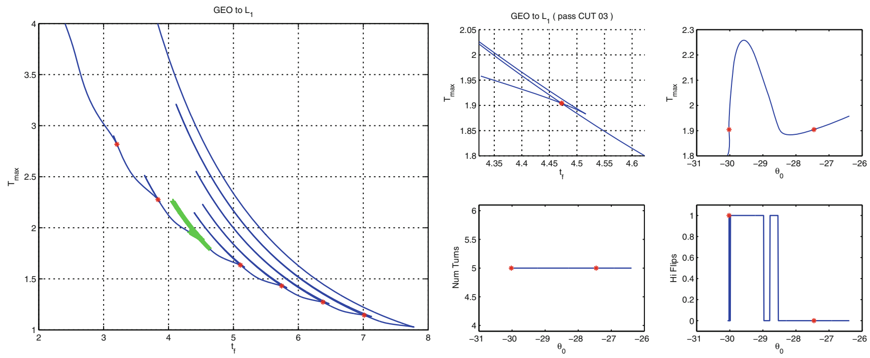

Fig. 77 For cut point n^o 3: (*left*) t_f versus ε homotopic curve with highlight of the cut passage in *green*; (*right*) analysis of the cut passage: (*top-left* subplot) t_f versus ε zoom, (*top-right* subplot) θ_0 versus ε, (*bottom-left* subplot) θ_0 versus num. turns around the Earth, (*bottom-right* subplot) θ_0 versus the number of times $|(H_1, H_2)|$ passes close to zero. *Red* points are values corresponding the each cut point

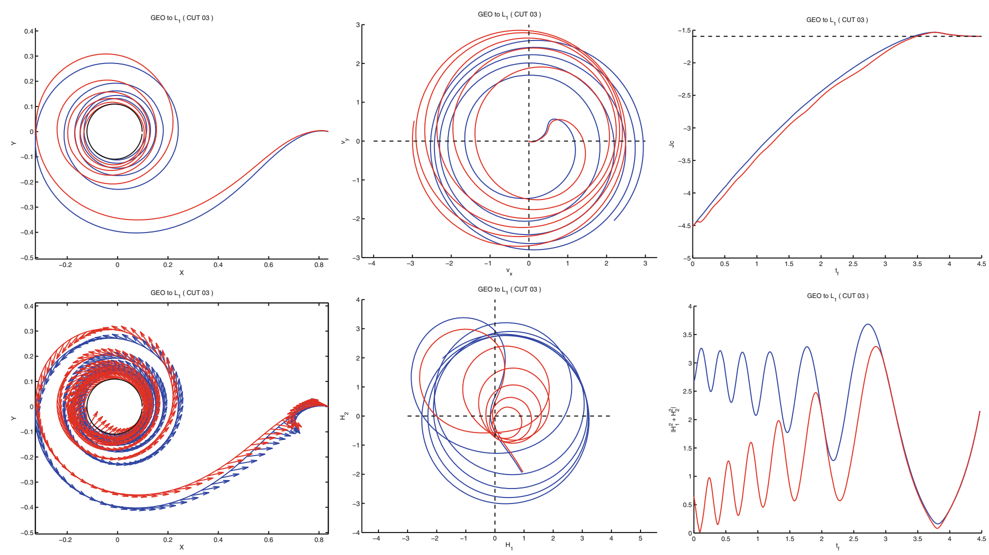

Fig. 78 For cut point n^o 3, *blue* orbits correspond to the first cut value and *red* orbits to the second cut value (*top-left*) $\{XY\}$ projection of the transfer trajectory, (*top-center*) $\{V_x V_y\}$ projection of the transfer trajectory, (*top-right*) t versus J_c (energy variation along the transfer trajectory), (*bottom-left*) control along the trajectory, (*bottom-center*) H_1 versus H_2, (*bottom-right*) t versus $|(H_1, H_2)|$

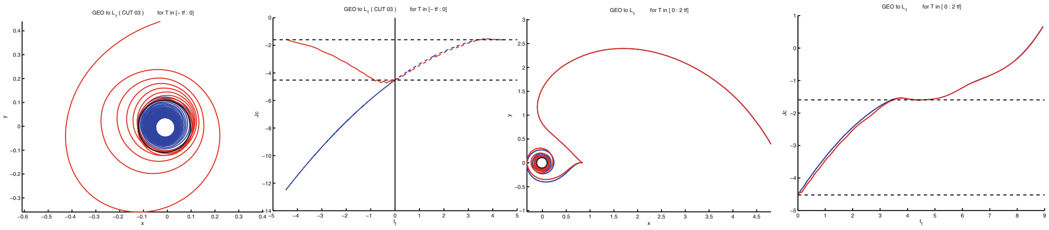

Fig. 79 For cut point n^o 3, (*left*) optimal solutions for $t \in [-t_f, 0]$ (XY projection and J_c variation), (*right*) optimal solutions for $t \in [0, 2t_f]$ (XY projection and J_c variation)

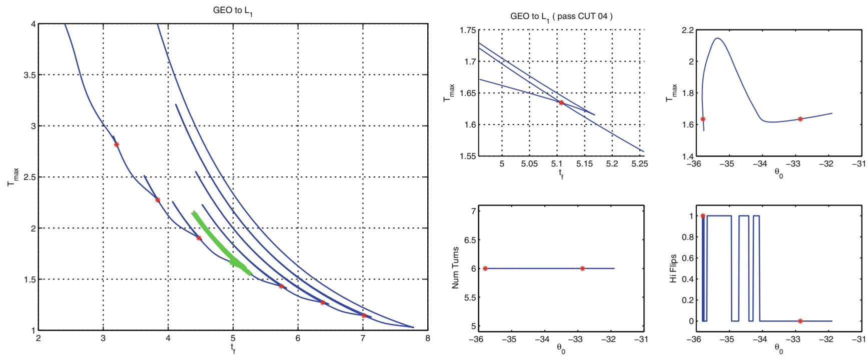

Fig. 80 For cut point n^o 4: (*left*) t_f versus ε homotopic curve with highlight of the cut passage in *green*; (*right*) analysis of the cut passage: (*top-left* subplot) t_f versus ε zoom, (*top-right* subplot) θ_0 versus ε, (*bottom-left* subplot) θ_0 versus num. turns around the Earth, (*bottom-right* subplot) θ_0 versus the number of times $|(H_1, H_2)|$ passes close to zero. *Red* points are values corresponding the each cut point

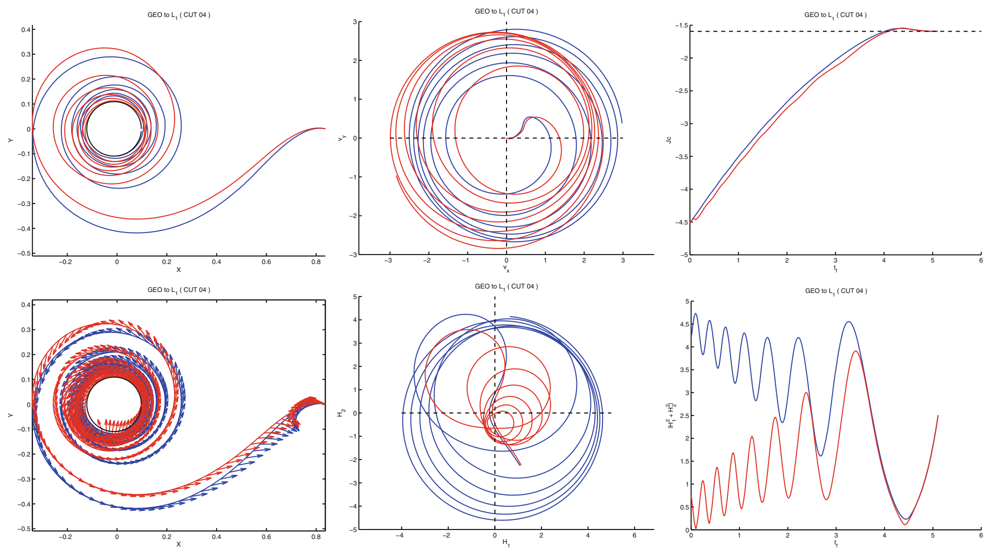

Fig. 81 For cut point n^o 4, *blue* orbits correspond to the first cut value and *red* orbits to the second cut value (*top-left*) $\{XY\}$ projection of the transfer trajectory, (*top-center*) $\{V_x V_y\}$ projection of the transfer trajectory, (*top-right*) t versus J_c (energy variation along the transfer trajectory), (*bottom-left*) control along the trajectory, (*bottom-center*) H_1 versus H_2, (*bottom-right*) t versus $|(H_1, H_2)|$

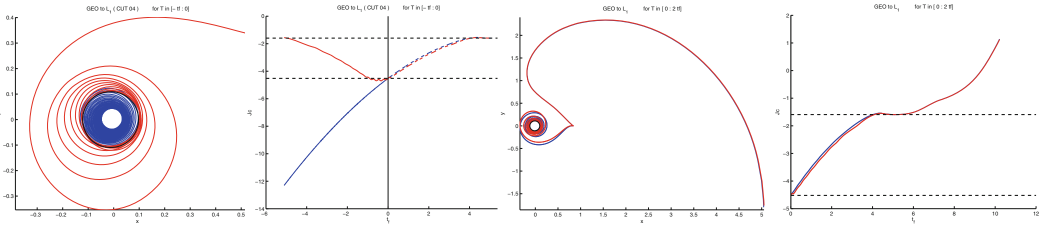

Fig. 82 For cut point n^o 4, (*left*) optimal solutions for $t \in [-t_f, 0]$ (XY projection and J_c variation), (*right*) optimal solutions for $t \in [0, 2t_f]$ (XY projection and J_c variation)

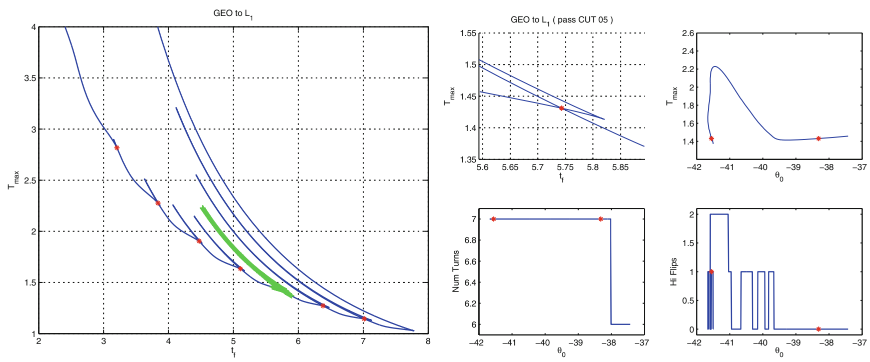

Fig. 83 For cut point n^o 5: (*left*) t_f versus ε homotopic curve with highlight of the cut passage in *green*; (*right*) analysis of the cut passage: (*top-left* subplot) t_f versus ε zoom, (*top-right* subplot) θ_0 versus ε, (*bottom-left* subplot) θ_0 versus num. turns around the Earth, (*bottom-right* subplot) θ_0 versus the number of times $|(H_1, H_2)|$ passes close to zero. *Red* points are values corresponding the each cut point

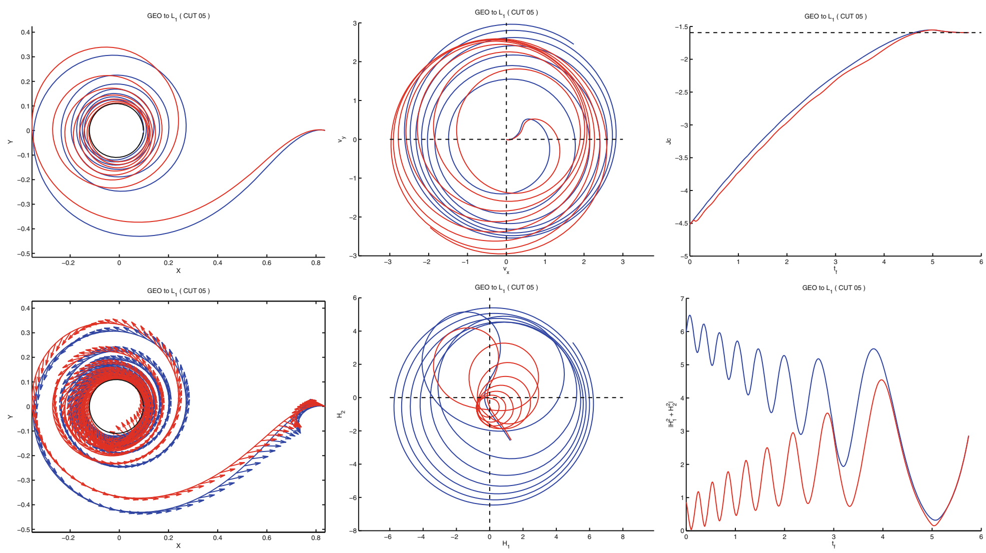

Fig. 84 For cut point n^o 5, *blue* orbits correspond to the first cut value and *red* orbits to the second cut value (*top-left*) $\{XY\}$ projection of the transfer trajectory, (*top-center*) $\{V_x V_y\}$ projection of the transfer trajectory, (*top-right*) t versus J_c (energy variation along the transfer trajectory), (*bottom-left*) control along the trajectory, (*bottom-center*) H_1 versus H_2, (*bottom-right*) t versus $|(H_1, H_2)|$

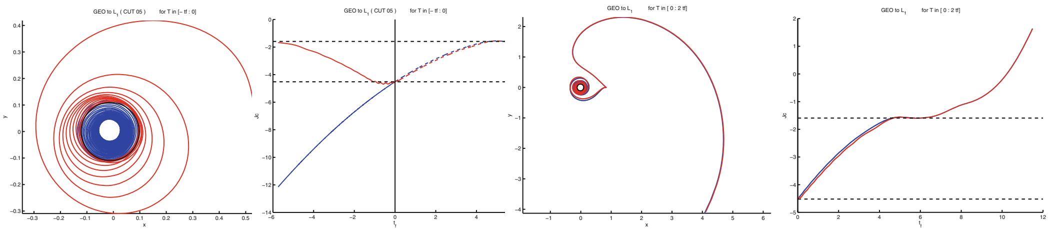

Fig. 85 For cut point n^o 5, (*left*) optimal solutions for $t \in [-t_f, 0]$ (XY projection and J_c variation), (*right*) optimal solutions for $t \in [0, 2t_f]$ (XY projection and J_c variation)

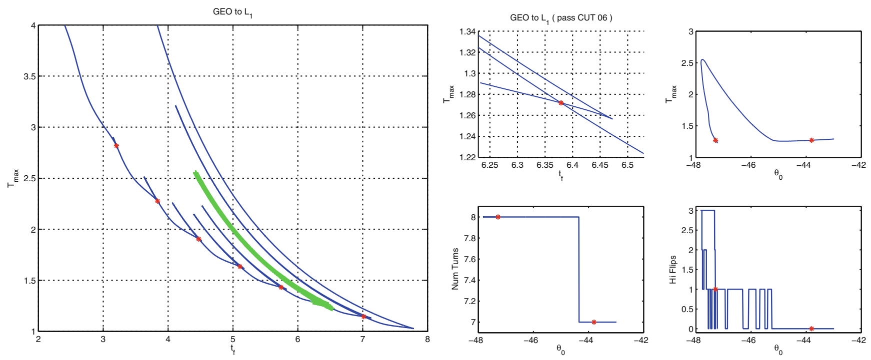

Fig. 86 For cut point n^o 6: (*left*) t_f versus ε homotopic curve with highlight of the cut passage in *green*; (*right*) analysis of the cut passage: (*top-left* subplot) t_f versus ε zoom, (*top-right* subplot) θ_0 versus ε, (*bottom-left* subplot) θ_0 versus num. turns around the Earth, (*bottom-right* subplot) θ_0 versus the number of times $|(H_1, H_2)|$ passes close to zero. *Red* points are values corresponding the each cut point

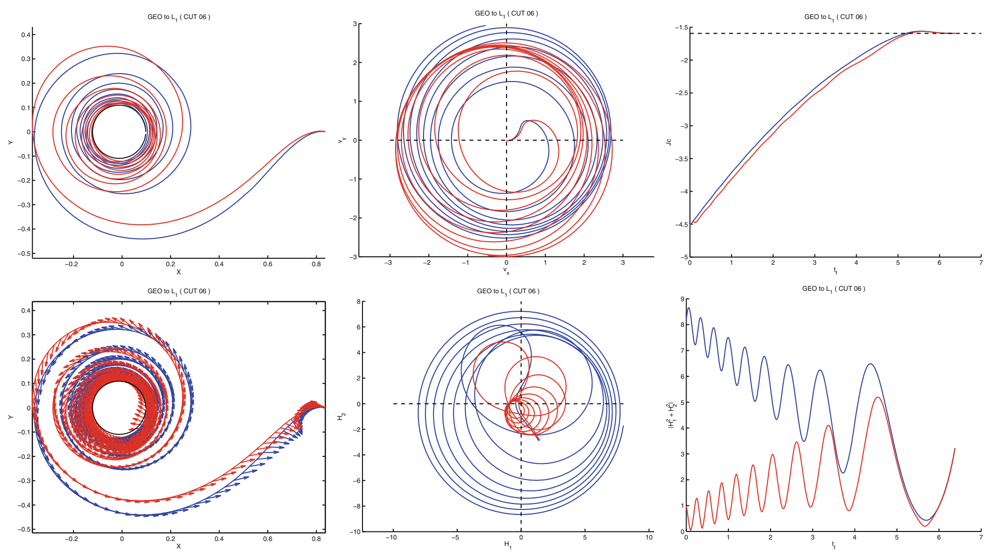

Fig. 87 For cut point n^o 6, *blue* orbits correspond to the first cut value and *red* orbits to the second cut value (*top-left*) $\{XY\}$ projection of the transfer trajectory, (*top-center*) $\{V_x V_y\}$ projection of the transfer trajectory, (*top-right*) t versus J_c (energy variation along the transfer trajectory), (*bottom-left*) control along the trajectory, (*bottom-center*) H_1 versus H_2, (*bottom-right*) t versus $|(H_1, H_2)|$

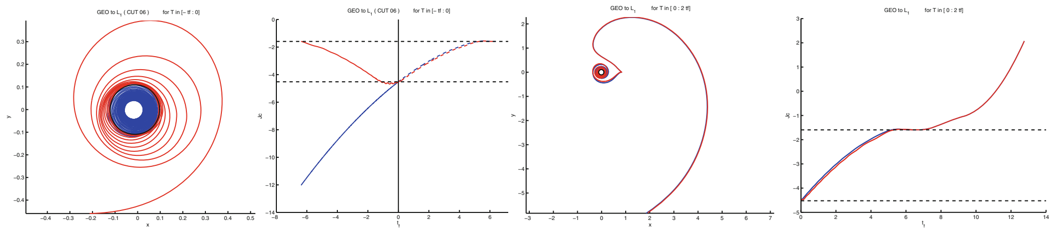

Fig. 88 For cut point n^o 6, (*left*) optimal solutions for $t \in [-t_f, 0]$ (XY projection and J_c variation), (*right*) optimal solutions for $t \in [0, 2t_f]$ (XY projection and J_c variation)

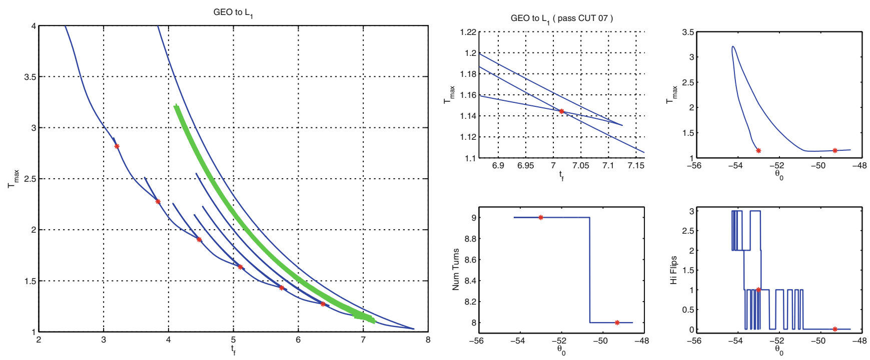

Fig. 89 For cut point n^o 7: (*left*) t_f versus ε homotopic curve with highlight of the cut passage in *green*; (*right*) analysis of the cut passage: (*top-left* subplot) t_f versus ε zoom, (*top-right* subplot) θ_0 versus ε, (*bottom-left* subplot) θ_0 versus num. turns around the Earth, (*bottom-right* subplot) θ_0 versus the number of times $|(H_1, H_2)|$ passes close to zero. *Red* points are values corresponding the each cut point

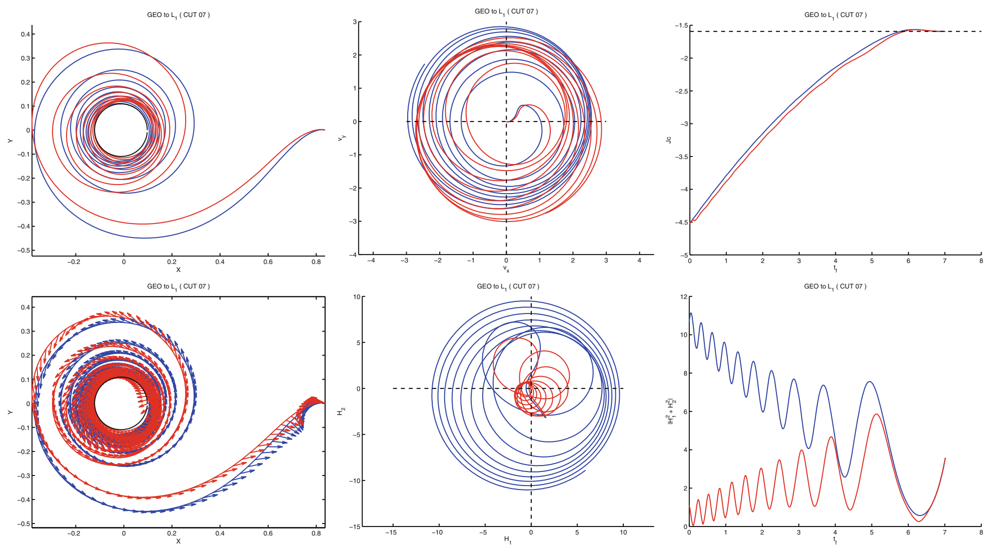

Fig. 90 For cut point n^o 7, *blue* orbits correspond to the first cut value and *red* orbits to the second cut value (*top-left*) $\{XY\}$ projection of the transfer trajectory, (*top-center*) $\{V_x V_y\}$ projection of the transfer trajectory, (*top-right*) t versus J_c (energy variation along the transfer trajectory), (*bottom-left*) control along the trajectory, (*bottom-center*) H_1 versus H_2, (*bottom-right*) t versus $|(H_1, H_2)|$

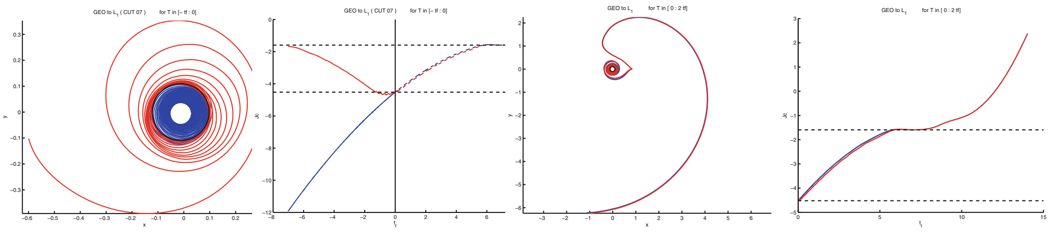

Fig. 91 For cut point n^o 7, (*left*) optimal solutions for $t \in [-t_f, 0]$ (XY projection and J_c variation), (*right*) optimal solutions for $t \in [0, 2t_f]$ (XY projection and J_c variation)

8 Summary of the Cut Points on the GEO to MO Transfer

In this Section we summarize the results for all the CUT points that we have found for the GEO to MO transfer problem. We recall that we have two classes of transfer trajectories, $\mathscr{C}_1$ and $\mathscr{C}_2$, and that in terms of transfer time, the solutions of type $\mathscr{C}_2$ are always better than those of type $\mathscr{C}_1$. Nevertheless, the behavior of the homotopic curve with respect to ε for the $\mathscr{C}_1$ type of solutions presents a less complex structure that the $\mathscr{C}_2$ type homotopic curve. In both cases we also find CUT points, where their initial conditions are summarized in Tables 30 and 31. We have done a similar analysis as the one for the GEO to L_1, and for each pair of cut points we have computed the transfer trajectory, the energy variation along the transfer trajectory, $J_c(t)$, the variation of the control-law along the trajectory and the variation of $H_{1,2}$. Moreover, we have integrated the optimal solutions back and forward in time, i.e. for $t \in [-t_f, 2t_t]$, where t_f is the transfer time. Finally, for the solutions along the homotopic curve close to cut point (i.e. $t_f^* \in [t_f - 0.15 : t_f + 0.15]$) we have computed transfer trajectories and some of their distinctive parameters, trying to characterize their passage. In the plots that we will see, the number of turns around the Earth, and the number of times that $|(H_1, H_2)|$ comes close to zero (in particular $|(H_1, H_2)| < 0.05$).

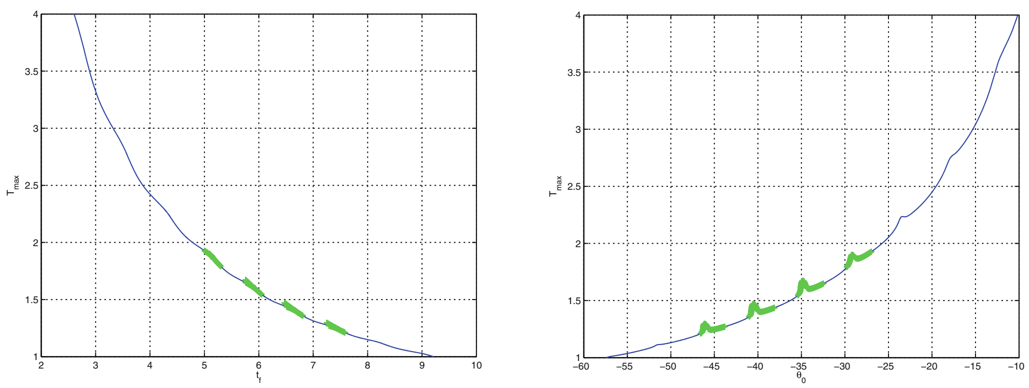

Fig. 92 For the GEO to Mo control problem, homotopic curve for $\varepsilon \in [1 : 10]$N for the $\mathscr{C}_1$ type of solutions. *Left* t_f (transfer time) versus ε projection. *Right* θ_0 (angle defining the initial position on the departure orbit) versus ε

8.1 $\mathscr{C}_1$ Cut Points

In Fig. 92 we show for the $\mathscr{C}_1$ type of solutions, the homotopic curve t_f versus ε and the same curve plotting θ_0 versus ε, where θ_0 in the angle that parameterizes the initial condition on the departure GEO orbit. In both plots we have highlighted in green the solutions close to the CUT pair, which are the solutions that we have analyzed. Moreover, Figs. 93, 94 and 95 summarize the results for the first cut point. Similarly, Figs. 96, 97 and 98 for the second cut point, Figs. 99, 100 and 101 for the third cut point, and finally Figs. 102, 103 and 104 for the fourth cut point.

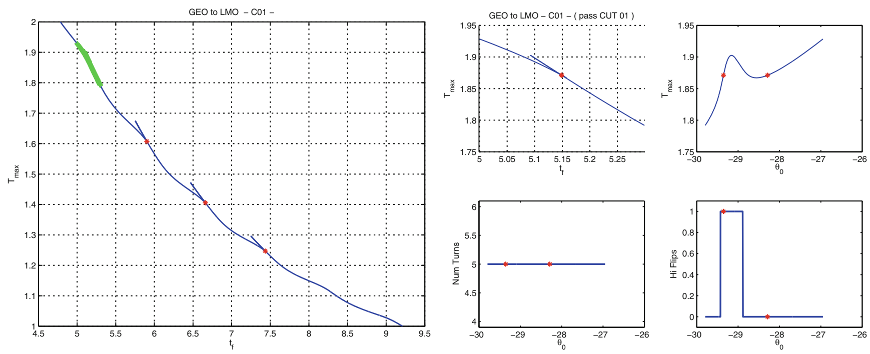

Fig. 93 $\mathscr{C}_1$ cut point n^o 1: (*left*) t_f versus ε homotopic curve with highlight of the cut passage in *green*; (*right*) analysis of the cut passage: (*top-left* subplot) t_f versus ε zoom, (*top-right* subplot) θ_0 versus ε, (*bottom-left* subplot) θ_0 versus num. turns around the Earth, (*bottom-right* subplot) θ_0 versus the number of times $|(H_1, H_2)|$ passes close to zero. *Red* points are values corresponding the each cut point

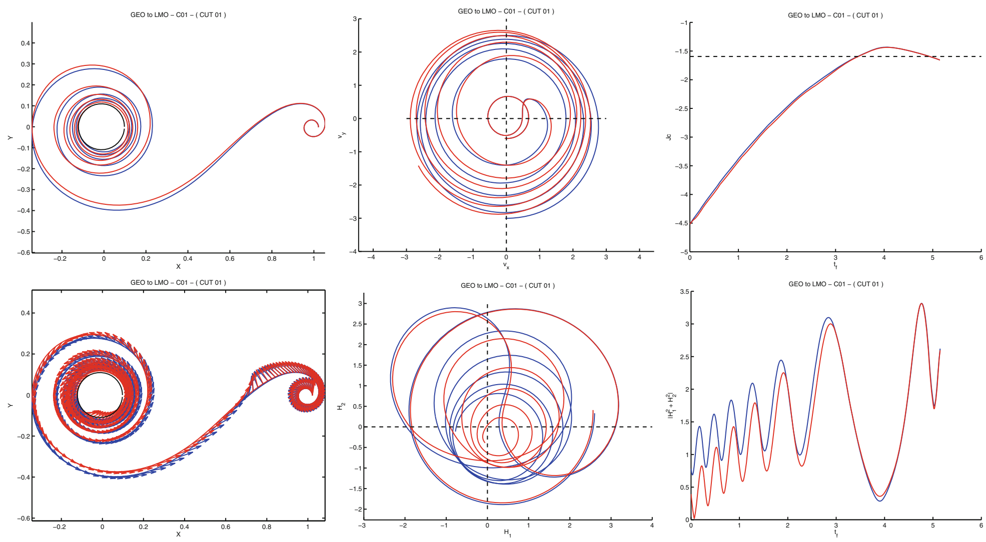

Fig. 94 $\mathscr{C}_1$ cut point n^o 1, *blue* orbits correspond to the first cut value and *red* orbits to the second cut value. (*top-left*) $\{XY\}$ projection of the transfer trajectory, (*top-center*) $\{V_x V_y\}$ projection of the transfer trajectory, (*top-right*) t versus J_c (energy variation along the transfer trajectory), (*bottom-left*) control along the trajectory, (*bottom-center*) H_1 versus H_2, (*bottom-right*) t versus $|(H_1, H_2)|$

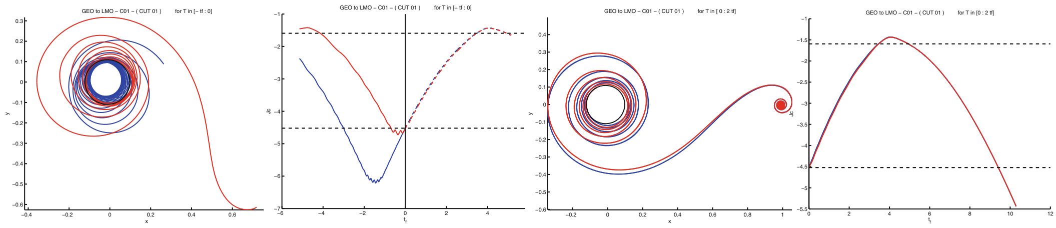

Fig. 95 $\mathscr{C}_1$ cut point n^o 1, (*left*) optimal solutions for $t \in [-t_f, 0]$ (XY projection and J_c variation), (*right*) optimal solutions for $t \in [0, 2t_f]$ (XY projection and J_c variation)

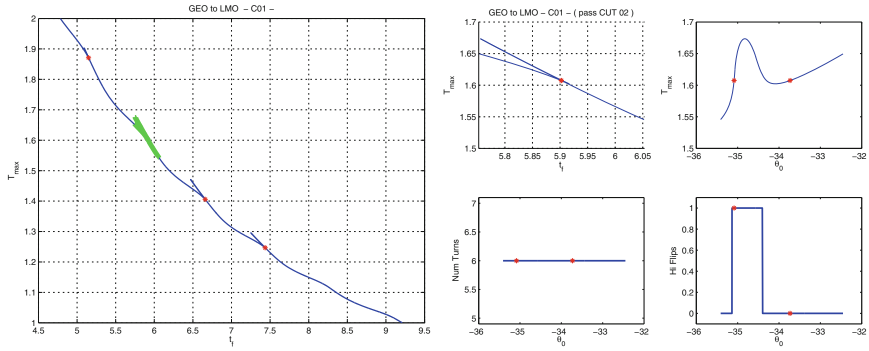

Fig. 96 $\mathscr{C}_1$ cut point n^o 2: (*left*) t_f versus ε homotopic curve with highlight of the cut passage in *green*; (*right*) analysis of the cut passage: (*top-left* subplot) t_f versus ε zoom, (*top-right* subplot) θ_0 versus ε, (*bottom-left* subplot) θ_0 versus num. turns around the Earth, (*bottom-right* subplot) θ_0 versus the number of times $|(H_1, H_2)|$ passes close to zero. *Red* points are values corresponding the each cut point

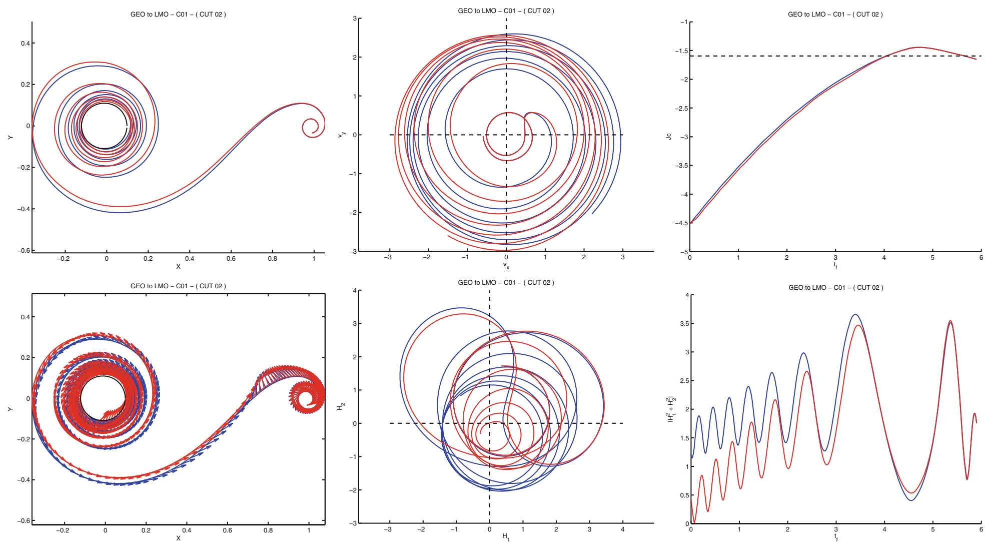

Fig. 97 $\mathscr{C}_1$ cut point n^o 2, *blue* orbits correspond to the first cut value and *red* orbits to the second cut value. (*top-left*) $\{XY\}$ projection of the transfer trajectory, (*top-center*) $\{V_x V_y\}$ projection of the transfer trajectory, (*top-right*) t versus J_c (energy variation along the transfer trajectory), (*bottom-left*) control along the trajectory, (*bottom-center*) H_1 versus H_2, (*bottom-right*) t versus $|(H_1, H_2)|$

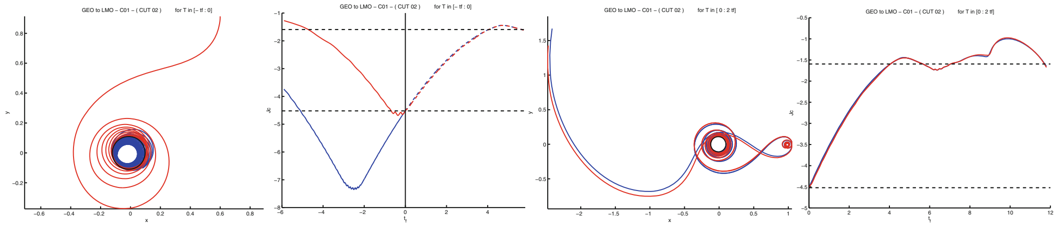

Fig. 98 $\mathscr{C}_1$ cut point n^o 2, (*left*) optimal solutions for $t \in [-t_f, 0]$ (XY projection and J_c variation), (*right*) optimal solutions for $t \in [0, 2t_f]$ (XY projection and J_c variation)

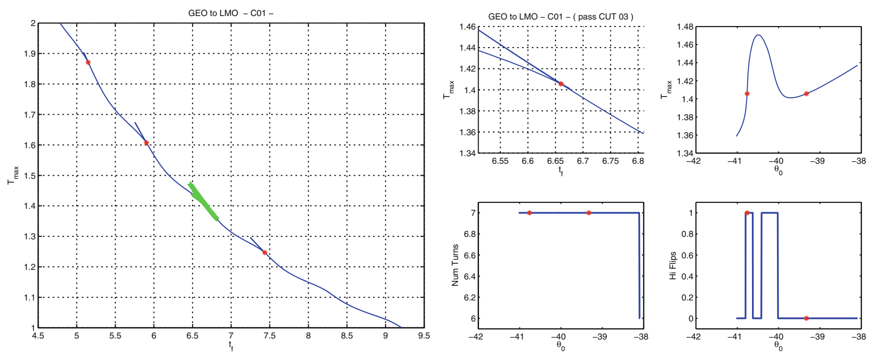

Fig. 99 $\mathscr{C}_1$ cut point n^o 3: (*left*) t_f versus ε homotopic curve with highlight of the cut passage in *green*; (*right*) analysis of the cut passage: (*top-left* subplot) t_f versus ε zoom, (*top-right* subplot) θ_0 versus ε, (*bottom-left* subplot) θ_0 versus num. turns around the Earth, (*bottom-right* subplot) θ_0 versus the number of times $|(H_1, H_2)|$ passes close to zero. *Red* points are values corresponding the each cut point

8.2 $\mathscr{C}_2$ *Cut Points*

In Fig. 105 we show for the $\mathscr{C}_2$ type of solutions, the homotopic curve t_f versus ε and the same curve plotting θ_0 versus ε, where θ_0 in the angle that parameterizes the initial condition on the departure GEO orbit. In both plots we have highlighted in green the solutions close to the CUT pair, which are the solutions that we have analyzed. Moreover, Figs. 106, 107 and 108 summarize the results for the first cut point. Similarly, Figs. 109, 110 and 111 for the second cut point, Figs. 112, 113 and 114 for the third cut point, Figs. 115, 116 and 117 for the forth cut point, Figs. 118, 119 and 120 for the fifth cut point, Figs. 121, 122 and 123 for the sixth cut point, Figs. 124, 125 and 126 for the seventh cut point, Figs. 127, 128 and 129 for the eighth cut point, and finally Figs. 130, 131 and 132 for the ninth cut point.

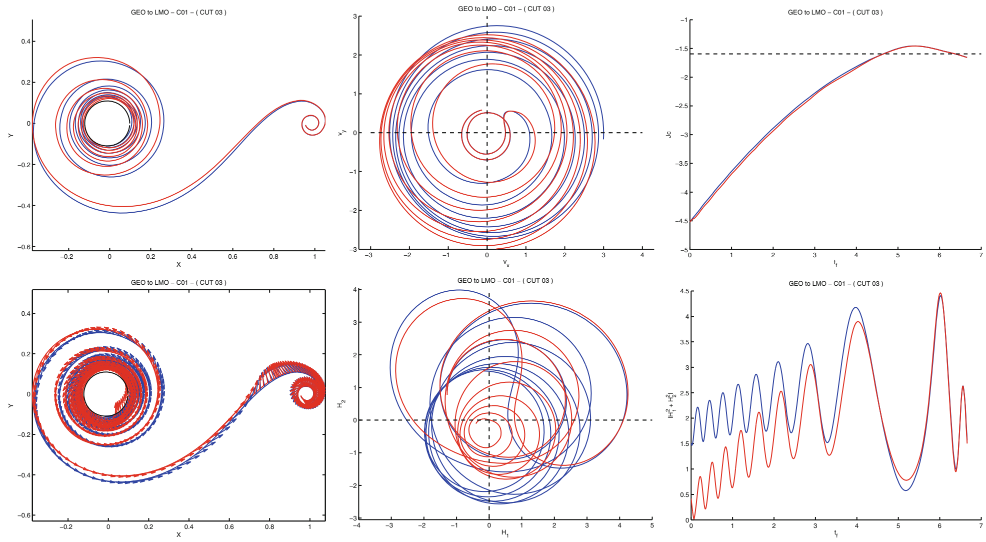

Fig. 100 $\mathscr{C}_1$ cut point n^o 3, *blue* orbits correspond to the first cut value and *red* orbits to the second cut value. (*top-left*) $\{XY\}$ projection of the transfer trajectory, (*top-center*) $\{V_x V_y\}$ projection of the transfer trajectory, (*top-right*) t versus J_c (energy variation along the transfer trajectory), (*bottom-left*) control along the trajectory, (*bottom-center*) H_1 versus H_2, (*bottom-right*) t versus $|(H_1, H_2)|$

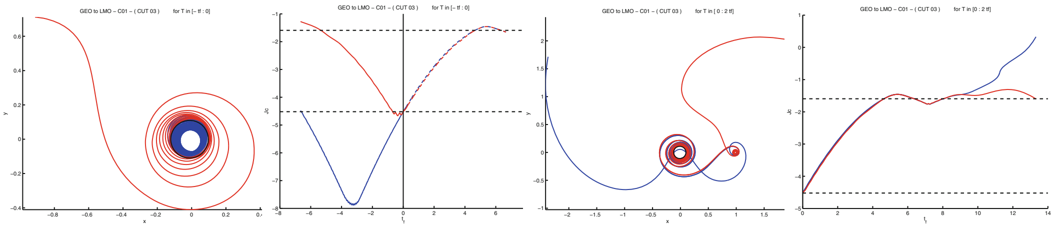

Fig. 101 $\mathscr{C}_1$ cut point n^o 3, (*left*) optimal solutions for $t \in [-t_f, 0]$ (XY projection and J_c variation), (*right*) optimal solutions for $t \in [0, 2t_f]$ (XY projection and J_c variation)

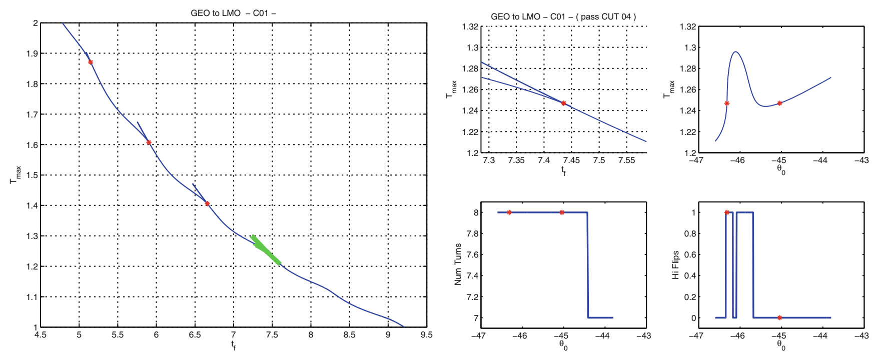

Fig. 102 $\mathscr{C}_1$ cut point n^o 4: (*left*) t_f versus ε homotopic curve with highlight of the cut passage in *green*; (*right*) analysis of the cut passage: (*top-left* subplot) t_f versus ε zoom, (*top-right* subplot) θ_0 versus ε, (*bottom-left* subplot) θ_0 versus num. turns around the Earth, (*bottom-right* subplot) θ_0 versus the number of times $|(H_1, H_2)|$ passes close to zero. *Red* points are values corresponding the each cut point

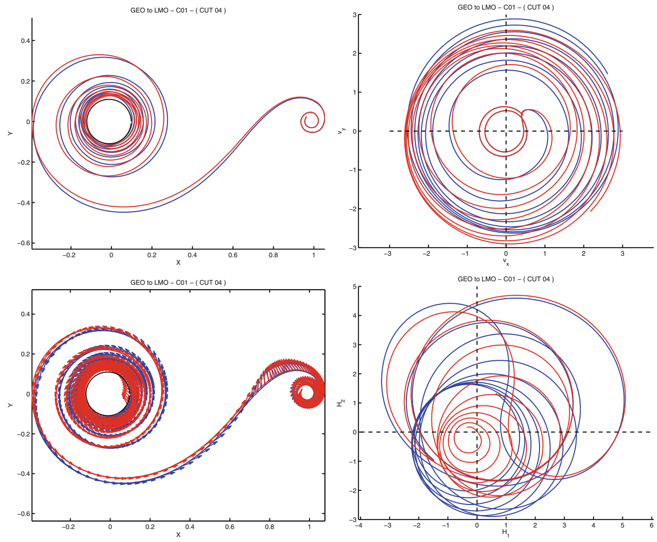

Fig. 103 $\mathscr{C}_1$ cut point n^o 4, *blue* orbits correspond to the first cut value and *red* orbits to the second cut value. (*top-left*) $\{XY\}$ projection of the transfer trajectory, (*top-center*) $\{V_x V_y\}$ projection of the transfer trajectory, (*top-right*) t versus J_c (energy variation along the transfer trajectory), (*bottom-left*) control along the trajectory, (*bottom-center*) H_1 versus H_2, (*bottom-right*) t versus $|(H_1, H_2)|$

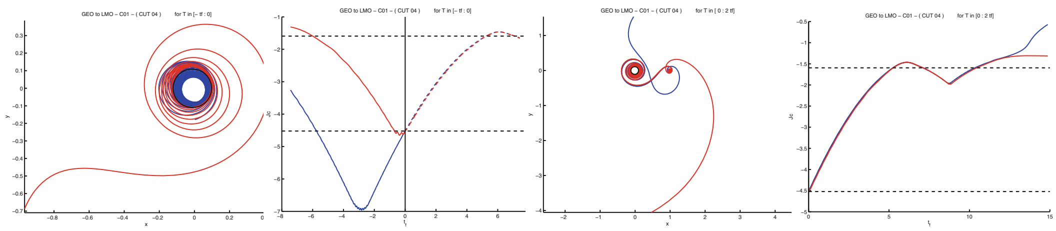

Fig. 104 $\mathscr{C}_1$ cut point n^o 4, (*left*) optimal solutions for $t \in [-t_f, 0]$ (XY projection and J_c variation), (*right*) optimal solutions for $t \in [0, 2t_f]$ (XY projection and J_c variation)

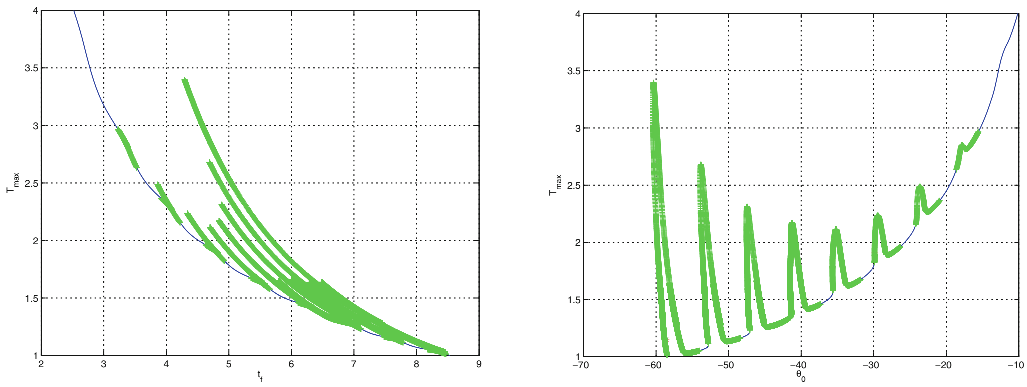

Fig. 105 For the GEO to Mo control problem, homotopic curve for $\varepsilon \in [1 : 10]$N for the $\mathscr{C}_2$ type of solutions. *Left* t_f (transfer time) versus ε projection. *Right* θ_0 (angle defining the initial position on the departure orbit) versus ε

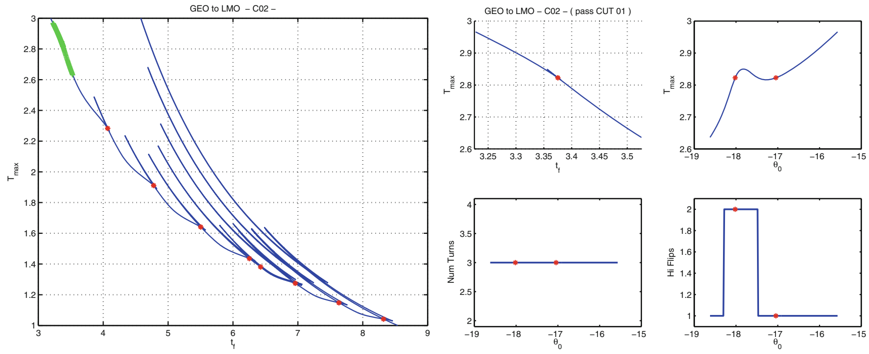

Fig. 106 $\mathscr{C}_2$ cut point n^o 1: (*left*) t_f versus ε homotopic curve with highlight of the cut passage in *green*; (*right*) analysis of the cut passage: (*top-left* subplot) t_f versus ε zoom, (*top-right* subplot) θ_0 versus ε, (*bottom-left* subplot) θ_0 versus num. turns around the Earth, (*bottom-right* subplot) θ_0 versus the number of times $|(H_1, H_2)|$ passes close to zero. *Red* points are values corresponding the each cut point

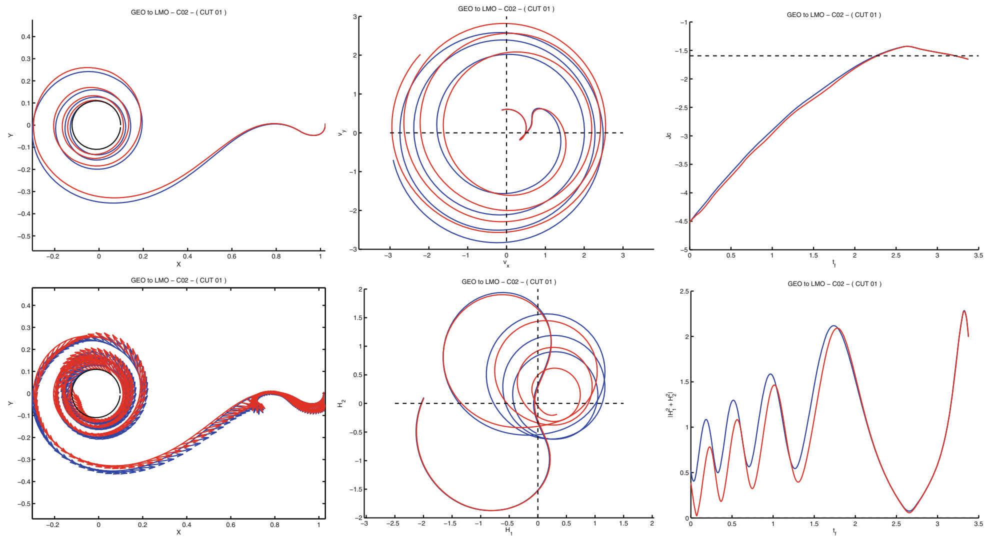

Fig. 107 $\mathscr{C}_2$ cut point n^o 1, *blue* orbits correspond to the first cut value and *red* orbits to the second cut value. (*top-left*) $\{XY\}$ projection of the transfer trajectory, (*top-center*) $\{V_x V_y\}$ projection of the transfer trajectory, (*top-right*) t versus J_c (energy variation along the transfer trajectory), (*bottom-left*) control along the trajectory, (*bottom-center*) H_1 versus H_2, (*bottom-right*) t versus $|(H_1, H_2)|$

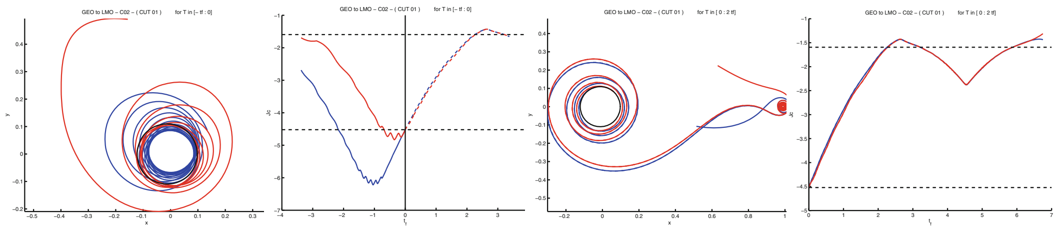

Fig. 108 $\mathscr{C}_2$ cut point n^o 1, (*left*) optimal solutions for $t \in [-t_f, 0]$ (XY projection and J_c variation), (*right*) optimal solutions for $t \in [0, 2t_f]$ (XY projection and J_c variation)

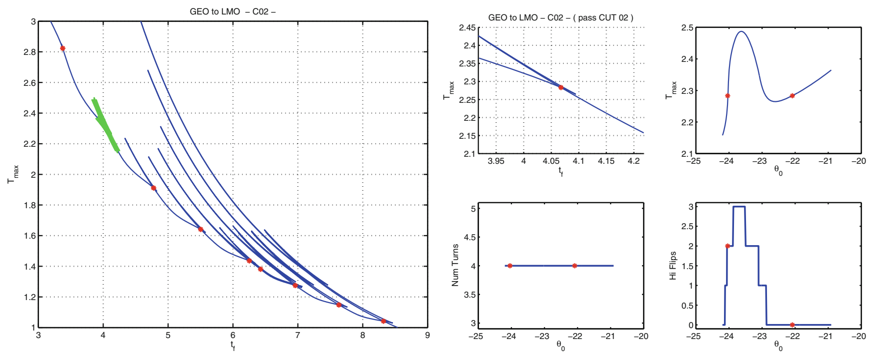

Fig. 109 $\mathscr{C}_2$ cut point n^o 2: (*left*) t_f versus ε homotopic curve with highlight of the cut passage in *green*; (*right*) analysis of the cut passage: (*top-left* subplot) t_f versus ε zoom, (*top-right* subplot) θ_0 versus ε, (*bottom-left* subplot) θ_0 versus num. turns around the Earth, (*bottom-right* subplot) θ_0 versus the number of times $|(H_1, H_2)|$ passes close to zero. *Red* points are values corresponding the each cut point

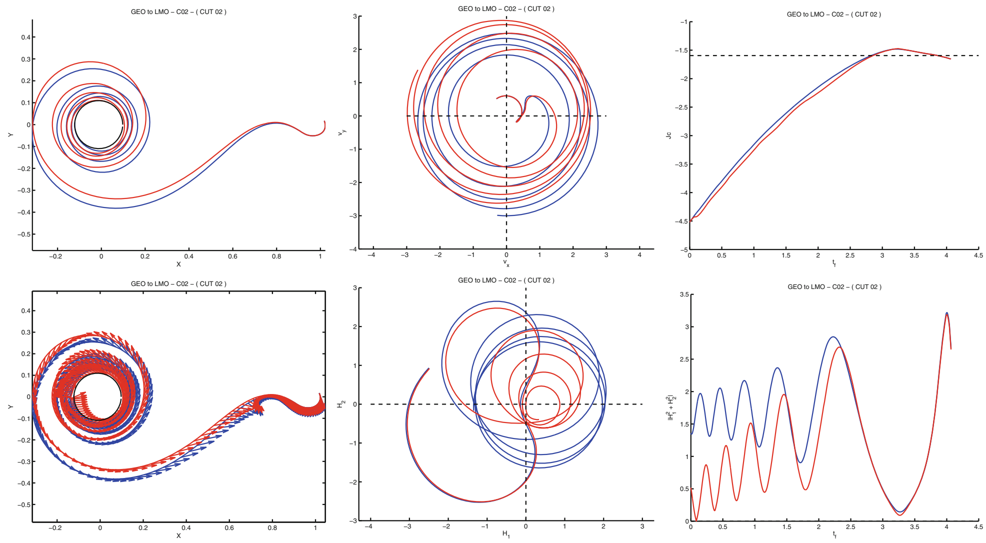

Fig. 110 $\mathscr{C}_2$ cut point n^o 2, *blue* orbits correspond to the first cut value and *red* orbits to the second cut value. (*top-left*) $\{XY\}$ projection of the transfer trajectory, (*top-center*) $\{V_x V_y\}$ projection of the transfer trajectory, (*top-right*) t versus J_c (energy variation along the transfer trajectory), (*bottom-left*) control along the trajectory, (*bottom-center*) H_1 versus H_2, (*bottom-right*) t versus $|(H_1, H_2)|$

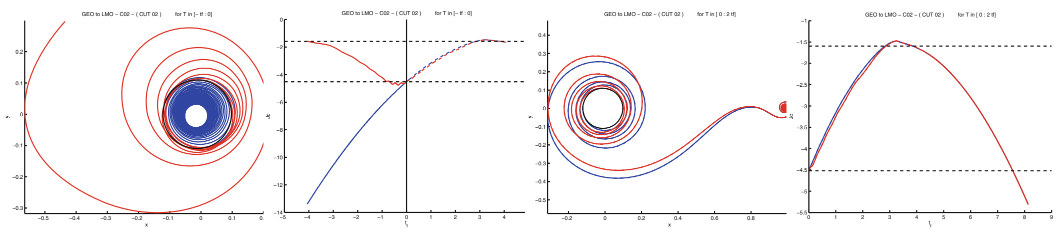

Fig. 111 $\mathscr{C}_2$ cut point n^o 2, (*left*) optimal solutions for $t \in [-t_f, 0]$ (XY projection and J_c variation), (*right*) optimal solutions for $t \in [0, 2t_f]$ (XY projection and J_c variation)

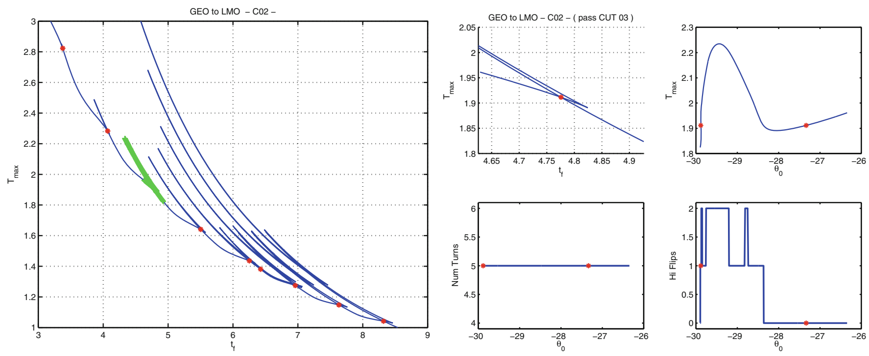

Fig. 112 $\mathscr{C}_2$ cut point n^o 3: (*left*) t_f versus ε homotopic curve with highlight of the cut passage in *green*; (*right*) analysis of the cut passage: (*top-left* subplot) t_f versus ε zoom, (*top-right* subplot) θ_0 versus ε, (*bottom-left* subplot) θ_0 versus num. turns around the Earth, (*bottom-right* subplot) θ_0 versus the number of times $|(H_1, H_2)|$ passes close to zero. *Red* points are values corresponding the each cut point

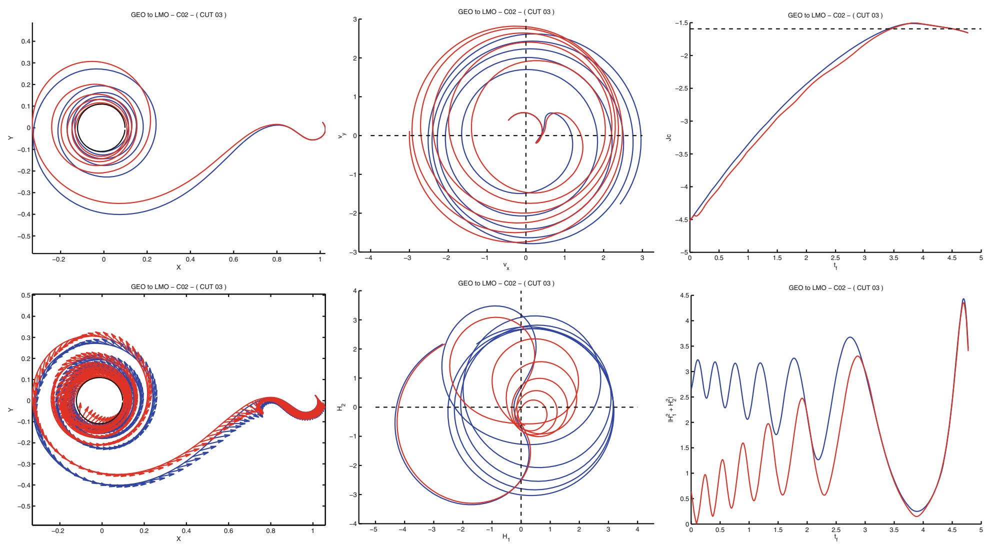

Fig. 113 $\mathscr{C}_2$ cut point n^o 3, *blue* orbits correspond to the first cut value and *red* orbits to the second cut value. (*top-left*) $\{XY\}$ projection of the transfer trajectory, (*top-center*) $\{V_x V_y\}$ projection of the transfer trajectory, (*top-right*) t versus J_c (energy variation along the transfer trajectory), (*bottom-left*) control along the trajectory, (*bottom-center*) H_1 versus H_2, (*bottom-right*) t versus $|(H_1, H_2)|$

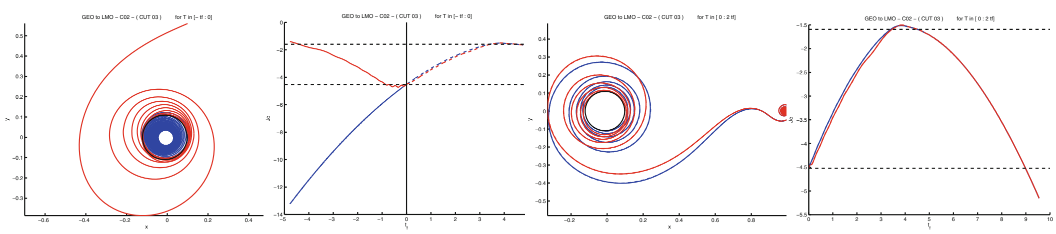

Fig. 114 $\mathscr{C}_2$ cut point n^o 3, (*left*) optimal solutions for $t \in [-t_f, 0]$ (XY projection and J_c variation), (*right*) optimal solutions for $t \in [0, 2t_f]$ (XY projection and J_c variation)

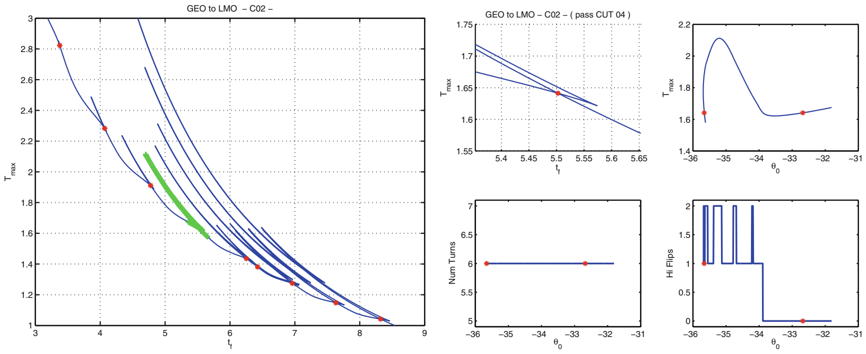

Fig. 115 $\mathscr{C}_2$ cut point n^o 4: (*left*) t_f versus ε homotopic curve with highlight of the cut passage in *green*; (*right*) analysis of the cut passage: (*top-left* subplot) t_f versus ε zoom, (*top-right* subplot) θ_0 versus ε, (*bottom-left* subplot) θ_0 versus num. turns around the Earth, (*bottom-right* subplot) θ_0 versus the number of times $|(H_1, H_2)|$ passes close to zero. *Red* points are values corresponding the each cut point

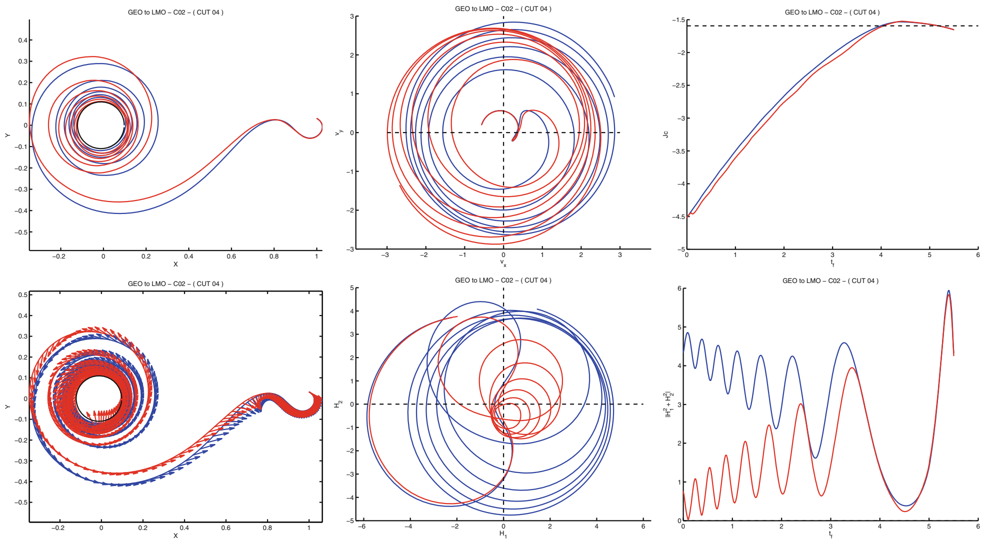

Fig. 116 $\mathscr{C}_2$ cut point n^o 4, *blue* orbits correspond to the first cut value and *red* orbits to the second cut value. (*top-left*) $\{XY\}$ projection of the transfer trajectory, (*top-center*) $\{V_x V_y\}$ projection of the transfer trajectory, (*top-right*) t versus J_c (energy variation along the transfer trajectory), (*bottom-left*) control along the trajectory, (*bottom-center*) H_1 versus H_2, (*bottom-right*) t versus $|(H_1, H_2)|$

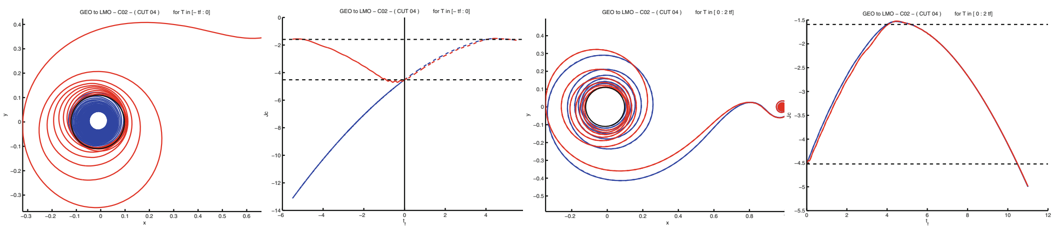

Fig. 117 $\mathscr{C}_2$ cut point n^o 4, (*left*) optimal solutions for $t \in [-t_f, 0]$ (XY projection and J_c variation), (*right*) optimal solutions for $t \in [0, 2t_f]$ (XY projection and J_c variation)

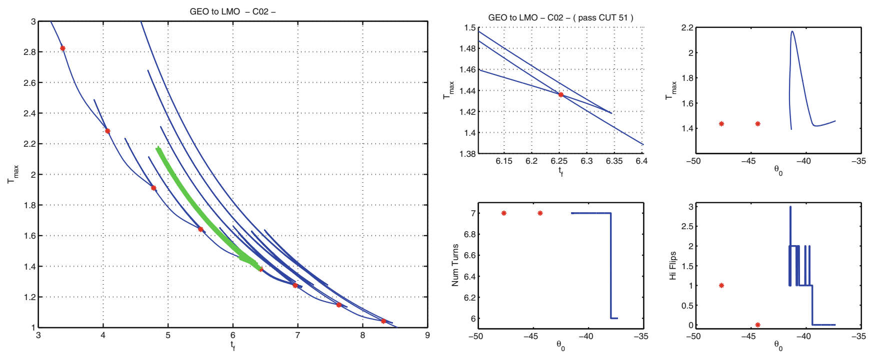

Fig. 118 $\mathscr{C}_2$ cut point n^o $5(a)$: (*left*) t_f versus ε homotopic curve with highlight of the cut passage in *green*; (*right*) analysis of the cut passage: (*top-left* subplot) t_f versus ε zoom, (*top-right* subplot) θ_0 versus ε, (*bottom-left* subplot) θ_0 versus num. turns around the Earth, (*bottom-right* subplot) θ_0 versus the number of times $|(H_1, H_2)|$ passes close to zero. *Red* points are values corresponding the each cut point

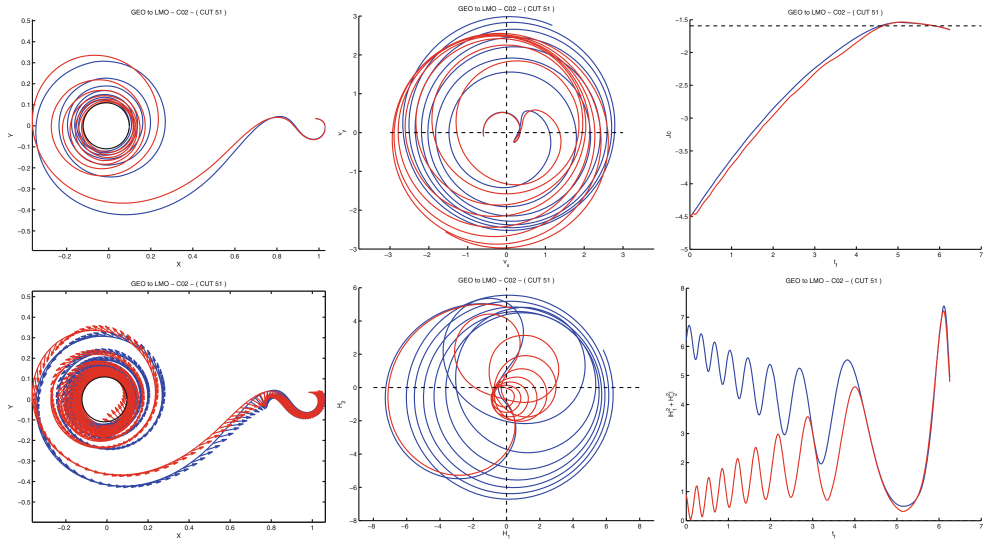

Fig. 119 $\mathscr{C}_2$ cut point n^o $5(a)$, *blue* orbits correspond to the first cut value and *red* orbits to the second cut value (*top-left*) $\{XY\}$ projection of the transfer trajectory, (*top-center*) $\{V_x V_y\}$ projection of the transfer trajectory, (*top-right*) t versus J_c (energy variation along the transfer trajectory), (*bottom-left*) control along the trajectory, (*bottom-center*) H_1 versus H_2, (*bottom-right*) t versus $|(H_1, H_2)|$

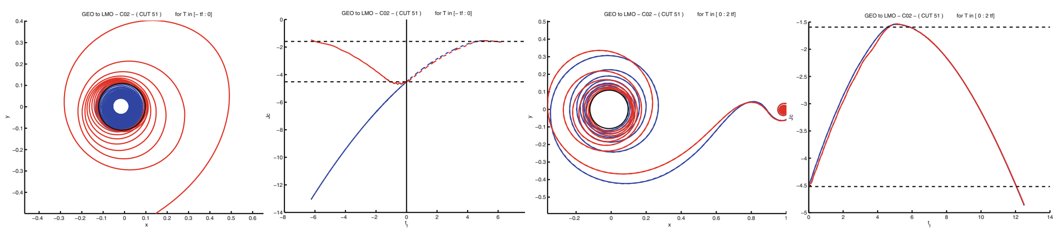

Fig. 120 $\mathscr{C}_2$ cut point n^o $5(a)$, (*left*) optimal solutions for $t \in [-t_f, 0]$ (XY projection and J_c variation), (*right*) optimal solutions for $t \in [0, 2t_f]$ (XY projection and J_c variation)

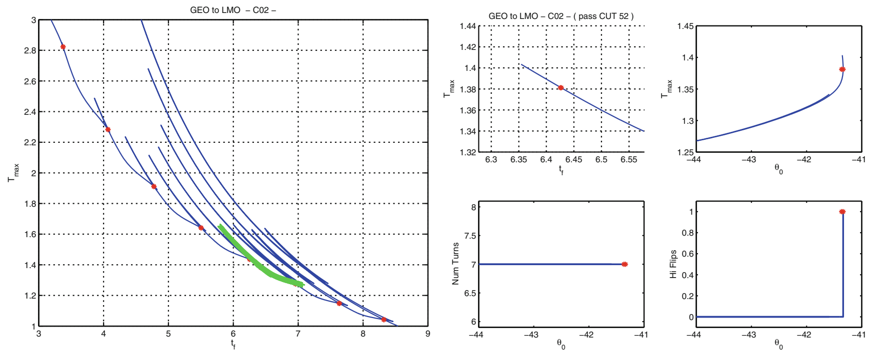

Fig. 121 $\mathscr{C}_2$ cut point n^o 5(b): (*left*) t_f versus ε homotopic curve with highlight of the cut passage in *green*; (*right*) analysis of the cut passage: (*top-left* subplot) t_f versus ε zoom, (*top-right* subplot) θ_0 versus ε, (*bottom-left* subplot) θ_0 versus num. turns around the Earth, (*bottom-right* subplot) θ_0 versus the number of times $|(H_1, H_2)|$ passes close to zero. *Red* points are values corresponding the each cut point

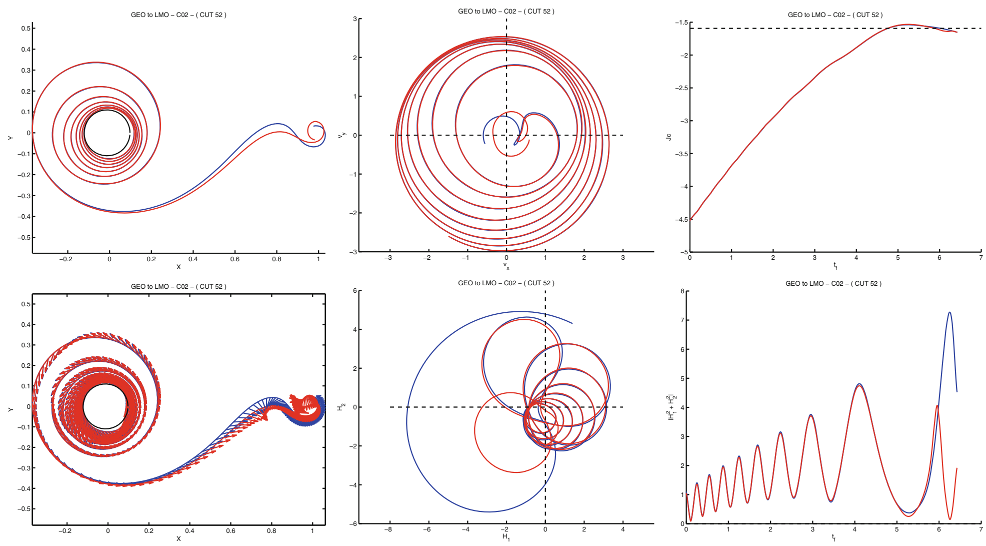

Fig. 122 $\mathscr{C}_2$ cut point n^o 5(b), *blue* orbits correspond to the first cut value and *red* orbits to the second cut value (*top-left*) $\{XY\}$ projection of the transfer trajectory, (*top-center*) $\{V_x V_y\}$ projection of the transfer trajectory, (*top-right*) t versus J_c (energy variation along the transfer trajectory), (*bottom-left*) control along the trajectory, (*bottom-center*) H_1 versus H_2, (*bottom-right*) t versus $|(H_1, H_2)|$

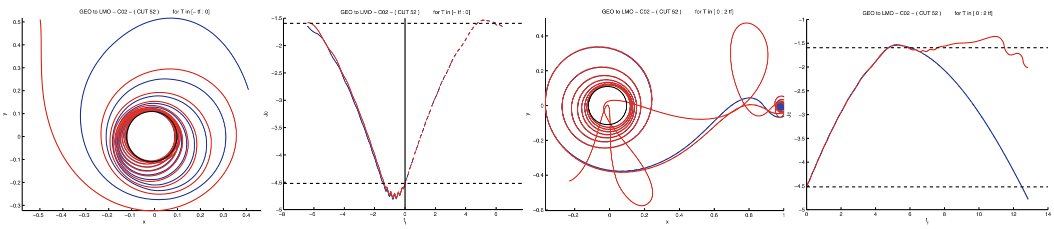

Fig. 123 $\mathscr{C}_2$ cut point n^o 5(b), (*left*) optimal solutions for $t \in [-t_f, 0]$ (XY projection and J_c variation), (*right*) optimal solutions for $t \in [0, 2t_f]$ (XY projection and J_c variation)

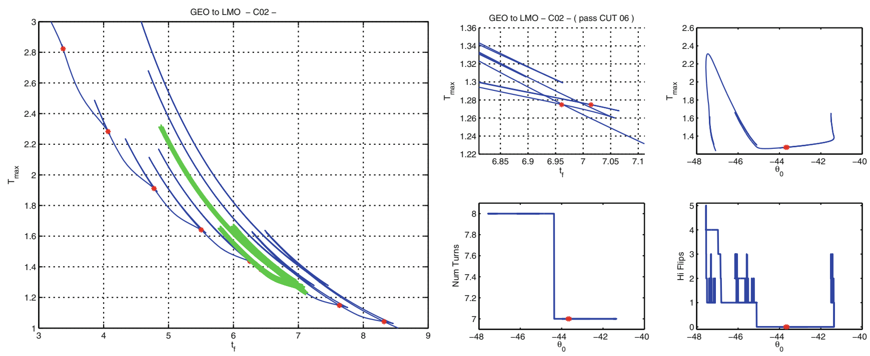

Fig. 124 $\mathscr{C}_2$ cut point n^o 6: (*left*) t_f versus ε homotopic curve with highlight of the cut passage in *green*; (*right*) analysis of the cut passage: (*top-left* subplot) t_f versus ε zoom, (*top-right* subplot) θ_0 versus ε, (*bottom-left* subplot) θ_0 versus num. turns around the Earth, (*bottom-right* subplot) θ_0 versus the number of times $|(H_1, H_2)|$ passes close to zero. *Red* points are values corresponding the each cut point

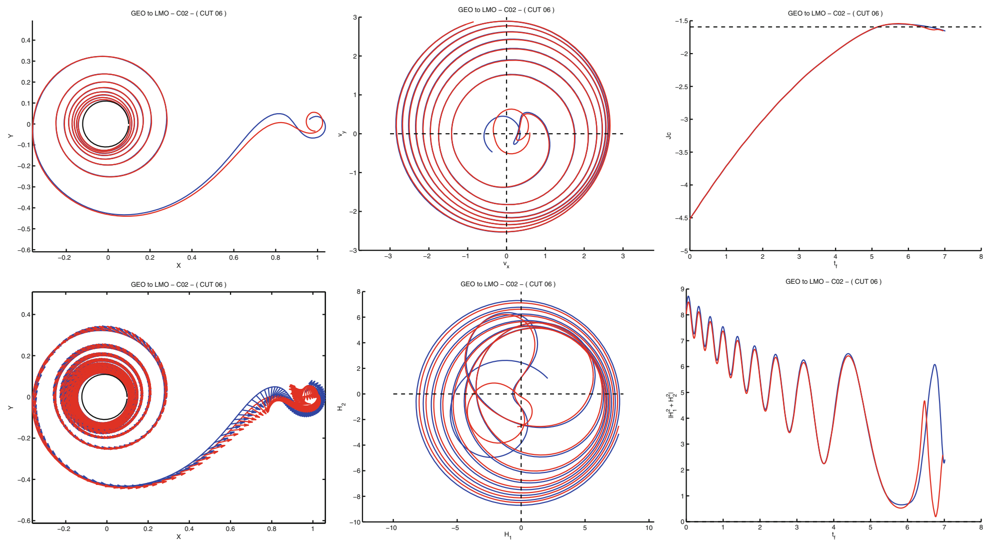

Fig. 125 $\mathscr{C}_2$ cut point n^o 6, *blue* orbits correspond to the first cut value and *red* orbits to the second cut value. (*top-left*) $\{XY\}$ projection of the transfer trajectory, (*top-center*) $\{V_x V_y\}$ projection of the transfer trajectory, (*top-right*) t versus J_c (energy variation along the transfer trajectory), (*bottom-left*) control along the trajectory, (*bottom-center*) H_1 versus H_2, (*bottom-right*) t versus $|(H_1, H_2)|$

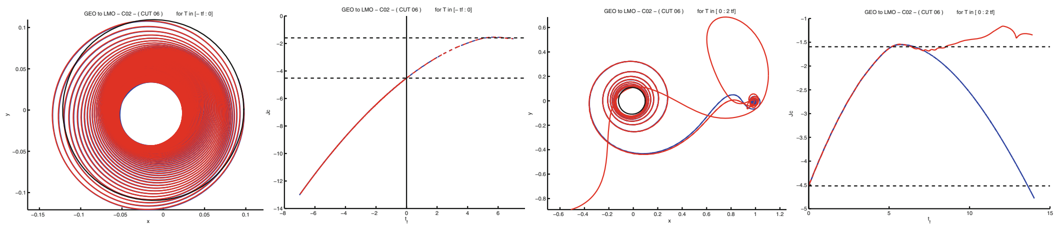

Fig. 126 $\mathscr{C}_2$ cut point n^o 6, (*left*) optimal solutions for $t \in [-t_f, 0]$ (XY projection and J_c variation), (*right*) optimal solutions for $t \in [0, 2t_f]$ (XY projection and J_c variation)

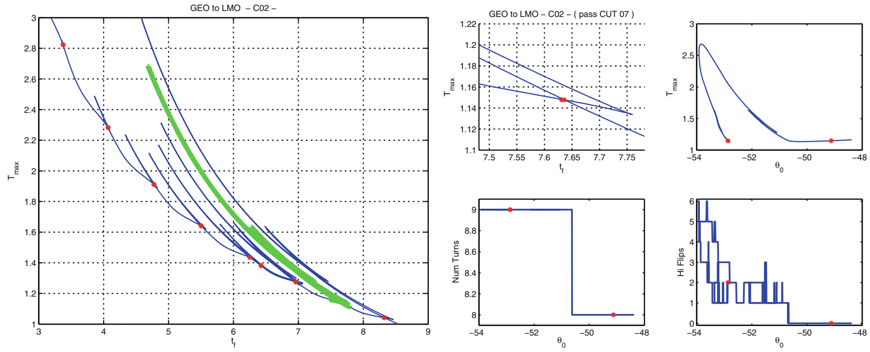

Fig. 127 $\mathscr{C}_2$ cut point n^o 7: (*left*) t_f verus ε homotopic curve with highlight of the cut passage in *green*; (*right*) analysis of the cut passage: (*top-left* subplot) t_f versus ε zoom, (*top-right* subplot) θ_0 versus ε, (*bottom-left* subplot) θ_0 versus num. turns around the Earth, (*bottom-right* subplot) θ_0 versus the number of times $|(H_1, H_2)|$ passes close to zero. *Red* points are values corresponding the each cut point

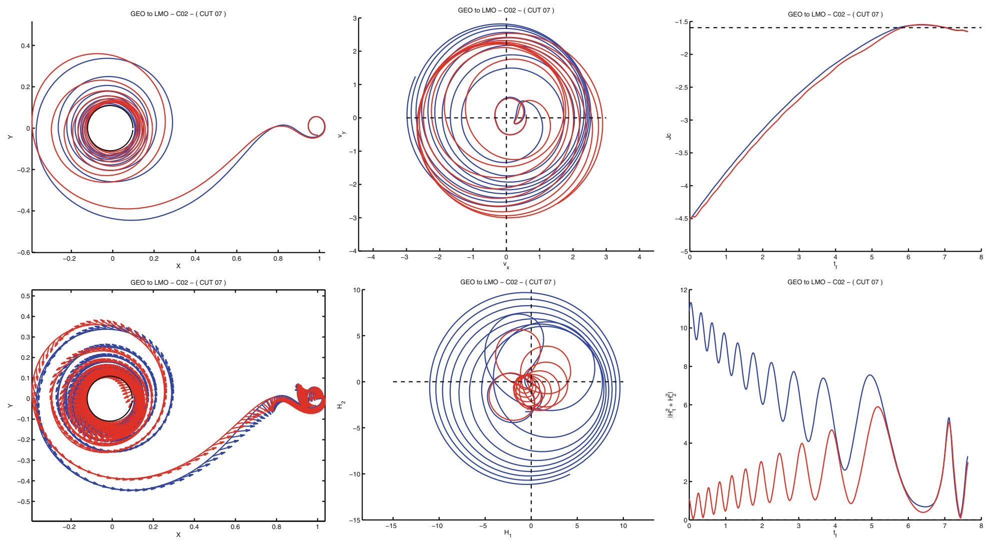

Fig. 128 $\mathscr{C}_2$ cut point n^o 7, *blue* orbits correspond to the first cut value and *red* orbits to the second cut value. (*top-left*) $\{XY\}$ projection of the transfer trajectory, (*top-center*) $\{V_x V_y\}$ projection of the transfer trajectory, (*top-right*) t versus J_c (energy variation along the transfer trajectory), (*bottom-left*) control along the trajectory, (*bottom-center*) H_1 versus H_2, (*bottom-right*) t versus $|(H_1, H_2)|$

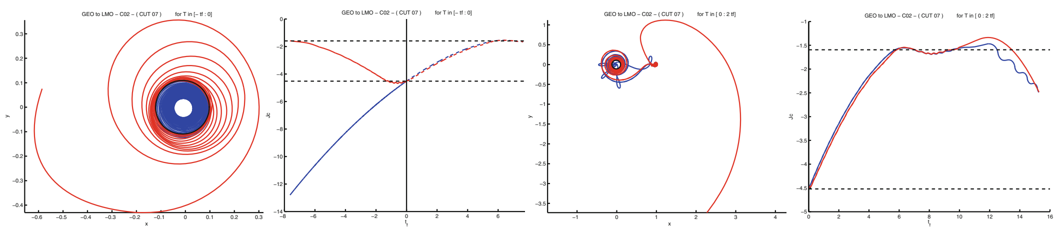

Fig. 129 $\mathscr{C}_2$ cut point n^o 7, (*left*) optimal solutions for $t \in [-t_f, 0]$ (XY projection and J_c variation), (*right*) optimal solutions for $t \in [0, 2t_f]$ (XY projection and J_c variation)

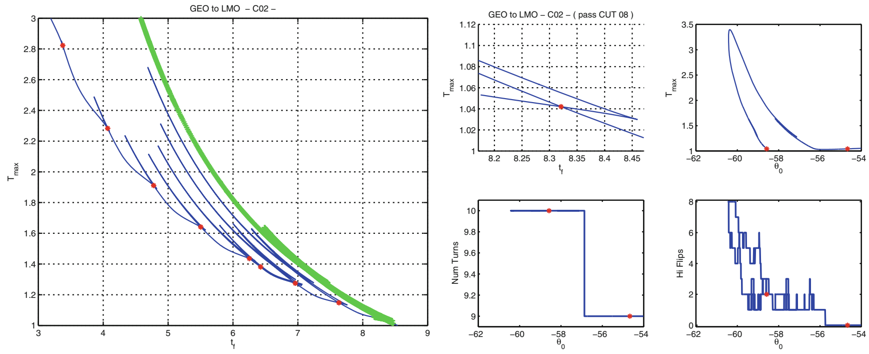

Fig. 130 $\mathscr{C}_2$ cut point n^o 8: (*left*) t_f versus ε homotopic curve with highlight of the cut passage in *green*; (*right*) analysis of the cut passage: (*top-left* subplot) t_f versus ε zoom, (*top-right* subplot) θ_0 versus ε, (*bottom-left* subplot) θ_0 versus num. turns around the Earth, (*bottom-right* subplot) θ_0 versus the number of times $|(H_1, H_2)|$ passes close to zero. *Red* points are values corresponding the each cut point

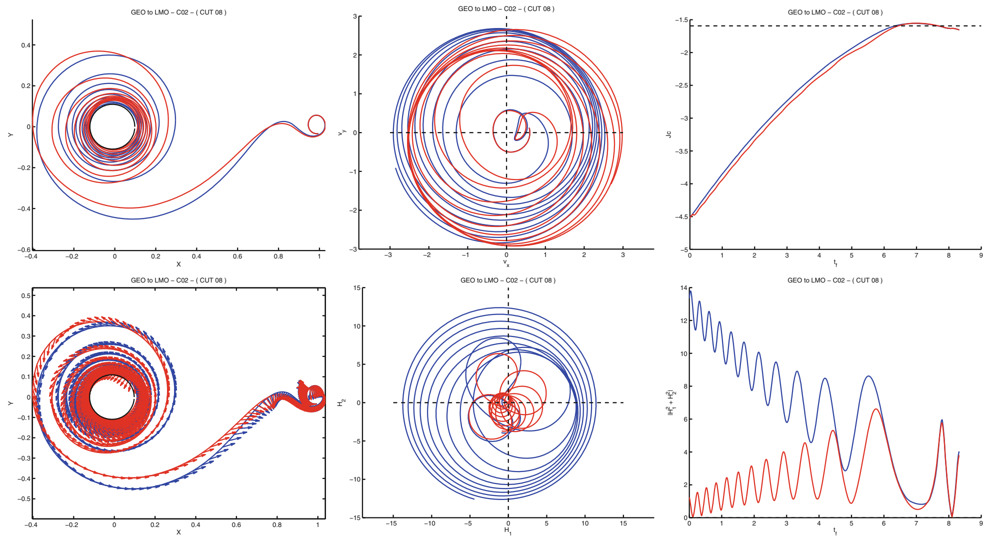

Fig. 131 $\mathscr{C}_2$ cut point n^o 8, *blue* orbits correspond to the first cut value and *red* orbits to the second cut value. (*top-left*) $\{XY\}$ projection of the transfer trajectory, (*top-center*) $\{V_x V_y\}$ projection of the transfer trajectory, (*top-right*) t versus J_c (energy variation along the transfer trajectory), (*bottom-left*) control along the trajectory, (*bottom-center*) H_1 versus H_2, (*bottom-right*) t versus $|(H_1, H_2)|$

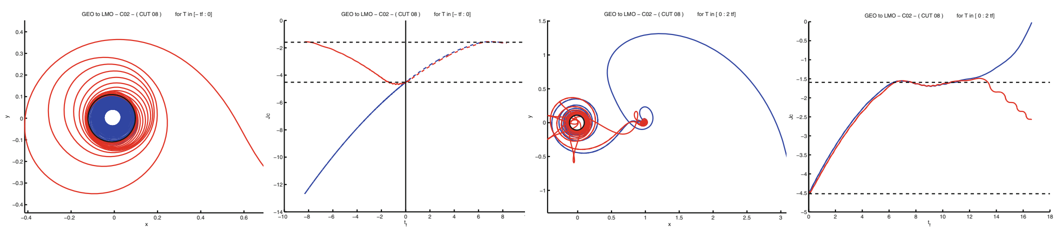

Fig. 132 $\mathscr{C}_2$ cut point n^o 8, (*left*) optimal solutions for $t \in [-t_f, 0]$ (XY projection and J_c variation), (*right*) optimal solutions for $t \in [0, 2t_f]$ (XY projection and J_c variation)

Acknowledgments This work has been supported by the Conseil Régional de Bourgogne grant no. 9201AAO049S0273.

References

1. Arnold VI (2004) Catastrophe theory. Springer, New York
2. BepiColombo mission: http://sci.esa.int/bepicolombo
3. Caillau JB, Chitour Y, Zheng Y (2015) L^1-Minimization for mechanical systems, pp 1–22
4. Caillau J-B, Cots O, Gergaud J (2012) Differential pathfollowing for regular optimal control problems. Optim Methods Softw 27(2):177–196
5. Caillau JB, Daoud B (2012) Minimum time control of the restricted three-body problem. SIAM J Control Optim 50(6):3178–3202 (2012). http://apo.enseeiht.fr/hampath
6. Caillau JB, Daoud B, Gergaud J (2011) Discrete and differential homotopy in circular restricted three-body control. Discrete Contin Dyn Syst Suppl:229–239 (2011) (Proceedings of 8th AIMS Conference on Dynamical Systems, Differential Equations and Applications, Dresden, May 2010)
7. Caillau J-B, Daoud B, Gergaud J (2012) Minimum fuel control of the planar circular restricted three-body problem. Celestial Mech Dyn Astron 114(1):137–150
8. Caillau J-B, Noailles J (2001) Coplanar control of a satellite around the Earth. ESAIM Control Optim Calc Var 6:239–258
9. Lisa Pathfinder mission: http://sci.esa.int/lisa-pathfinder
10. Zhang C, Topputo F, Bernelli-Zazzera F, Zhao Y-S (2015) Low-thrust minimum-fuel optimization in the circular restricted three-body problem. J Guid Control Dyn 38:1501–1510